Orbit Space Reduction for Symmetric Dynamical Systems with an Application to Laser Dynamics

Submitted by Victoria Crockett,

to the University of Exeter as a thesis for the degree of

Doctor of Philosophy in Mathematics, September 2010.

Abstract

This work considers the effect of symmetries on analysing bifurcations in dynamical systems. We consider an example of a laser with strong optical feedback which is modelled using coupled non-linear differential equations. A stationary point can be found in space, which can then be continued in parameter space using software such as AUTO. This software will then detect and continue bifurcations which indicate change in dynamics as parameters are varied. Due to symmetries in the equations, using AUTO may require the system of equations to be reduced in order to study periodic orbits of the original system as (relative) equilibria of the reduced system. Reasons for this are explored as well as considering how the equations can be changed or reduced to remove the symmetry. Invariant and Equivariant theory provide the tools for reducing the system of equations to the orbit space, allowing further analysis of the lasers dynamics.

Acknowledgements

First and foremost I would like to sincerely thank Dr Sebastian Wieczorek and Prof Peter Ashwin for their support throughout my thesis.

I am grateful also, to Bookham technologies and Great Western Research, without whom I would not have had this opportunity.

I would also like to thank the various fellow Ph.D. candidates at the University of Exeter Mathematics department with whom I have enjoyed many conversations and discussions regarding our research and who have helped to maintain my passion for the subject and its advancement. Noteably Catherine Luke, John Wordsworth, Tim Paulden, James Kent, Paul Truman, Dan Holdaway, and Rachel Lowe.

I would also like to thank those at Exeter College for giving me time to complete the writing process.

There has also been a great deal of support from friends in Exeter over the years which has been invaluable. I would like to mention Gill Hatwell, Jane Grief, Steph Thomson, Becki Wordsworth, Hannah Newton, Maddy Morgan, and many more for your wonderful friendships and encouragement. I would like to give a special mention to Jack Matthews for his love, support and proof reading skills.

During my time at Exeter there have been many challenges and throughout my time here I have had the continuing support from my parents, Paul and Adrienne Crockett, my siblings and many extended family members - who I am very close to and very thankful for.

I would like to dedicate this thesis to my late Grandfather David Crockett, who

passed away before he could see its final result. He was a great man, extremely creative and well educated and always took an interest in my work.

Contents

List of Figures

List of Tables

Chapter 1

Introduction

In this chapter I introduce and discuss motivations and methods for modelling lasers. This will include an introduction to the history and reasons behind the methods used in the modelling of lasers. This will allow the reader to understand the particular methods chosen in modelling a laser with strong optical feedback later in the thesis. Later, I will consider again the influence that previous work has had in determining the process and direction of my research.

In addition to this I will introduce the subject of symmetries in systems of differential equations. I will discuss how symmetries in systems, though often prized for their beauty, can cause difficulties in analysis. I will consider linear symmetries and how these affect bifurcations in systems of ODEs.

We will see that group theory provides us with the means to describe symmetries and link these to solutions of our equations. This introduction will define the tools needed to do this and will give some examples of groups to be used.

1.1 Introduction to the Modelling of Lasers

A laser is a device for producing coherent light, which has many applications, particularly in communications and data storage, such as reading DVDs. A simple laser consists of an optical cavity containing a special material known as a gain medium, through which the light passes back and forth between mirrors. The gain medium can be composed of a variety of materials in any state, generally chosen for properties that allow lasing to occur at various frequencies. For lasing to occur some initial energy must be applied to the medium, a process known as pumping. Pump energy can be optical or electrical, but is used to excite electrons into higher energy states which collectively form what is called population inversion. Once the energy applied to the medium by the pump reaches a certain threshold i.e. when a critical density of excited electrons, or population inversion threshold is reached, then an initial stimulus of light can be applied to start coherent light emission. As this stimulated light passes back and forth within the laser cavity, it stimulates further emissions, provided the pump energy input remains above the threshold. Usually the coupling mirror will be partially transparent to allow the stimulated light to be directed out of the gain medium and into a coupled cavity (often a fibre optic cable).

Spontaneous and stimulated emission was considered by Einstein in 1917 [7] in a paper which predicted that photons could stimulate identical coherent photons by interacting with electrons in excited atoms. This was done by using probability coefficients for absorption, spontaneous emission, and stimulated emission of electromagnetic radiation to re-derive Plank's law of radiation. The existence of stimulated

emission was then confirmed by Rudolf W. Ladenburg in 1928 [33] and observation of lasing was made in 1960 by Maiman [25]. Exploration of chaos produced in lasers was first reported in a loss modulated CO_2 laser [1] and in a multimode He-Ne laser [37] at the end of the twentieth century and through the development of semiconductor lasers in the paper by Lang and Kobayashi [24]. Further information on the history of the laser can be found in *The Laser Guide Book* by Hecht [14] and in [13].

More recent challenges in modelling lasers have involved lasers coupled to additional lasers or with feedback from an external mirror, so that the light re-enters the gain medium out of phase as in the Lang and Kobayashi paper and noteably [28] and [34]. Such laser systems produce highly complex behaviour and are modelled by systems of coupled non-linear differential equations as seen in [20] and [38]. These systems of equations cannot be solved exactly, but the dynamics can be described, and continuation software such as AUTO [6] can be used to track stationary or periodic points in parameter space, detecting and mapping any changes to the dynamics.

During experimental operations, regions of stability may be stumbled upon possibly without realising which operating parameters may have had the right effect, although since this is not intuitive, results are often difficult to reproduce. In addition to this, in some cases it is necessary to find regions of instability, for instance in secure communications [35]. This would require, though, that the decoding laser is operating in identical circumstances so that the hidden signal can be removed

cleanly.

It is therefore necessary to understand stability and types of instability. Ideally this should be done by analytical methods, though unfortunately this is only possible in the most simple cases. In more complicated set ups we often need to use numerical methods such as simulation or path-following (continuation) software [6].

In order to map the stability in parameter space we may need to use numerical models to find and illustrate the transitions between these regions. To do this we need to find a suitable mathematical model to analyse. Then, starting from a steady state solution we can use continuation software (such as AUTO) to 'follow' this steady state as parameters are varied. This software will detect changes in the solution's stability known as bifurcations by examining the changing eigenvalues of the Jacobian of the system of equations [23], indicating the point at which a boundary is reached where the stability of the laser may change. Similarly to the method by which the steady state was followed, bifurcation points can then be followed to produce a map of the stable and unstable regions of operation on varying two parameters for the laser with a description of the changes that will take place as boundaries are crossed.

Often mathematical models of lasers will naturally be symmetric [21]. This might be from symmetries in the set up or from symmetries within each laser caused by the invariance under the phase shift of the complex-valued electric field. Symmetries can cause problems for software continuation of bifurcations for a number of reasons.

- Eigenvalues of symmetric bifurcations may be multiple, but path following

programmes such as AUTO expect a single real eigenvalue or a complex pair of eigenvalues to pass through zero at a bifurcation.

- Symmetric systems with continuous group symmetries may have "relative equilibria" that are periodic orbits or even tori in the original system.

- Nonlinear terms mean that bifurcations may not be generic - multiple solutions may branch out or emerge at a bifurcation.

For the rest of this chapter we review standard methods for understanding and analysing dynamics of ODEs with symmetries before discussing the orbit space reduction. This is a way of removing the symmetries by identifying all points that are symmetrically related.

Orbit space reduction techniques were introduced by Chossat [3] and Lauterbach [4] as a tool for analysing equivariant dynamical systems, here we consider numerical uses of orbit space reduction.

1.2 Symmetries of ODEs

Symmetric patterns in nature or in experimental work are important to note as often patterns can change suddenly with a given parameter variation around that same symmetry. The patterns have symmetries which may still be dominant in systems of equations which might be used to model them. In real life the system is unlikely to have perfect symmetry, but will be present in its idealization. In addition to this, it could be said that the bifurcation is associated with the change of symmetry that

is observed.

From this perspective it is clear that symmetry in systems can produce beautiful patterns and [9], in fact, without some initial symmetry to be changed, the bifurcation points indicated by the fascinating sudden changes of symmetry may not occur for us to then study. However, once a set of equations are applied to a problem they inherit the system's idealised symmetry and this may then cause difficulties in its analysis, as discussed in the example of a laser with strong optical feedback later in this thesis.

Linear symmetries Bifurcations are associated with changes to a pattern in the system, or to look at it another way, a point where the symmetry changes.

We consider symmetry groups that are groups of linear transformations that act orthogonally [11]. Since bifurcation theory applies locally then we should be primarily concerned with operators which act in linear spaces.

For dynamical systems defined by ODEs, the symmetries impose restrictions on both the form of the solutions and the way bifurcations may take place. One can identify two subthemes:

1. Geometric: Transformation groups, fixed point subspaces and singularities.

2. Algebraic: Group representation theory and also equivariant singularity theory.

In fact in [11] for the orbit space reduction we discuss, both themes are inter-twined.

A symmetry is a transformation of a space, S, that preserves some given structure. Let Γ be the set of these transformations which can be described as a group, and assume S is the real vector space $\mathbb{R}^n$. The symmetries or transformations we consider are linear mappings $\gamma : \mathbb{R}^n \to \mathbb{R}^n$. Here the given structure that we are preserving during these transformations will be the set of solutions of an ODE, for example, for a bifurcation problem.

For example, consider the bifurcation problem

$$\dot{x} = f(x, \lambda)$$

where equilibria are given by

$$f(x, \lambda) = 0 \tag{1.1}$$

where $f : \mathbb{R}^n \times \mathbb{R} \to \mathbb{R}^n$ is a smooth (C^∞) mapping, λ being the bifurcation parameter. The presence of symmetries Γ means that for all $\gamma \in \Gamma$

$$f(\gamma x, \lambda) = \gamma f(x, \lambda)$$

so that every $\gamma \in \Gamma$ commutes with f. It follows that x is a solution to (1.1) if and only if γx is, so the solution set to (1.1) is preserved by the symmetries $\gamma \in \Gamma$.

1.3 Group theory and dynamics

Group theory provides us with the means to describe symmetry in a system of ODEs and to make rigorous statements about how the symmetries relate to solutions and their stabilities. Let us quickly define the basics:

Wallace [36] gives the following definitions surrounding sets: **set** A collection or assembly of objects is called a set. Each object is said to be an **element** of the set. Let A be a set. If A consists of a finite number of elements, say $a_1, a_2, ..., a_N$ (where the notation presumes the elements are distinct) then we write

$$A = \{a_1, a_2, ..., a_N\}$$

and A is said to be a **finite set** of **cardinality** N, written $N = |A|$. If A does not have a finite number of elements A is called an infinite set. The set consisting of no elements is called the empty set or the null set.

Subset A set A is said to be a subset of a set B if every element of A is also an element of B. We write

$$A \subseteq B$$

to indicate that A is a subset of B and so on.

Mappings Let A and B be sets. Let there be a rule or prescription, denoted by f, by which to each element a of A there is assigned a unique element, denoted by $f(b)$, of B. Then the rule is said to be a mapping or map or function from A to B. We write

$$a \to f(a) \ (a \in A)$$

and to indicate that f is a mapping on sets, we use both of the following notations:

$$f : A \to B \text{ and } A \overset{f}{\to} B$$

A is called the domain of f and B is called the codomain of f.

Wallace [36] also gives the following definitions: **Group** Let G be a non-empty set on which there is defined a binary operation so that the outcome of the operation between a and b $(a, b \in G)$ is denoted by ab. Then G is called a **group** if the following axioms hold.

1. For all $a, b \in G, ab \in G$ (closure)
2. For all $a, b, c \in G, (ab)c = a(bc)$ (associativity)
3. There exists $e \in G$ such that for all $a \in G, ea = a$ (existence of identity).
4. For each $a \in G$ there exists an element denoted by a^{-1} such that $a^{-1}a = e$ (existence of inverse).

Finite group A group G is said to be finite if the set G is a finite set, otherwise the group is said to be infinite. If G is finite the **order** of G, written $|G|$ (which is the number of elements in G) is finite and G has **finite order**. An infinite group is said to have **infinite order**.

Subgroup Let H be a non-empty subset of the group G which is also a group under the multiplication in G. Then H is called a subgroup of G. **Subgroup Criterion** A non-empty subset H of the group G is a subgroup of G if and only if for all $a, b \in H, ab \in H$ and $a^{-1} \in H$.

Conjugate Let H be a subgroup of the group G. Any subgroup of the form $x^{-1}Hx$ for some $x \in G$ is called a conjugate of H. A subgroup H which coincides with all its conjugates is said to be **normal** in G. Thus H is normal in G if and only if $x^{-1}Hx = H$ for all $x \in G$ or equivalently, $xH = Hx$ for all $x \in G$.

Homomorphism We are here concerned with mappings which preserve algebraic structure. Such mappings are called 'homomorphisms' (Greek: homo - same, morph - form). More precisely we have the following definition which we make for semigroups. Let S and T be semigroups and let $f : S \to T$ be a mapping such that

$$f(xy) = f(x)f(y)$$

for all $x, y \in S$. Then f is said to be a homomorphism from S into T.

Kernel Let G and H be groups and let $f : G \to H$ be a homomorphism. Then the sub-group $K = \{x \in G | f(x) = e_H\}$ is a normal subgroup of G which is called the kernel of f written Ker f.

Wallace also gives the following definitions for Rings: By a **polynomial in** x **over** $\mathbb{R}$ we understand an expression $a(x)$ of the form

$$a(x) = a_0 + a_1x + ... + a_mx^m$$

where the so-called **coefficients** $a_0, a_1, ..., a_m$ are real numbers, and x is sometimes called an '**indeterminate**'. If all of the coefficients are 0 the polynomial is said to be the **zero polynomial**, denoted by 0. If $a(x)$ is not the zero polynomial and if $a_m \neq 0$ then $a(x)$ is said to have **degree** m, briefly $\deg(a(x)) = m$.

Axioms and Rings Let R be a non-empty set in which there are defined two binary operations called **addition** and **multiplication**. For $a, b \in R$ the outcome of the addition of a and b, called the **sum** of a and b, is denoted by $a + b$ ('a plus b') and the outcome of the multiplication of a by b, called the **product** of a by b, is denoted by the simple juxtaposition ab ('a times b'). Then R is called a **ring** if the following axioms hold:

1. Axioms of addition

   - For all $a, b \in R, a + b \in R$ (closure)
   - For all $a, b, c \in R, (a + b) + c = a + (b + c)$ (associativity).
   - There exists a distinguished element denoted by 0 such that for all $a \in R, a + 0 = 0 + a = a$ (0 is 'zero')
   - For any $a \in R$ there exists an element denoted by $-a \in R$ such that $a + (-a) = (-a) + a = 0$ (the inverse of addition).
   - For all $a, b \in R, a + b = b + a$ (commutativity).

2. Axioms of Multiplication

   - For all $a, b \in R, ab \in R$ (closure)
   - For all $a, b, c \in R, (ab)c = a(bc)$ (associativity)

3. Axioms of Distributivity

   - For all $a, b, c \in R, a(b + c) = ab + ac$ (distributivity)
   - For all $a, b, c \in R, (a + b)c = ac + bc$ (distributivity).

Subring Let S be a non-empty subset of the ring R which is also a ring under the addition and multiplication in R. Then S is called a subring of R.

As discussed in [16, p201] a **module**, M, is defined as follows: Let R be any ring; a nonempty set M is said to be a *module* over R if M is an abelian group under an operation + such that for every $r \in R$ and $m \in M$ there exists an element rm in M subject to

- $r(a+b) = ra + rb$;
- $r(sa) = (rs)a$;
- $(r+s)a = ra + sa$

for all $a, b \in M$ and $r, s \in R$.

Examples of groups In particular, Lie groups will prove to be useful during the discussions of symmetries in dynamical systems, as a well developed theory of continuous symmetry as they form smooth differentiable manifolds.

Lie group [11, p25]. Let $GL(n)$ denote the group of all invertible linear transformations of the vector space $\mathbb{R}^n$ into itself, or equivalently the group of nonsingular $n \times n$ matrices over $\mathbb{R}$. A Lie group is a closed subgroup Γ of $GL(n)$ for some n. These are often also known as linear Lie groups. For example, the real invertible matrices form a group under multiplication, denoted by $GL_2(\mathbb{R})$:

$$GL_2(\mathbb{R}) = \left\{ A = \begin{pmatrix} a & b \\ c & d \end{pmatrix} : \det A \neq 0 \right\}$$

The space of all $n \times n$ matrices may be identified with $\mathbb{R}^{n^2}$, which contains $GL(n)$ as an open subset. If Γ is a closed subgroup then it is a closed subset of $GL(n)$ as well as a subgroup of $GL(n)$. A Lie subgroup of Γ is just a closed subgroup in the same sense.

The following groups are all isomorphic to Lie groups. This is not an exhaustive list, but introduces examples that are used commonly in describing the symmetries in dynamical systems. See [4] for more details.

The orthogonal group $\mathbf{O}(n)$: The group of $n \times n$ matrices, A, satisfying $AA^t = I_n$.

The special orthogonal group $\mathbf{SO}(n)$: all $A \in \mathbf{O}(n)$ such that $\det(A) = 1$. This is also known as the n-dimensional rotation group. For example $\mathbf{SO}(2)$ is made up of planar rotations

$$R_\theta = \begin{pmatrix} \cos\theta & -\sin\theta \\ \sin\theta & \cos\theta \end{pmatrix}$$

and can be identified with $\mathbf{S}^1$, the circle group.

The cyclic group $\mathbf{Z}_n$ consists of 2×2 matrices generated by $\mathbb{R}$.

The dihedral group $\mathbf{D}_n$ of order $2n$, generated by $\mathbf{Z}_n$ with an element of order 2 that does not commute with $\mathbf{Z}_n$. This is the symmetry of a regular n-gon in the plane.

In addition to these, all finite groups are isomorphic to Lie groups.

More generally, we will consider compact groups of Lie type, as in Golubitsky, Stewart and Schaeffer [11, p25]. They split the discussion of Lie groups into three parts:

1. Basic definitions and examples.

2. Representation theory.

3. Existence of an invariant integral - so we can use averaging arguments which allow for identification of any representation of a compact Lie group with a group of orthogonal transformations.

Note that a Lie group can be seen as a manifold (for example, we can think of $\mathbf{S}^1$ as a circle) with a group property - we can combine two points on the manifold

to give a third such that the group axioms are satisfied. All the examples of groups above are Lie groups and have well-defined dimension which is the dimension of this manifold.

Chapter 2

Differential equations with symmetries

In this chapter I consider the analysis of differential equations with symmetries. I will start by considering how symmetries (as described in the previous chapter) may affect bifurcation problems. I will then consider particular cases where symmetry is a problem for analysis of a system of equations; considering how symmetries can be removed. Following this I will introduce invariants and equivariants and discuss how these can be used to remove symmetries by reducing a system to its orbit space.

Suppose a system has symmetry $\Gamma \subseteq \mathbf{O}(n)$ and phase space $\mathbb{R}^n$. This means we assume that for $x \in \mathbb{R}^n$ the ODEs

$$\dot{x} = f(x) \tag{2.1}$$

must satisfy

$$f(\gamma x) = \gamma f(x)$$

for all $\gamma \in \Gamma$ and all $x \in \mathbb{R}^n$. We say the ODE $f(x)$ has symmetries Γ. We verify that the symmetries of our systems of equations can be described in the language of groups. If γ and δ are symmetries of the system then we need to show that γ^{-1} and $\gamma\delta$ are also symmetries. To see this, we set $y = \gamma x$ then $f(y) = \gamma f(\gamma^{-1}y)$ and multiply by γ^{-1} and then secondly $f(\gamma\delta x) = \gamma f(\delta x) = \gamma\delta f(x)$. Hence, the set of symmetries, Γ, of our system of equations forms a group.

We use this language to describe the type of dynamics that might occur.

Symmetries of arbitrary points $x_0 \in \mathbb{R}^n$ form a subgroup of Γ called the *isotropy subgroup* of x_0, defined by

$$\Sigma_{x_0} = \{\gamma \in \Gamma : \gamma x_0 = x_0\}.$$

Solutions to symmetric systems typically come in symmetric families; more precisely, if we have $x_0 \in \mathbb{R}^n$ then the *group orbit* through x_0 is defined by

$$\Gamma x_0 = \{\gamma x_0 : \gamma \in \Gamma\}.$$

One can show from (2.1) that if x_0 is a steady solution, then every point in the group orbit will also be a steady solution. We say $Y \subset \mathbb{R}^n$ is *invariant* under Γ if $\Gamma Y = Y$. As a special case, Y is *fixed* under Γ if $\gamma y = y$ for all $\gamma \in \Gamma$ and $y \in Y$. Note that every subset that is fixed under Γ is also invariant under Γ (not vice versa though).

For any subgroup $G \subset \Gamma$ we define the *fixed point subspace* associated to G as

$$\mathrm{Fix}(G) = \{y \in \mathbb{R}^n \ : \ \gamma y = y \ \text{ for all } \gamma \in G\}.$$

As discussed previously, one of the problems with having symmetries in the system is the high multiplicity of eigenvalues. Techniques have been developed [11] to simplify analysis of symmetric bifurcation problems, using methods that exploit the symmetries. These techniques include restriction to fixed point subspaces, invariant theory and equivariant theory.

Consider some H, an isotropy subgroup, and note $H \subseteq N(H)$ where

$$N(H) = \{g \in G : gH = Hg\}$$

(ie H is within the *normaliser* of H, $N(H)$). Suppose for some $h \in G$ that

$$\begin{aligned} h\text{Fix}(H) = \text{Fix}(H) & \\ \Leftrightarrow \quad & \{hx \in V : Hx = x\} = \{x \in V : Hx = x\} \\ \Leftrightarrow \quad & \{y \in V : Hh^{-1}y = h^{-1}y\} = \{x \in V : Hx = x\} \\ \Leftrightarrow \quad & \{y \in V : hHh^{-1}y = y\} = \{x \in V : Hx = x\} \\ \Leftrightarrow \quad & hHh^{-1} = H \\ \Leftrightarrow \quad & hH = Hh \\ \Leftrightarrow \quad & h \in N(H) \end{aligned}$$

So h fixes $\text{Fix}(H)$ if and only if $h \in N(H)$.

For example, if we consider the dihedral group acting on $\mathbb{C} \cong \mathbb{R}^2$

$$\mathbf{D}_3 = \langle \{z \to \overline{z}, z \to e^{2\pi i/3} z\} \rangle = \langle \{\kappa, \rho\} \rangle = \{e, \rho, \rho^2, \kappa, \rho\kappa, \rho^2\kappa\}$$

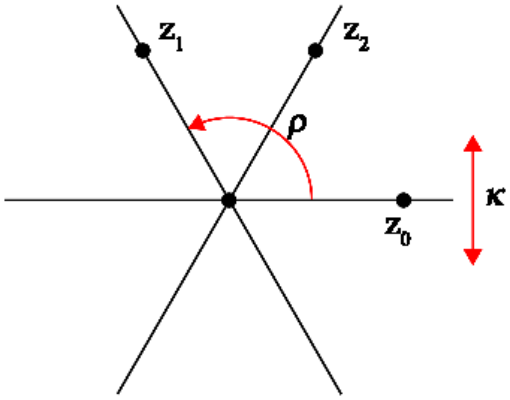

Figure 2.1: The reflections, κ, and rotations, ρ that generate the dihedral group $\mathbf{D}_3$ acting on the plane $\mathbb{C}$.

(where $\kappa^2 = \rho^3 = e$). One can verify that the isotropy subgroups are

$$\begin{aligned} G_{z_0} &= \{e, \kappa\} \\ G_0 &= D_3 \\ G_z &= \{e\} \\ G_{z_1} &= \{e, \rho^2\kappa\} \\ G_{z_2} &= \{e, \rho\kappa\} \end{aligned}$$

Where z is a general point in $\mathbb{C}$, z_0 is a point on the real axis, $z_1 = e^{\frac{2\pi i}{3}} z_0$ and $z_2 = e^{\frac{4\pi i}{3}} z_0$. Note that G_{z_0}, G_{z_1}, and G_{z_2} are conjugate to Z_2. $\mathbf{D}_3$ is trivial ($N(\mathbf{D}_3) = \mathbf{D}_3$) as is G_z ($N(e) = e$) and $N(G_{z_0}) = G_{z_0}$.

Every orbit $x(t)$ for a system with symmetry Γ is a dynamically invariant subset of X on which each $\gamma \in \Gamma$ acts by either leaving the orbit invariant, or by mapping it to a different orbit. A *relative equilibrium* is an equilibrium in the orbit space,

while in phase space it is an invariant group orbit. For a finite group the relative equilibrium must consist of a finite set of equilibrium, but for an infinite group there may be non-trivial (e.g. periodic) motion on the relative equilibrium in phase space [22]. This is discussed in more detail in [4, Chapter 7].

2.1 Symmetries for bifurcation problems

Consider a bifurcation problem

$$\dot{x} = f(x, \lambda)$$

with parameter, λ, with a symmetry group Γ of f for all values of λ. We assume $f(0, \lambda) = 0$ and f is singular at $\lambda = 0$ meaning there is a bifurcation at $(0, 0)$ [11].

A question is for which of the isotropy subgroups, Σ, could there be branches bifurcating from the steady states which have Σ as their group of symmetries.

A basic result is in [11, p11] The fundamental observation about one-dimensional fixed-point subspaces is the *equivariant branching lemma*, which asserts that generically, for each Σ satisfying

$$\dim \mathrm{Fix}(\Sigma) = 1,$$

there exists a unique branch of nontrivial steady-state solutions to $g = 0$ lying in $\mathrm{Fix}(\Sigma) \times \mathbb{R}$. "Algebraically this shows the existence of sub-groups with **D** fixed-point subspace." This is also an example of how symmetry makes it difficult to do bifurcation analysis as you get eigenvalues of high multiplicity. [11] says, however, that "these same symmetries help simplify the search for solutions".

An example application Golubitsky, Stewart and Schaeffer [11] give the example of a hosepipe suspended vertically, where water flows through the pipe at some rate λ. For larger values of λ the pipe will start to oscillate with either standing or rotating waves. The hose is circular and they assume a circularly symmetric model so the ODE has all rotations and reflections about the origin in the horizontal plane as its symmetries - the group of symmetries is $\mathbf{O}(2)$. This means the symmetries of periodic solutions from Hopf bifurcation are isotropy subgroups inside $\mathbf{O}(2) \times \mathbf{S}^1$:

- The standing waves have $\mathbf{Z}_2$ reflective symmetry inside $\mathbf{O}(2)$ and also a spatiotemporal reflection inside $\mathbf{O}(2) \times \mathbf{S}^1$.
- The rotating waves have $\widetilde{\mathbf{SO}}(2) = (\theta, \theta) : \theta \in \mathbf{S}^1$. Here $\mathbf{S}^1$ is identified with the rotations in $\mathbf{O}(2)$.

In this example there is an analogy between steady-state and Hopf bifurcation, where they replace Γ by $\Gamma \times \mathbf{S}^1$.

2.2 Reduction of symmetries and the orbit space

According to [11] the study of bifurcation problems with symmetry is complicated because symmetry often forces eigenvalues of high multiplicity. Even after Liapunov-Schmidt reduction, it is necessary to study bifurcation problems with several state variables. Techniques exist to simplify the analysis of symmetric bifurcation problems, and these exploit the very symmetries that cause the initial complication!

The three techniques Golubitsky, Stewart and Schaeffer [11] describe are:

1. Restriction to fixed-point subspaces.

2. Invariant theory.

3. Equivariant singularity theory.

It is natural to try and simplify the problem by removing the symmetries and going to an "orbit space". This means we write the original system in terms of what happens to all symmetric images of a single point rather than just a single point.

The idea of orbit space reduction is to investigate the system of differential equations modulo the group action. The system of differential equations is transformed to another system on a space with a complicated structure. The stratification of this set is found from the structure of orbit types of the group action, where the orbit types correspond to sets of points that have a given isotropy. The orbit space reduction is performed with the help of a Hilbert basis, described in section 2.3, of the ring of invariants.

We define the *orbit space* for the action of Γ on $V = \mathbb{R}^n$ to be

$$V/\Gamma = \{\Gamma x \ : \ x \in \mathbb{R}^n\}$$

where we "glue together" points that are on the same group orbit, i.e. we treat Γx as a point in the new space for each x. Note that Γx is a compact manifold, with dimension

$$\dim \Gamma x = \dim \Gamma - \dim \Sigma_x.$$

Unfortunately, for a typical compact group Γ acting on $\mathbb{R}^n$, the orbit space is not typically a manifold- it may have singularities and edges of varying dimension and

be quite hard to visualise geometrically.

Following work of Chossat [3], it is possible to introduce new variables that are combinations of the old ones, in order to re-write the system equations in a finite dimensional representation of the orbit space of the original system. The question will be how to do this in the most efficient way - to avoid wasting time re-doing your equations with different combinations of variables only to find that the symmetries remain.

2.3 Invariants and Equivariants: Generators and Bases

Let us define the set of *invariant polynomial functions*

$$\mathcal{P}(\Gamma) = \{f : \mathbb{R}^n \to \mathbb{R} \text{ polynomial } : f(\gamma x) = f(x) \ \forall \ \gamma \in \Gamma, x \in \mathbb{R}^n\}$$

As noted by [11], $\mathcal{P}$ is a ring called the *ring of invariants*. Namely, if $f, g \in \mathcal{P}(\Gamma)$ then $f(x)g(x)$ and $f(x) + g(x)$ are in $\mathcal{P}(\Gamma)$. That is, we can multiply and add (but not divide) polynomial invariants to obtain new polynomial invariants.

We also define the *module of equivariant polynomials over the ring of invariant polynomials*:

$$\widetilde{\mathcal{P}}(\Gamma) = \{f : \mathbb{R}^n \to \mathbb{R}^n \text{ polynomial } : f(\gamma x) = \gamma f(x) \forall \gamma \in \Gamma, x \in \mathbb{R}^n\}.$$

As discussed in [11], this is a module over the ring of invariants because (a) one can add equivariants to get a new equivariant and (b) equivariants can be multiplied by invariants to give an equivariant.

We will observe that there is a finite subset, $\mathcal{P}$, of invariant polynomials $\{u_1, ..., u_\ell\}$ such that every invariant polynomial can be written as a polynomial function of this $\{u_1, ..., u_\ell\}$. We call this set a *Hilbert basis* for the ring. The set of all invariant polynomials is a ring (sums and products of Γ-invariant polynomials are again Γ-invariant).

This following fundamental result (see [11]) shows that for compact group actions, the space of invariant functions is finitely generated and, helpfully, that a Hilbert basis will always exist.

Theorem 1 (Theorem 4.2 - Hilbert-Weyl Theorem)**.** *Suppose that* Γ *is a compact Lie group acting on* $\mathbb{R}^n$*. Then there is a finite Hilbert basis for the ring* $\mathcal{P}(\Gamma)$*.*

Using a Hilbert basis will remove the symmetries from the system of ODEs. However, since there is no unique Hilbert basis there will be many ways this can be done. For our purpose though, we will require that the number of ODEs in the system should be kept as low as possible for ease of numerical computation and for other reasons discussed later. Since the number of ODEs in the system is dictated by the size of the Hilbert basis, we therefore wish to find a way to quickly find a (since it is not necessarily unique) minimal Hilbert basis or the size of the minimal basis.

We say there is a *relation* between elements in a Hilbert basis if there is a non-trivial polynomial of the basis elements that is satisfied identically.

The ring $\mathcal{P}(\Gamma)$ is defined to be a *polynomial ring* if there is a Hilbert basis with no relations in it. We will later see example 2.2 which has a Hilbert basis with a relation

so the ring $\mathcal{P}$ is not a polynomial ring. Golubitsky, Stewart and Schaeffer (p47 and p72) [11] give a test to check if a Hilbert basis makes a polynomial ring. This could also be used to check that there are no relations if this is not immediately obvious. When you have a polynomial ring obtained from the Hilbert basis $\{u_1, ..., u_\ell\}$ then every invariant polynomial f has uniquely the form $f(x) = h(u_1(x), ..., u_\ell(x))$.

We will see that the ring of invariants we are interested in will always be finitely generated and therefore have a Hilbert basis. Unfortunately, Hilbert bases are not necessarily unique, may be of large size even for relatively simple groups, and moreover, there may be relations between basis elements. To avoid adding more than the necessary dimensions to our calculations we need to ensure that the basis of variables we choose is a minimal Hilbert basis.

Suppose we have a Hilbert basis $\{u_1, \cdots, u_\ell\}$ for $\mathcal{P}(\Gamma)$, the set of Γ-invariant polynomials. We will use this Hilbert basis to represent the system in the orbit space [3].

Simple examples: The ring of real polynomials of a single variable x is finitely generated by $\{x\}$. The ring of even polynomials of a single variable x is finitely generated by $\{x^2\}$. The module of odd polynomials if a single variable is generated by $\{x\}$ over the ring of even polynomials (note that this simply means that any odd polynomial can be written as $xf(x)$ where f is even.

Note that one does not need to consider invariants from $\mathbb{R}^n \to \mathbb{R}^d$ for any $d > 1$:

for example, $f : \mathbb{R}^n \to \mathbb{R}^2$ is invariant

$$\begin{pmatrix} f_1(\gamma(x)) \\ f_2(\gamma(x)) \end{pmatrix} = \begin{pmatrix} f_1(x) \\ f_2(x) \end{pmatrix}$$

if and only if f_1 and f_2 are in $\mathcal{P}(\Gamma)$.

Computing a Hilbert basis is often cumbersome but elementary, we restrict to the set of monomials of a given order and determine which (combinations) of these are invariant for all generators of the group.

Smooth maps As we are concerned not just with polynomial vector fields, it is useful to generalise the results above to smooth maps. We define

$$\mathcal{E}(\Gamma) = \{f : \mathbb{R}^n \to \mathbb{R} \text{ smooth } : f(\gamma x) = f(x) \ \forall \ \gamma \in \Gamma, x \in \mathbb{R}^n\}$$

and $\mathcal{E} \subset \mathcal{P}$ and similarly $\widetilde{\mathcal{E}}$ the set of smooth equivariants. The following results from [11] indicate that the results for polynomials generalise easily to smooth functions (more precisely, for germs of smooth functions - See Appendix A). Let $\mathcal{E}_s$ be the ring of smooth (C^∞) germs of functions $\mathbb{R}^s \to \mathbb{R}$.

Theorem 2 (Theorem 4.3 - Schwarz (1975))**.** *Let Γ be a compact Lie group acting on $\mathbb{R}^n$. Let $\{u_1, ..., u_\ell\}$ be a Hilbert basis for the Γ-invariant polynomials $\mathcal{P}(\Gamma)$ and let $f \in \mathcal{E}(\Gamma)$. Then there exists a smooth germ $h \in \mathcal{E}_s$ such that*

$$f(x) = h(u_1(x), ..., u_\ell(x)).$$

To summarise, it is clear that any function of the form $f(x) = h(u_1(x), ..., u_\ell(x))$ where $u_1 : \mathbb{R}^n \to \mathbb{R}$, $h : \mathbb{R}^\ell \to \mathbb{R}$ is invariant- what the Theorem tells us is that in fact all invariant functions can be written in this way.

The module of smooth equivariants is also finitely generated as stated in the following result:

Theorem 3 (Theorem 5.3 Poenaru (1976))**.** *Let Γ be a compact Lie group and let $g_1, ..., g_r$ generate the module $\widetilde{\mathcal{P}}(\Gamma)$ of Γ-equivariant polynomials over the ring $\mathcal{P}(\Gamma)$. Then $g_1, ..., g_r$ generate the module $\widetilde{\mathcal{E}}(\Gamma)$ over the ring $\mathcal{E}(\Gamma)$.*

2.4 Using invariants for orbit space reduction

One can use invariants to reduce a system to a representation of the orbit space embedded in $\mathbb{R}^\ell$, where s is the dimension of a Hilbert basis for the invariant $\mathcal{P}(\Gamma)$ by simply considering the map

$$\Pi(x) := (u_1(x), ..., u_\ell(x)). \tag{2.2}$$

Suppose that there are k independent polynomial relations between the elements in the Hilbert basis:

$$\{r_1(u_1, \cdots, u_\ell), \cdots, r_k(u_1, \cdots, u_\ell)\}$$

where $r_i = 0$ and the orbit space will be a space of dimension $\ell - k$.

Let us write

$$\mathcal{O} = \Pi(\mathbb{R}^n) \subset \mathbb{R}^\ell$$

to denote the orbit space and assume that the group acts nontrivially. As discussed in Chossat [3], this is a semi-algebraic set and so can be written as a union of manifolds of different dimensions associated with the images of the fixed point subspaces - these manifold are called *strata* of the orbit space.

The *trivial stratum* of $\mathcal{O}$ is the image of the set of points with trivial symmetry. If we write

$$L = \{x \in \mathbb{R}^n \ : \ \Sigma_x = I\}$$

then the trivial stratum can be written

$$\tilde{\mathcal{O}} = \Pi(L).$$

Note that $\tilde{\mathcal{O}}$ is a manifold, and that

$$\mathcal{O} = \mathrm{clos}(\tilde{\mathcal{O}})$$

is the closure of the trivial stratum.

Example: $\mathbf{SO}(2)$ acting on $\mathbb{R}^3$. Take a Hilbert basis for invariants to be $\{\Pi_1, \Pi_2\} = \{x^2 + y^2, z\}$. The (x, y)-plane becomes the Π_2 axis (the non-trivial stratum) and the trivial stratum is all positive Π_2.

This is a simple example of a stratified manifold, more generally there may be relations between the invariants. So later we consider a different basis $(\Pi_1, \Pi_2, \Pi_3) = (x^2+y^2, z, (x^2+y^2)^2)$ which is a Hilbert basis, but not minimal as there is the relation $\Pi_1^2 = \Pi_3$.

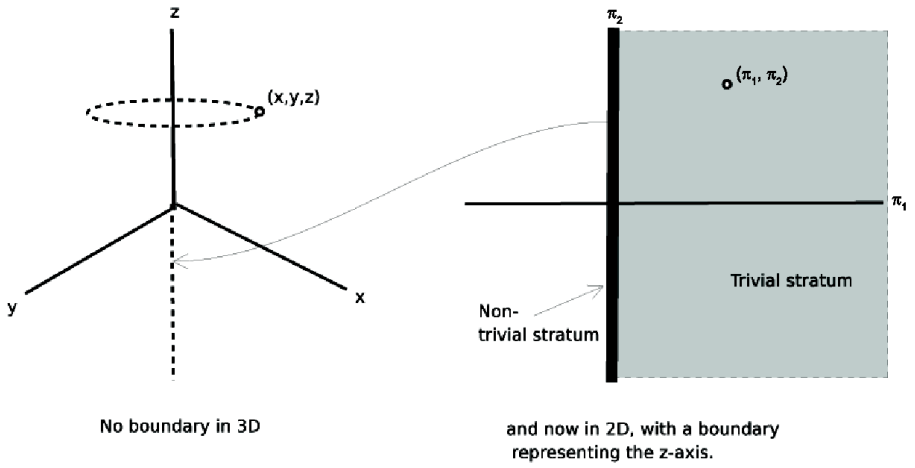

Figure 2.2: $\mathbf{SO}(2)$ acting on $\mathbb{R}^3$. The left image represents the dynamics in the original system with a point (x, y, z) on the periodic orbit. On the right, we have the reduced system with its strata.

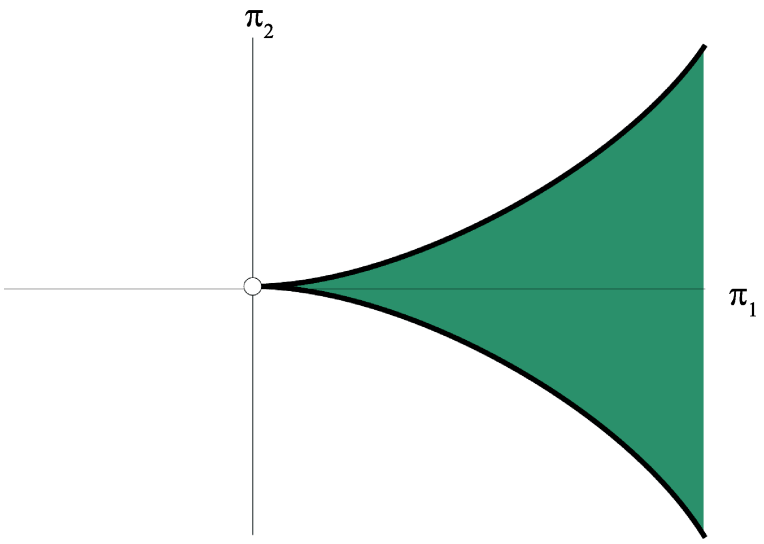

Figure 2.3: $\mathbf{D}_3$ acting on $\mathbb{R}^2$. The image shows the reduced system and its strata: the point $(0, 0)$, the curved boundaries, and the shaded region in between.

Example: $\mathbf{D}_3$ on $\mathbb{R}^2$. Consider

$$\mathbf{D}_3 = \langle \{ z \to e^{2i\pi/3} z, z \to \overline{z} \} \rangle.$$

A Hilbert basis for invariants is given by

$$u = |z|^2, \quad v = z^3 + \overline{z}^3$$

This is an application of the calculation found in [11, p53]. So we can first claim every $\mathbf{D}_3$-equivariant germ $g \in \widetilde{\mathcal{E}}(\mathbf{D}_3)$ has the form

$$g(z) = p(u, v)z + q(u, v)\overline{z}^2.$$

We start with $\mathbf{D}_3$-equivariant polynomial g of the form

$$g(z) = \sum b_{jk} z^j \overline{z}^k$$

with b_{jk} real.

It is worth noting that the Hilbert map is not unique as the Hilbert basis used is itself not unique. The example where $\mathbf{D}_3$ acts on $\mathbb{R}^2$ from [3] shows this. Finding the orders of the generators for either a ring or a module could be the next step. See [3, p169] for information including Molien's Theorem. This would not give the best basis to use, but it would give the size of the smallest basis possible and would give a check to determine whether the basis used is minimal.

Generally the invariance of the group is responsible for the degeneracies in the equations. The number of bifurcating equilibria may not be clear or points on the group orbit may not be equilibria - on a relative equilibria the vector field is tangent

to the group orbit rather than disappearing, which means the dynamics may be periodic.

If the manifold is smooth and finite dimensional, and if the group is compact and acting smoothly on the Manifold then the orbit space can be represented as a stratified manifold in a vector space. For examples of Orbit space reduction in dynamical systems, see [3, p194].

Note that this example, where $\mathbf{D}_3$ acts on $\mathbb{R}^2$ has three strata (see Figure 2.3).

Now note that the dimension of the orbit space of Γ acting on V is defined as the dimension of the principal stratum, i.e. the stratum with the highest dimension.

$$\begin{aligned} \dim(V/\Gamma) &= \dim(V) - \dim(\Gamma x) \\ &= \dim(V) - \dim(\Gamma) + \dim \Sigma_x \end{aligned}$$

If there are relations between elements of the Hilbert basis that are equalities then the dimension is lower than the dimension of the space $\mathbb{R}^\ell$ where the orbit space is realised. If there are inequalities rather than equalities these dimensions may be the same as the following example illustrates.

Example: $\mathbf{SO}(2)$: a Hilbert basis with relation. Consider the example where $\mathbf{SO}(2)$ acts by rotations in the (x, y)-plane for $(x, y, z) \in \mathbb{R}^3$. Let $(\Pi_1, \Pi_2, \Pi_3) = (x^2 + y^2, z, (x^2 + y^2)^2)$ be a Hilbert basis for the invariants, then there is a relation

$$\Pi_3 = \Pi_1^2$$

because by design Π_3 was specified as such. This example is similar to the laser system in the sense that the invariants are not independent, but in this case it is

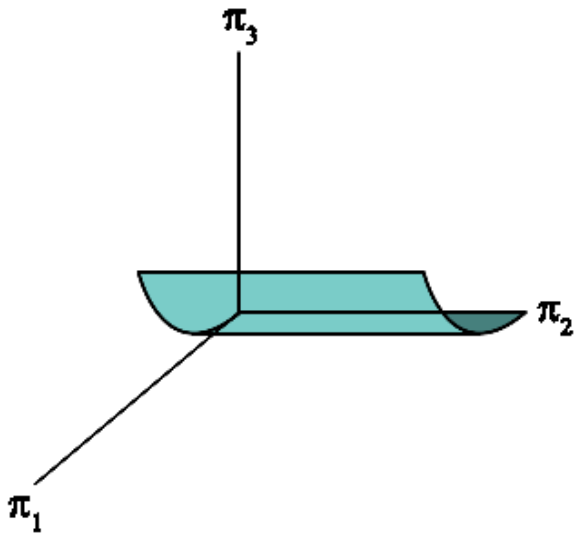

Figure 2.4: **SO**(2): a Hilbert basis with relation: The surface $\Pi_3 = \Pi_1^2$, $\Pi_1 > 0$ is the orbit space for this action of **SO**(2).

not a minimal basis.

Chapter 3

Eigenvalues for orbit space reduced systems

In this chapter I will review the work of Koenig and Chossat [3, 19] which relate to reduction of a system to the orbit space using invariants, in particular relating eigenvalues of linearised systems in these cases. I will discuss how eigenvalues of the reduced system can be related to the eigenvalues of the original system. In this way we can interpret the bifurcations in the reduced system as bifurcations in the original system. Following this I will consider a method for choosing a basis of invariants required for the orbit space reduction. I will give an example showing how different bases of invariants can give different eigenvalues. Finally I will discuss some differences between finding eigenvalues on the trivial and nontrivial strata.

3.1 Review of main results from Koenig and Chossat

In [3] the paper starts with an example which shows how to build the orbit space explicitly and then reduce the dynamics to it. The main results of [3] relate the eigenvalues of the linearised flow to that on the orbit space. The following sections of [3] give a general method for general compact group actions and list some basic properties of the dynamics in the reduced system.

Recall that Γx is the orbit of a point $x \in V = \mathbb{R}^n$ under the action of Γ.

Invariant polynomials and representation of the orbit space Starting with $\mathcal{P}(\Gamma)$ as the ring of Γ-invariant polynomials in $V = \mathbb{R}^n$, recall that invariance means for any $p \in \mathcal{P}(\Gamma)$, $p(g^{-1}x) = p(x)$ for all $(g, x) \in \Gamma \times V$. The Hilbert and Weyl result says that $\mathcal{P}(\Gamma)$ has a Hilbert basis, i.e. there is a family of invariant polynomials $\{\Pi_1, ..., \Pi_l\}$ such that for any $p \in \mathcal{P}(\Gamma)$ a polynomial $\widehat{p}$ of l variables exists such that $p(x) = \widehat{p}(\Pi_1(x), ..., \Pi_l(x))$.

This basis can be chosen to be minimal (have smallest number of elements for any Hilbert basis) and to consist of homogeneous polynomials, but the basis is in general not unique. In addition, its elements may not be algebraically independent but may satisfy a number of relations as previously discussed.

Projecting equivariant vector fields: computation and properties Suppose that

$$\dot{x} = X(x) \tag{3.1}$$

is a given Γ-equivariant vector field. Let $\Pi_1, ..., \Pi_l$ be a Hilbert basis for the ring of Γ-invariant polynomials, where we note that $I_k = \Pi_k(x)$ are invariants. We can express the vector field on the orbit space in terms of the invariants

$$\dot{\Pi}_i(x) = d\Pi_i(x)\dot{x} = d\Pi_i(x)X(x) =: \widehat{X}_i(x)$$

for $i = 1, \cdots, l$, where $d\Pi_i$ denotes the Jacobian of the map Π_i.

Note that $\widehat{X}_i(x)$ is a Γ-invariant smooth function of x and so by Schwarz's theorem it can be expressed as function of the Π_js; there exists a smooth function $\tilde{X}_i : \mathbb{R}^\ell \to \mathbb{R}$ such that

$$\widehat{X}_i(x) = \tilde{X}_i(\Pi_1(x), \cdots, \Pi_l(x))$$

for $i = 1, ..., l$ and all $x \in \mathbb{R}^n$. Let $\tilde{X} = (\tilde{X}_1, ..., \tilde{X}_l)$ - this defines a smooth map to $\mathbb{R}^\ell$ and hence there is a projection of 3.1 onto a smooth vector field

$$\dot{\Pi} = \tilde{X}(\Pi) \tag{3.2}$$

that represents the vector field on the orbit space $\mathcal{O}$ extended to $\mathbb{R}^\ell$.

Unfortunately, although the vector field on the orbit space is uniquely specified, if there are any relations satisfied by the Hilbert basis elements then the orbit space vector field (3.2) is not uniquely defined on $\mathbb{R}^\ell$. For example, suppose that there is a polynomial relation that satisfies $p(\Pi_1, \cdots, \Pi_l) = 0$ on the orbit space; then

$$\dot{\Pi} = \tilde{X}(\Pi) + p(\Pi)\tilde{Z}(\Pi)$$

will give the same dynamics on the orbit space for any non-trivial vector field $\tilde{Z}$ on $\mathbb{R}^\ell$. We will see an example of this in Section 3.3.

A key result is the following theorem which is also in Koenig's work [19]:

Theorem 4. *[3, Theorem 3.7] Let $X(x) = L_s x + L_n x + R(x)$ be a Γ-equivariant vector field in V, where L_s is the semisimple linear part of X. Similarly let $\tilde{X}(\Pi) = \tilde{L}_s\Pi + \tilde{L}_n\Pi + \tilde{R}(\Pi)$ be the projected vector field on the orbit space. Note that $X(0) = 0$ implies $\tilde{X}(0) = 0$. Then there exists a choice of generators $\Pi_1, ..., \Pi_l$ such that:*

(i) $\tilde{L}_s$ is the projection of L_s and is semisimple;

(ii) $\tilde{L}_n\Pi + \tilde{R}(\Pi)$ is the projection of $L_n x + R(x)$;

(iii) The eigenvalues of $\tilde{L}_s$ are linear combinations with positive integer coefficients of the eigenvalues of L_s.

Note that any linear map A can be decomposed into

$$A = A_s + A_n$$

where A_s is *semi-simple* (i.e. it can be diagonalized), A_n is *nilpotent* (i.e. $(A_n)^k = 0$ for some finite k) and $A_s A_n = A_n A_s$ [17] and any eigenvalue of A must be an eigenvalue of A_s

In consequence this raises several questions:

- How are the eigenvalues from the original system combined to form the new eigenvalues for a given choice of invariants and how do we choose these in the best way?

- In the case that there are algebraic constraints, there may be 'fake' eigenvalues corresponding to perturbations in directions transverse to $\mathcal{O}$. Is it possible to control these eigenvalues?

- Do these additional 'fake' eigenvalues produce 'false bifurcations' (see example in Section 3.4) in the reduced system (i.e. bifurcations that do not exist in our original system or model)?

Clearly it will be useful to find a way of either

- Preventing eigenvalues from being combined in such a way as to produce false bifurcations.

- Analysing the regions of parameter space in which these combinations are likely to occur. Once these regions are known we must check results using the original system of equations if that particular region has no restrictions on using it.

Possible methods to minimise the impact of false bifurcations include deliberately choosing a non-minimal Hilbert basis which would confine regions where false bifurcations may take place to a less bothersome region of parameter space.

3.2 Relating eigenvalues of orbit space to eigenvalues of the original system

Suppose that a Γ-equivariant system

$$\dot{x} = f(x)$$

is reduced to the orbit space $\dot{y} = g(y)$ and $x(t) = \Psi_t(x_0)$ in $\mathbb{R}^n$ goes to $y(t) = \Phi_t(y_0)$ in $\mathbb{R}^s$, where $\Psi_t(x_0)$ is the solution of $\dot{x} = f(x)$ with $x(0) = x_0$ and $\Phi_t(y_0)$ is the solution of $\dot{y} = g(y)$ with $y(0) = y_0$. We assume as before that $y = \Pi(x)$ is the orbit space reduction. Then for all $t > 0$,

$$\Pi \circ \Psi_t(x(0)) = \Phi_t \circ \Pi(x(0)) \tag{3.3}$$

In the special case that Π^{-1} exists then

$$x(t) = \Pi^{-1}(\Phi_t(\Pi(x(0)))$$

which implies, writing $d = \frac{\partial}{\partial x_i}$, that

$$\frac{dx}{dt} = d\Pi^{-1}(\Phi_t \circ \Pi(x(0)))\underbrace{\frac{d\Phi_t}{dt}(\Pi(x_0))}_{g(\Pi(x(t))}$$

$$\left.\frac{dx}{dt}\right|_t = f(x) = d\Pi^{-1}(\Pi(x))g(\Pi(x)) \tag{3.4}$$

and so

$$f(x) = d\Pi^{-1}(\Pi(x))g(\Pi(x)).$$

More generally Π^{-1} does not exist for all x, but we will still have

$$d\Pi(x)f(x) = g(\Pi(x)). \tag{3.5}$$

Theorem 5. *Suppose x_0 is a relative equilibrium of $\dot{x} = f(x)$. Then $y_0 = \Pi(x_0)$ is an equilibrium of $\dot{y} = g(y)$.*

Proof. If $\dot{x} = f(x)$ has a relative equilibrium at $x = x_0$ that means that Γx_0 is invariant under Ψ_t. From (3.3) and the fact that $y_0 = \Pi(x)$ is the same for any $x \in \Gamma x_0$, this means that $\Phi_t(y_0) = y_0$ for all t. Hence $g(y) = 0$. □

The fact that $g(\Pi(x))$ is Γ-invariant implies, using (3.5), that

$$g(\Pi(x_0)) = 0 = d\Pi(x_0)f(x_0)$$

and hence

$$f(x_0) \in \ker(d\Pi(x_0))$$

We can differentiate (3.5) again to give

$$d(d\Pi)(x)f(x) + d\Pi(x)df(x) = dg(\Pi(x)d\Pi(x) \tag{3.6}$$

and use this in the next result.

Theorem 6. *Suppose v_0 is an eigenvector of $df(x_0)$ with eigenvalue λ_0 and x_0 is an equilibrium. If $w_0 = d\Pi(x_0)v_0 \neq 0$, then λ_0 is an eigenvalue of $dg(\Pi(x_0))$ with eigenvector w_0.*

Proof. Suppose $\dot{x} = f(x)$ has an equilibrium at $x = x_0$ and so $f(x_0) = 0$. Then from 3.6

$$d\Pi(x_0)df(x_0) = dg(\Pi(x_0))d\Pi(x_0) \tag{3.7}$$

Suppose $df(x_0)$ has eigenvector v_0 and eigenvalue λ_0 which means that $df(x_0)v_0 = \lambda_0 v_0$. So (3.2) becomes

$$d\Pi(x_0)\lambda_0 v_0 = dg(\Pi(x_0))d\Pi(x_0)v_0$$

$$\lambda_0 \underbrace{d\Pi(x_0)v_0}_{w_0} = dg(\Pi(x_0)) \underbrace{d\Pi(x_0)v_0}_{w_0}$$

However, note that it is possible that w_0 is zero even if v_0 is non-zero - in which case this equation tells us nothing about eigenvalues of dg. If however

$$d\Pi(x_0)v_0 = w_0 \neq 0$$

then we can show that w_0 is an eigenvector of $dg(\Pi(x_0))$ with eigenvalue λ_0. This is because

$$d(d\Pi)(x_0)f(x_0)v_0 + d\Pi(x_0)df(x_0)v_0 = dg(\Pi(x_0))d\Pi(x_0)v_0$$

$$\Rightarrow \underbrace{d(d\Pi)(x_0)f(x_0)v_0}_{\text{zero as } f(x_0)=0} + \lambda_0 \underbrace{(d\Pi(x_0)v_0)}_{w_0} = dg(\Pi(x_0)) \underbrace{d\Pi(x_0)v_0}_{w_0}$$

$$\lambda_0 w_0 = dg(\Pi(x_0))w_0.$$

□

Note however that (a) some eigenvectors v_0 may be in $ker(d\Pi(x_0))$ and (b) other eigenvalues w_0 may not be in the image of $d\Pi(x_0)$. These are the eigenvalues that change under orbit space reduction. This result is proved in the case where x_0 is

an equilibrium, but it may be possible to extend to the case where x_0 is a relative equilibrium.

3.3 Example of how different invariants can give different eigenvalues

Consider $\mathbf{Z}_2$ acting by $x \mapsto -x$ and the $\mathbf{Z}_2$-symmetric ODE

$$\dot{x} = f(x)$$

for $x \in \mathbb{R}$. The symmetry here simply implies that $f(x)$ is an odd function. For this symmetry, the invariants are generated by $S = \{I = x^2\}$ meaning a representation of the orbit space is

$$\Pi_1(x) = x^2$$

where one can see that

$$\mathcal{O} = \{y \ : \ y \geq 0\}.$$

To show that the eigenvalues of the orbit space system may be augmented by additional 'fake' eigenvalues, we consider

$$\dot{x} = xf(x^2)$$

with $x \to -x$ (with additional invariants). If we choose the invariants $\Pi_1 = x^2$ and $\Pi_2 = x^4$ as the basis, then there is a relation $\Pi_1^2 = \Pi_2$ and the trivial stratum corresponds to

$$\{(\Pi_1, \Pi_2) : \Pi_1 > 0 \text{ and } \Pi_2 = \Pi_1^2\}$$

. The system of equations can be written in many ways. clearly one way is

$$\dot{\Pi}_1 = 2x^2 f(x^2) = 2\Pi_1 f(\Pi_1)$$

$$\dot{\Pi}_2 = 4x^4 f(x^2) = 4\Pi_2 f(\Pi_1)$$

Suppose then we look at a specific example where $f(x^2) = 1 - x^2$. Then for any α we can write the equations as

$$\dot{\Pi}_1 = 2\Pi_1 - \Pi_1^2$$

$$\dot{\Pi}_2 = 4\Pi_2 - 4\Pi_1\Pi_2 + \alpha(\Pi_1^2 - \Pi_2)$$

Hence, the Jacobian is

$$J = \begin{pmatrix} 2 - 2\Pi_1 & 0 \\ -4\Pi_2 + 2\alpha\Pi_1 & 4 - 4\Pi_1 - \alpha \end{pmatrix} \tag{3.8}$$

and for example, when $\Pi_1 = 1, \Pi_2 = 1$ this becomes

$$J = \begin{pmatrix} 0 & 0 \\ -4 + 2\alpha & -\alpha \end{pmatrix}$$

which has an arbitrary eigenvalue $-\alpha$ that clearly depends on the choice of equation in the orbit space.

3.4 Eigenvalues on nontrivial strata

The following example shows a 'fake' eigenvalue can appear in the dynamics on the orbit space.

Consider the linear vector field X defined by the system

$$\begin{aligned} \dot{x} &= ax + by \\ \dot{y} &= cy. \end{aligned}$$

It is equivariant by the action of Z_2 defined by $(x, y) \mapsto (-x, -y)$. We have seen that the orbit space can be defined as the image of the map

$$(x, y) \mapsto (\Pi_1 = x^2, \Pi_2 = y^2, \Pi_3 = xy)$$

A straightforward calculation shows that the projected $\tilde{X}$ yields the system in $\mathbb{R}^3$

$$\dot{\Pi}_1 = 2a\Pi_1 + 2b\Pi_3$$

$$\dot{\Pi}_2 = 2c\Pi_2$$

$$\dot{\Pi}_3 = b\Pi_2 + (a + c)\Pi_3.$$

If $a = -c \neq 0$, 0 is a hyperbolic equilibrium of X, while $\tilde{X}$ has a zero eigenvalue at the origin in $\mathbb{R}^3$. This extra eigenvalue is a 'fake' eigenvalue for the dynamics on the orbit space. In general, these extra 'fake' eigenvalues may pass through zero at a false bifurcation - in this case the eigenvalue is forced to remain zero.

Chapter 4

Orbit space reduction for $\mathbf{SO}(2)$ symmetry

In this chapter I will give an example of how invariants may be used to reduce a system with symmetry to the orbit space. In doing so the symmetries in the system are removed making numerical analysis possible. I will then show in a practical application of the ideas in Chapter 3 how the eigenvalues of the Jacobian of the reduced system can be related back to the original system in order to complete a bifurcation analysis.

In this example I consider $\mathbf{SO}(2)$ acting on $(x, y)^T \in \mathbb{R}^2$ in the normal way, by

$$\begin{pmatrix} x \\ y \end{pmatrix} \rightarrow \begin{pmatrix} \cos(\theta) & -\sin(\theta) \\ \sin(\theta) & \cos(\theta) \end{pmatrix} \begin{pmatrix} x \\ y \end{pmatrix}$$

For convenience from here on we write the invariants as generators of $I_1, \cdots, I_u$.

The invariants are generated by $I = r^2 = x^2 + y^2$. The general equivariant vector

field in coordinates $z = x + iy$, according to [11] is $\dot{z} = (f(|z|^2) + ig(|z|^2))z$

$$\begin{pmatrix} \dot{x} \\ \\ \dot{y} \end{pmatrix} = f(I) \begin{pmatrix} x \\ \\ y \end{pmatrix} + g(I) \begin{pmatrix} y \\ \\ -x \end{pmatrix}$$
$$= \begin{pmatrix} f(r^2) & g(r^2) \\ \\ -g(r^2) & f(r^2) \end{pmatrix} \begin{pmatrix} x \\ \\ y \end{pmatrix}$$

Which can be written as a reduced system in the orbit space as an equation for the invariant:

$$I = x^2 + y^2 = r^2$$

$$\begin{aligned} \dot{I} &= 2x\dot{x} + 2y\dot{y} \\ &= 2xf(I)x + 2yf(I)y \\ &= 2If(I) \end{aligned} \tag{4.1}$$

For a relative equilibrium $\dot{I} = 0$ meaning from (4.2) $I = 0$ or $f(I) = 0$. These correspond to the 2 strata; $I = 0$ corresponds to points with isotropy $\mathbf{SO}(2)$, $I > 0$ corresponds to points with trivial isotropy. We now discuss how the Jacobian J_I for the reduced system can be related to the Jacobian J_x for the original system. The first Jacobian is

$$J_I = 2f(I) + 2If'(I) \tag{4.2}$$

Note that in the original coordinates the Jacobian at $(0, 0)$ is

$$J_x = \begin{pmatrix} f(0) & g(0) \\ \\ -g(0) & f(0) \end{pmatrix}$$

with eigenvalues $f(0) \pm ig(0)$. Away from $(0,0)$ the relative equilibrium is not an equilibrium unless we go into a rotating frame. We do this by finding a $\sigma \in \mathbb{R}$ such that the relative equilibrium (x_0, y_0) satisfies

$$\begin{pmatrix} \dot{x_0} \\ \dot{y_0} \end{pmatrix} = \begin{pmatrix} 0 & \sigma \\ -\sigma & 0 \end{pmatrix} \begin{pmatrix} x_0 \\ y_0 \end{pmatrix}$$

This implies that

$$\begin{pmatrix} f(I_0) & g(I_0) - \sigma \\ -g(I_0) + \sigma & f(I_0) \end{pmatrix} \begin{pmatrix} x_0 \\ y_0 \end{pmatrix} = 0$$

We now choose $\sigma = g(I_0)$ and note $f(I_0) = 0$ on the equilibrium. In the rotating frame:

$$\begin{aligned} \dot{x} &= xf(I) + y(g(I) - g(I_0)) \\ \dot{y} &= -x(g(I) - g(I_0)) + yf(I) \end{aligned}$$

So

$$J_x = \begin{pmatrix} f(r^2) + 2x^2 f'(r^2) + 2xyg'(r^2) & g(r^2) - g(r_0^2) + 2xyf'(r^2) + 2y^2 g'(r^2) \\ -(g(r^2) - g(r_0^2)) - 2x^2 g'(r^2) + 2xyf'(r^2) & -2xyg'(r^2) + 2y^2 f'(r^2) + f(r^2) \end{pmatrix} \tag{4.3}$$

We evaluate this on the equilibrium: $r = r_0$, $x = x_0$, etc. Now choose a typical point on the relative equilibrium such that $y_0 = 0$:

$$J_x = \begin{pmatrix} f(r_0^2) & 0 \\ 0 & f(r_0^2) \end{pmatrix} + 2x_0^2 \begin{pmatrix} f'(r_0^2) & 0 \\ -g'(r_0^2) & 0 \end{pmatrix} \tag{4.4}$$

We now compare the eigenvalues of the two Jacobians for the original system of equations in the rotating frame, (4.4), and the reduced system, (4.2). Considering

(4.2) we have two cases for a relative equilibrium; Either $I_0 = 0$ in which case

$$J_I = 2f(0)$$

$$J_x = \begin{pmatrix} f(0) & 0 \\ 0 & f(0) \end{pmatrix}$$

where the eigenvalues in the reduced system are double the eigenvalues from the original system.

Or, alternatively, $f(I_0) = 0$ in which case

$$J_I = 2I_0 f'(I_0)$$

$$J_x = 2I_0 \begin{pmatrix} f'(I_0) & 0 \\ -g'(I_0) & 0 \end{pmatrix}$$

where the eigenvalues remain the same; one eigenvalue is 0 because of the rotating frame.

4.1 Reduction of equations for $\mathbf{SO}(2)$ acting on $\mathbb{R}^2$

We now consider more non-trivial actions of $\mathbf{SO}(2)$ that will be relevant for our laser system; although the computations here are not complete they indicate some of the complexity of the problem. let us consider $\mathbf{SO}(2)$ acting on $\mathbb{C}^2$ by

$$(E_1, E_2) \to (e^{i\phi}E_1, e^{i\phi}E_2). \tag{4.5}$$

For convenience we will sometimes write $E_1 = x_1 + iy_1$ $E_2 = x_2 + iy_2$ in the section below. A Hilbert basis for the invariants $\mathcal{P}(\mathbf{SO}(2))$ is given by

$$\begin{aligned} I_1 &= |E_1|^2 = x_1^2 + y_1^2 \\ I_2 &= |E_2|^2 = x_2^2 + y_2^2 \\ I_3 &= Re(E_1 E_2^*) = x_1 x_2 + y_1 y_2 \\ I_4 &= Im(E_1 E_2^*) = y_1 x_2 - x_1 y_2 \end{aligned} \tag{4.6}$$

while a basis for the Equivariants is given by

$$U_1 = \begin{pmatrix} x_1 \\ y_1 \\ 0 \\ 0 \end{pmatrix}, \; U_2 = \begin{pmatrix} 0 \\ 0 \\ x_2 \\ y_2 \end{pmatrix}, \; U_3 = \begin{pmatrix} y_1 \\ -x_1 \\ 0 \\ 0 \end{pmatrix}, \; U_4 = \begin{pmatrix} 0 \\ 0 \\ y_2 \\ -x_2 \end{pmatrix}. \tag{4.7}$$

$$U_5 = \begin{pmatrix} x_2 \\ y_2 \\ 0 \\ 0 \end{pmatrix}, \; U_6 = \begin{pmatrix} 0 \\ 0 \\ x_1 \\ y_1 \end{pmatrix}, \; U_7 = \begin{pmatrix} y_2 \\ -x_2 \\ 0 \\ 0 \end{pmatrix}, \; U_8 = \begin{pmatrix} 0 \\ 0 \\ y_1 \\ -x_1 \end{pmatrix}. \tag{4.8}$$

Note that by Poenaru's theorem there must be smooth functions f_k of the invariants such that

$$\begin{pmatrix} \dot{x}_1 \\ \dot{y}_1 \\ \dot{x}_2 \\ \dot{y}_2 \end{pmatrix} = \sum_{k=1}^{8} f_k(I_1, I_2, I_3, I_4) U_k. \tag{4.9}$$

We derive the equivalent to the general equation (4.9) in the orbit space given

by

$$\Pi(E_1, E_2) = (I_1, I_2, I_3, I_4).$$

with the relation $I_1 I_2 = I_3^2 + I_4^2$.

Writing the equation in component form we have

$$\dot{x}_1 = x_1 f_1 + y_1 f_3 + x_2 f_5 + y_2 f_7 \tag{4.10}$$

$$\dot{y}_1 = y_1 f_1 - x_1 f_3 + y_2 f_5 - x_2 f_7 \tag{4.11}$$

$$\dot{x}_2 = x_2 f_2 + y_2 f_4 + x_1 f_6 + y_1 f_8 \tag{4.12}$$

$$\dot{y}_2 = y_2 f_2 - x_2 f_4 + y_1 f_6 - x_1 f_8 \tag{4.13}$$

and so

$$\dot{I}_1 = 2x_1\dot{x}_1 + 2y_1\dot{y}_1 \tag{4.14}$$

$$= 2(x_1^2 + y_1^2) f_1 + 2(x_1 x_2 + y_1 y_2) f_5 + 2(x_1 y_2 - x_2 y_1) f_7 \tag{4.15}$$

and so

$$\dot{I}_1 = 2f_1 I_1 + 2f_5 I_3 - 2f_7 I_4 \tag{4.16}$$

similarly,

$$\dot{I}_2 = 2f_2 I_2 + 2f_6 I_3 + 2f_8 I_4 \tag{4.17}$$

$$\begin{aligned}
\dot{I}_3 &= x_1\dot{x}_2 + x_2\dot{x}_1 + y_1\dot{y}_2 + y_2\dot{y}_1 \\
&= (x_1 x_2 + y_1 y_2) f_1 + (x_1 x_2 + y_1 y_2) f_2 + (x_2 y_1 - x_1 y_2) f_3 \\
&\quad + (x_1 y_2 - x_2 y_1) f_4 + (x_2^2 + y_2^2) f_5 + (x_1^2 + y_1^2) f_6
\end{aligned}$$

so we have

$$\dot{I}_3 = f_1 I_3 + f_2 I_3 + f_3 I_4 - f_4 I_4 + f_5 I_2 + f_6 I_1 \tag{4.18}$$

and finally

$$\begin{aligned}
\dot{I}_4 &= y_1\dot{x}_2 + x_2\dot{y}_1 - x_1\dot{y}_2 - y_2\dot{x}_1 \\
&= (-x_1y_2 + x_2y_1)f_1 + (x_2y_1 - x_1y_2)f_2 + (-y_1y_2 - x_1x_2)f_3 \\
&\quad +(y_1y_2 + x_1x_2)f_4 + (-y_2^2 - x_2^2)f_7 + (y_1^2 + x_1^2)f_8
\end{aligned}$$

and so

$$\dot{I}_4 = f_1 I_4 + f_2 I_4 - f_3 I_3 + f_4 I_3 - f_7 I_2 + f_8 I_1 \tag{4.19}$$

Our set of equations for the reduced system is therefore:

$$\begin{aligned}
\dot{I}_1 &= 2f_1 I_1 + 2f_5 I_3 - 2f_7 I_4 \\
\dot{I}_2 &= 2f_2 I_2 + 2f_6 I_3 + 2f_8 I_4 \\
\dot{I}_3 &= f_1 I_3 + f_2 I_3 + f_3 I_4 - f_4 I_4 + f_5 I_2 + f_6 I_1 \\
\dot{I}_4 &= f_1 I_4 + f_2 I_4 - f_3 I_3 + f_4 I_3 - f_7 I_2 + f_8 I_1
\end{aligned} \tag{4.20}$$

For a relative equilibrium to occur the left hand sides of (4.20) need to be zero. There are two cases corresponding to the two strata of the orbit space:

- $I_1 = I_2 = I_3 = I_4 = 0$
- $f_3 = f_4$ with all other functions of invariants equal to zero.

In order to describe how the original system (4.13) is related to the reduced system (4.20) we need to compare the eigenvalues of their Jacobians. J_I is the

Jacobian matrix for system (4.20), J_x is the Jacobian matrix for system (4.13). J_H is the matrix containing all partial derivatives of the functions of invariants.

First consider J_I:

$$J_I = \begin{pmatrix} 2f_1 & 0 & 2f_5 & -2f_7 \\ 0 & 2f_2 & 2f_6 & 2f_8 \\ f_6 & f_5 & f_1+f_2 & f_3-f_4 \\ f_8 & -f_7 & f_4-f_3 & f_1+f_2 \end{pmatrix} + J_H \tag{4.21}$$

Where J_H are the additional terms that involve gradients of the f_i.

For relative equilibrium $I_1 = I_2 = I_3 = I_4 = 0$ we also have the Jacobian for equations 4.13

$$J_x = \begin{pmatrix} f_1 & f_3 & f_5 & f_7 \\ -f_3 & f_1 & -f_7 & f_5 \\ f_6 & f_8 & f_2 & f_4 \\ -f_8 & f_6 & -f_4 & f_2 \end{pmatrix} \tag{4.22}$$

Now we need to compare the eigenvalues of J_I and J_x for each of the two cases of equilibrium, in order to find the relationship between the functions of invariants and the eigenvalues of the original system.

For the first case J_x remains the same and J_I becomes:

$$J_I = \begin{pmatrix} 2f_1 & 0 & 2f_5 & -2f_7 \\ 0 & 2f_2 & 2f_6 & 2f_8 \\ f_6 & f_5 & f_1+f_2 & f_3-f_4 \\ f_8 & -f_7 & f_4-f_3 & f_1+f_2 \end{pmatrix} \tag{4.23}$$

For the second case $J_I = J_H$ and J_x becomes

$$J_x = \begin{pmatrix} 0 & f_3 & 0 & 0 \\ -f_3 & 0 & 0 & 0 \\ 0 & 0 & 0 & f_3 \\ 0 & 0 & -f_3 & 0 \end{pmatrix} \tag{4.24}$$

We have not been able to find explicitly results that relate the eigenvalues of these Jacobians in general.

Chapter 5

Modelling an external-cavity laser

In this chapter I will introduce an example of a laser system where there is strong optical feedback. As I will show, the system of equations governing the laser's operation respects certain symmetries. As a result, an orbit space reduction that draws on the previous chapters of this thesis is required in order to carry out bifurcation analysis and determine the laser's stable and unstable operating regions. I will focus on codimension-one bifurcations of equilibria and periodic orbits, and will also look in more detail at certain codimension-two bifurcations.

5.1 Introduction

Although lasers have been studied for half a century, it is only recently that coupled systems of lasers have been considered in real-life applications for their diverse dynamics and sometimes chaotic behaviour [27, 12, 15, 8, 10]. This unstable behaviour may be of benefit in certain new applications such as secure communications but

generally it is to be avoided because it reduces predictability of the system's dynamics. Semiconductor lasers, in particular, are very sensitive to external influences and a lot of work has been done to understand their stability properties. For example, semiconductor laser systems with optical injection can demonstrate highly non-linear behaviour as shown in [42] via an understanding of their non-linear dynamics.

Research on modelling and analysing these systems varies and different types of models may restrict what methods you can then use to analyse bifurcations. Simpler models may be less rigorous, but are easier to analyse. These models assume that the spatio-temporal electric field can be seperated into space and time dependent parts giving equations for the modal amplitudes from the wave equation and the profile of the modes from the Helmholtz equation. In earlier models the modes in each resonator are considered seperately and some forcing is added to the electric field equation to represent the effect of the external resonators. Non-linear behaviour in coupled lasers are considered by Wieczorek and Chow in [39, 40] where they use the composite cavity mode approach to analyse their systems. This gives equations for the electric field associated with the composite structure rather than each individual laser.

In this paper we use a composite-cavity-mode approach to modelling nonlinear behaviour of a laser coupled to a passive optical resonator. We vary the transmissivity T of the mirror separating the laser from the passive resonator (and other parameters) to examine how the lasing behaviour changes with the coupling between the cavities. For the remainder of this section we derive the dynamical equations

(5.21) that determine the behaviour of the modes, and give an idea of their dynamical complexity. Subsequent sections perform a bifurcation analysis of the system with the assistance of the path-following programme AUTO.

5.1.1 Composite cavity mode model

An optical fibre incorporating a grating attached to the laser may substantially affect the stability of the laser. Considering the simplest case of a grating as a mirror that reflects most light back into the laser, we have strong optical feedback. The setup we consider in this paper is shown schematically in Figure 5.1.

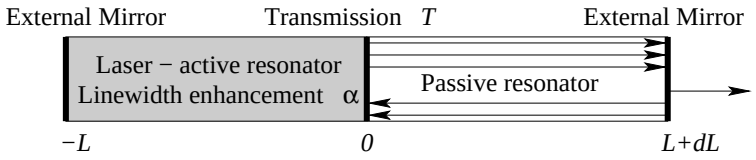

Figure 5.1: A laser strongly coupled to an external cavity: the shaded region is an active lasing material, the right is a passive resonant cavity. The two regions are strongly coupled by a partial mirror with transmissivity T.

The real valued electric field within such a coupled-laser system, $\mathcal{E}(z,t)$, is described by the electromagnetic wave equation

$$\frac{\partial^2}{\partial z^2}\mathcal{E}(z,t) - \frac{n^2(z)}{c^2}\frac{\partial^2}{\partial t^2}\mathcal{E}(z,t) - \mu_0\sigma(z)\frac{\partial}{\partial t}\mathcal{E}(z,t) = \mu_0\frac{\partial^2}{\partial t^2}\mathcal{P}(z,t), \qquad (5.1)$$

where we assumed plane wave conditions as in [39] and z is along the field propagation direction. The left-hand side of this partial differential equation describes electric field propagation and losses within the coupled-laser structure whose physi-

cal structure is specified by the space-dependent refractive index $n(z)$ and boundary conditions. Here, μ_0 is the permeability of vacuum, ϵ_0 is the permittivity of vacuum, $c = 1/\sqrt{\mu_0\epsilon_0}$ is the speed of light, and the conductivity of the material, $\sigma(z)$, represents losses. The inhomogeneous term on the right-hand side involves the active-medium polarisation, $\mathcal{P}(z,t)$, and represents the source of the propagating electric field. To calculate polarisation and population inversion within each laser, Eqn. (5.1) has to be combined with a suitable quantum-mechanical description of the active medium. The resulting PDE model is known as the Maxwell-Bloch equations.

In semiclassical laser theory [29], the inhomogeneous wave equation (5.1) is solved by expanding the electric field

$$\mathcal{E}(z,t) = \frac{1}{2}\sum_j u_j(z)a_j(t) + \bar{u}_j(z)\bar{a}_j(t) \ , \tag{5.2}$$

and the active-medium polarisation

$$\mathcal{P}(z,t) = \frac{1}{2}\sum_j u_j(z)b_j(t) + \bar{u}_j(z)\bar{b}_j(t) \ , \tag{5.3}$$

where the bar denotes complex conjugation. The *passive composite-cavity modes*, $u_j(z)$, are the solutions to the homogeneous wave equation and the time-dependent, complex-valued coefficients of the field expansion, $a_j(t)$, are the corresponding electric field amplitudes. We will first calculate the composite-cavity modes and then briefly sketch the derivation of ordinary differential equations for the slowly-varying part of the complex-valued coefficients, $a_j(t)$.

Assuming a passive cavity ($\mathcal{P}(z) = 0$) without losses ($\sigma(z) = 0$) we get the

homogeneous wave equation

$$\frac{\partial^2}{\partial z^2}\,\mathcal{E}(z,t) = \mu_0\,\epsilon_0\,\epsilon_b(z)\,\frac{\partial^2}{\partial t^2}\mathcal{E}(z,t). \tag{5.4}$$

where $\epsilon_b(z)$ is the dielectric constant, which is the square of the refractive index. Following Spencer and Lamb [32], we define for the coupled-cavity structure in Fig. 5.1 the refractive index squared as:

$$n^2(z) = \Theta(-L_A, 0)(z)\,n_A^2 + \Theta(0, L_B)(z)\,n_B^2 + \frac{\eta}{k}\,\delta(z), \tag{5.5}$$

where the rectangular function

$$\begin{aligned} \Theta(x_1, x_2)(z) &= 1 \text{ for } x_1 < z < x_2, \\ \Theta(x_1, x_2)(z) &= 0 \text{ for } x_1 > z > x_2, \end{aligned} \tag{5.6}$$

$\delta(z)$ is the Dirac delta function, and $k = \Omega/c$ is the wave vector in vacuum. The coupling mirror at $z = 0$ with transmission coefficient T is modeled as a dielectric "bump" with a coupling coefficient η given by

$$\eta = (n_A + n_B)\sqrt{\frac{1-T}{T}}. \tag{5.7}$$

The electric field with complex amplitude $\mathcal{E}_0$ and associated with a passive composite-cavity eigenmode, $u(z)$,

$$\mathcal{E}(z,t) = \mathcal{E}_0\,u(z)\,\exp(-i\Omega t) + \bar{\mathcal{E}}_0\,\bar{u}(z)\,\exp(i\Omega t), \tag{5.8}$$

is substituted into Eq. (5.4) to yield:

$$\frac{d^2}{dz^2}\,u(z) = -\mu_0\,\epsilon_0\,\epsilon_b(z)\,\Omega^2\,u(z). \tag{5.9}$$

As shown in Refs. [32, 5], each eigenfunction satisfies the boundary conditions

$$\frac{d}{dz}\,u(0^+) - \frac{d}{dz}\,u(0^-) = -k\,\eta\,u(0), \tag{5.10}$$

$$u(0^+) = u(0^-), \tag{5.11}$$

$$u(-L_A) = u(L_B) = 0. \tag{5.12}$$

where 0^+ and 0^- denote positions infinitesimally before and after the coupling mirror, and $z = -L_A, L_B$ are the end mirror positions. The n^{th} mode solution of equation (5.9) satisfying the boundary conditions (5.10)–(5.12) can be written as a piecewise function

$$\begin{aligned} u_n(z) &= A_n \sin\left[k_n n_A (z + L_A)\right] \quad \text{for} \quad -L_A \le z \le 0 \\ u_n(z) &= B_n \sin\left[k_n n_B (z - L_B)\right] \quad \text{for} \quad 0 \le z \le L_B. \end{aligned} \tag{5.13}$$

The eigenmodes obey the orthogonality relation

$$\int_{-L_A}^{L^B} dz\, n^2(z)\, u_n(z)\, u_m(z) = \mathcal{N}\,\delta_{nm} \tag{5.14}$$

with the normalization constant

$$\mathcal{N} = n^2 L,$$

where $n = n_A$ and $L = L_A$ and this is assumed throughout. From the orthogonality relation we get

$$\begin{aligned} A_n^2\, n_A^2\, L_A \left(\frac{1}{2} - \frac{\sin(2k_n n_A L_A)}{4k_n n_A L_A}\right)\sqrt{T} + B_n^2\, n_B^2\, L_B \left(\frac{1}{2} - \frac{\sin(2k_n n_B L_B)}{4k_n n_B L_B}\right)\sqrt{T} + \\ A_n^2\,\frac{(n_A + n_B)}{k_n}\,\sin^2(k_n n_A L_A)\sqrt{1-T} = \mathcal{N}\sqrt{T} \end{aligned} \tag{5.15}$$

which needs to be solved simultaneously with the boundary conditions (5.10) and (5.11):

$$\sqrt{T}\,[B_n\,n_B\,\cos(k_n n_B L_B) - A_n\,n_A\,\cos(k_n n_A L_A)] = \tag{5.16}$$
$$-\sqrt{1-T}\,A_n\,(n_A + n_B)\,\sin(k_n n_A L_A),$$

and

$$A_n\,\sin(k_n n_A L_A) = -B_n\,\sin(k_n n_B L_B), \tag{5.17}$$

to obtain the frequencies, $\Omega_n = k_n c$, and amplitudes, A_n and B_n, of the composite-cavity modes. We introduce the relative optical-length difference

$$\frac{dL^\star}{\lambda} = n\frac{L_B - L_A}{\lambda}, \tag{5.18}$$

where $\lambda = 1\mu m$ is approximately the wavelength of the free-running (no external cavity) laser. It turns out that the coupled-cavity system in Fig. 5.1 can be modelled with just two composite-cavity modes, namely $u_1(z)$ and $u_2(z)$.

In calculating the complex-valued coefficients, $a_j(t)$, it is common to separate in $a_j(t)$ a term oscillating at a fast optical frequency, ν:

$$a_j(t) = E_j(t)\,e^{-i\nu t}, \tag{5.19}$$

and study the slowly-varying, complex-valued field amplitude $E_j(t)$. Inserting the modal expansion (5.2) into (5.1), using (5.19), calculating polarisation $\mathcal{P}(z,t)$ using quantum mechanics, neglecting small terms in line with the semiclassical laser theory [29], and adiabatically eliminating polarisation (class-B lasers) [39] leads to a

set of ordinary differential equations for the complex-valued amplitudes, $E_1(t)$ and $E_2(t)$, associated with the two composite-cavity modes considered [40]:

$$\begin{aligned}\dot{E}_1 &= -\gamma C_{11}E_1 - i\Omega_1 E_1 \\ &\quad +C_{11}\gamma\left[C_{11}^A(F - i\alpha\beta N)E_1 + C_{21}^A(F - i\alpha G)E_2\right] \\ \dot{E}_2 &= -\gamma C_{22}E_2 - i\Omega_2 E_2 \\ &\quad +C_{22}\gamma\left[C_{22}^A(F - i\alpha\beta N)E_2 + C_{21}^A(F - i\alpha G)E_1\right]\end{aligned} \tag{5.20}$$

with

$$F = (1 + \beta N) \quad \text{and} \quad G = \beta(1 + N).$$

Here, the fixed normalised parameters γ and β can be expressed in terms of real laser parameters

$$\gamma = \frac{\gamma_E}{2\gamma_N}, \quad \beta = 1 + \frac{2c\Gamma\xi N_{ts}}{n\gamma_E}$$

given in Table 5.1. The parameter α is called the linewidth enhancement factor and quantifies the magnitude of coupling between the amplitude and phase of the complex-valued field $E_j(t)$. Equations (5.21) depend implicitly on the bifurcation parameters T and $dL^\star$ through the normalised composite-mode frequencies Ω_1 and Ω_2, and the modal integrals [39]

$$C_{nm} = \frac{1}{L}\int_{-L_A}^{L_B} dz\, u_n(z)\, u_m(z) = C_{nm}^A + C_{nm}^B, \tag{5.21}$$

where

$$C_{nm}^A = \frac{1}{2L}A_n A_m \left(\frac{\sin[(k_n - k_m)n_A L_A]}{(k_n - k_m)n_A} - \frac{\sin[(k_n + k_m)n_A L_A]}{(k_n + k_m)n_A}\right), \tag{5.22}$$

$$C^B_{nm} = \frac{1}{2L} B_n B_m \left(\frac{\sin[(k_n - k_m)n_B L_B]}{(k_n - k_m)n_B} - \frac{\sin[(k_n + k_m)n_B L_B]}{(k_n + k_m)n_B} \right). \tag{5.23}$$

Note that C^A_{nm} are not constants, they depend on the modes which themselves depend on dL^* and T. Therefore the transcendental equation (5.16) needs to be re-calculated at each point for each of the two modes as AUTO varies the parameters.

Finally, we give the equation for the real-valued population inversion inside the laser, N, derived in Ref. [40]:

$$\dot{N} = \Lambda - (1 + N) - F \sum_{k,n=1}^{2} C^A_{kn} E_k E^*_n, \tag{5.24}$$

where Λ is the normalised pump rate.

Computations using the original system (5.21) and (5.24) were done by transforming the system to a rotating frame. We change coordinates to

$$\begin{aligned} X &= |E_1| \\ Y + iZ &= E_2 e^{-i \arg(E_1)} \end{aligned} \tag{5.25}$$

Then equation (5.21) and (5.24) become

$$\begin{aligned}
\dot{X} &= -\gamma C_{11} X + \gamma C_{11}[C^A_{11}(1 + \beta N)X + C^A_{12}((1 + \beta N)Y + \alpha\beta(1 + N)Z)] \qquad (5.26)\\
\dot{Y} &= -\gamma C_{22} Y - (\omega_1 - \omega_2)Z + \gamma C_{22} C^A_{22}((1 + \beta N)Y + \alpha\beta N Z) \\
&\quad + \gamma C_{22} C^A_{12}(1 + \beta N)X - \gamma C_{11}[C^A_{11}\alpha\beta N + C^A_{12}(\alpha\beta(1 + N)Y - (1 + \beta N)Z)/X]Z \\
\dot{Z} &= -\gamma C_{22} Z - (\omega_2 - \omega_1)Y + \gamma C_{22} C^A_{22}((1 + \beta N)Z - \alpha\beta N Y) \\
&\quad - \gamma C_{22} C^A_{12}\alpha\beta(1 + N)X + \gamma C_{11}[C^A_{11}\alpha\beta N + Z(\alpha\beta(1 + N)Y - (1 + \beta N)Z)/X]Y \\
\dot{N} &= \Lambda - (1 + N) - (1 + \beta N)[C^A_{11} X^2 + 2C^A_{12} XY + C^A_{22}(Y^2 + Z^2)]
\end{aligned}$$

Note that this system has one fewer dimension (it is independent of the $\arg(E_1)$), but it has the disadvantage - it has a singularity at $E_1 = 0$ (Note the terms $1/X$ in (5.26)). In the next section we will use symmetries more explicitly to perform a reduction that is valid even when $E_1 = 0$. Figure 5.2 displays some numerically approximated bifurcation diagrams using equations (5.26) as detailed in Appendix D.

5.2 Symmetries in the system

The system of equations, (5.21) describing the evolution of the laser is problematic if we try and follow branches of solutions. This is due to the presence of the S^1-symmetry: the equations are equivariant under

$$(E_1, E_2, N) \to (e^{i\phi}E_1, e^{i\phi}E_2, N)$$

for any $\phi \in [0, 2\pi)$. This means that nontrivial equilibria are no longer generic; the simplest nontrivial solutions are periodic orbits. It introduces an additional "drift" frequency to all solutions and will make quasiperiodic behaviour typical and allows the change of coordinates (5.25). To remove this problem we will consider transformations that "reduce" the symmetry; the problem then becomes one that certain symmetry reductions may have singularities; for instance if we reduce the electric field so that E_1 is real and positive by choosing and appropriate ϕ, this will have a degeneracy when $E_1 = 0$.

To overcome this, we consider a coordinate change to a set of group invariant

coordinates:

$$I_1 = |E_1|^2, \qquad I_2 = |E_2|^2, \qquad I_3 = \mathrm{Re}(E_1 E_2^*), \qquad I_4 = \mathrm{Im}(E_1 E_2^*), \qquad I_5 = N$$

for which (5.21) and (5.24) can be written as

$$\begin{aligned}
\dot{I}_1 = \; & -2C_{11}\gamma I_1 + 2C_{11}\gamma\{C_{11}^A F I_1 + C_{21}^A[F I_3 - \alpha G I_4]\}, \\
\dot{I}_2 = \; & -2C_{22}\gamma I_2 + 2C_{22}\gamma\{C_{22}^A F I_2 + C_{21}^A[F I_3 + \alpha G I_4]\}, \\
\dot{I}_3 = \; & -(C_{11}+C_{22})\gamma I_3 - \Omega_{21} I_4 + C_{11}\gamma C_{11}^A (F I_3 + \alpha G I_4) \\
& + C_{22}\gamma C_{22}^A (F I_3 - \alpha\beta N I_4) + C_{21}^A \gamma F (C_{11} I_2 + C_{22} I_1), \\
\dot{I}_4 = \; & -(C_{11}+C_{22})\gamma I_4 + \Omega_{21} I_3 + C_{11}\gamma C_{11}^A (F I_4 - \alpha\beta N I_3) \\
& + C_{22}\gamma C_{22}^A (F I_4 + \alpha\beta N I_3) + C_{21}^A \alpha G (C_{22}\gamma I_1 - C_{11}\gamma I_2), \\
\dot{I}_5 = \; & \Lambda - (I_5 + 1) - F(C_{11}^A I_1 + C_{22}^A I_2 + 2C_{21}^A I_3),
\end{aligned} \tag{5.27}$$

where we introduce the frequency detuning

$$\Omega_{21} = \Omega_2 - \Omega_1.$$

5.3 Relating the dynamics in each system of equations

Here we consider how the dynamics in the symmetry reduced system (5.27), in the rotating frame (5.26), and in the original system (5.21) and (5.24) are related. An equilibrium in the reduced system corresponds to a degenerate equilibrium in the rotating frame which in the original system is a relative equilibrium, or periodic orbit. Periodic orbits in the reduced system are also periodic orbits in the rotating

frame (though these are degenerate) and are relative periodic orbits that are tori in the original system. Further details can be found in [3, p17] and bifurcations of relative equilibria are discussed in [22].

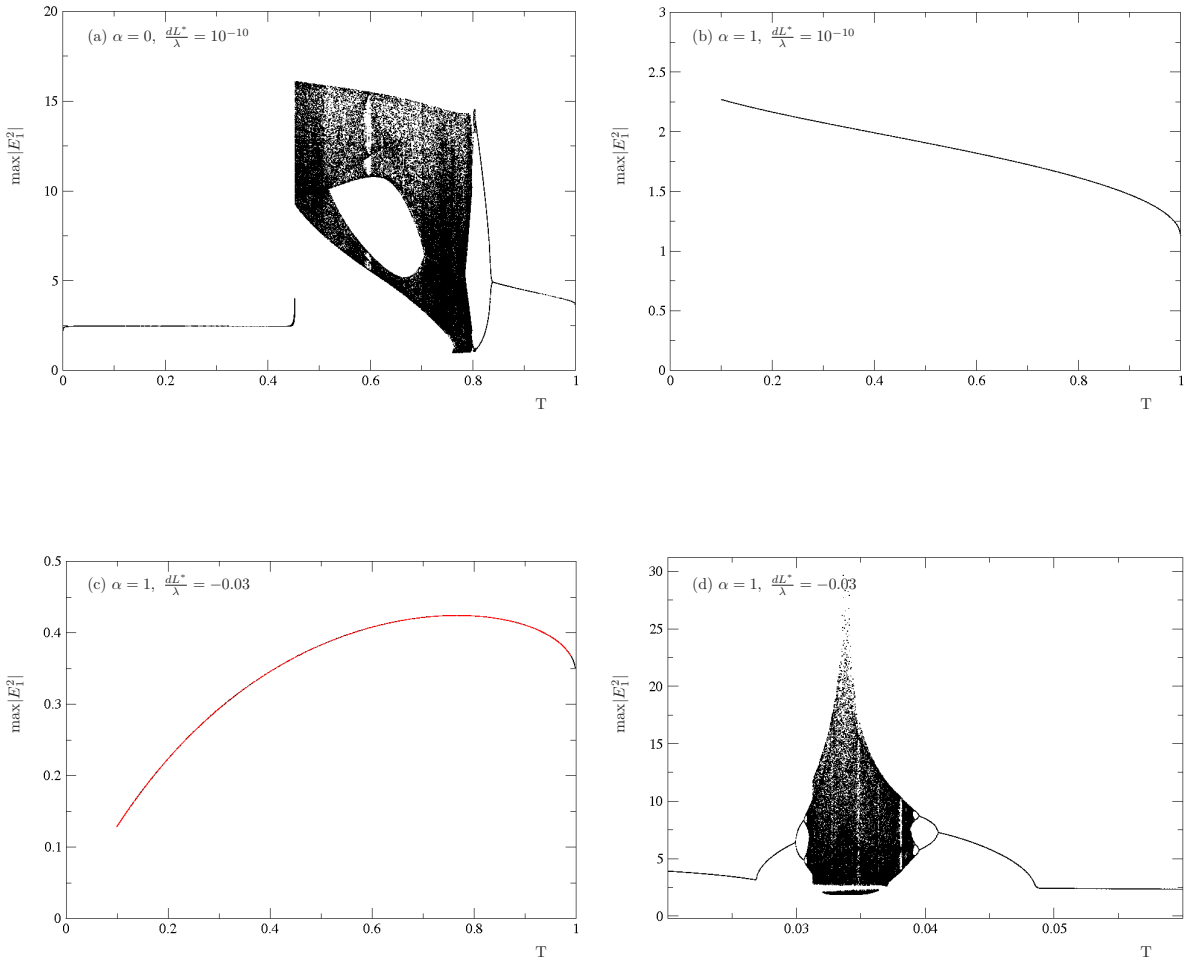

Figure 5.2: We scan T between 0 (uncoupled cavities) and 1 (fully coupled) and plot the values of maxima of the electric fields of one of the modes $|E_1|^2$ on a timeseries. Of the panels (a) and (b) show $dL^*/\lambda = 10^{-10}$ and $\alpha = 0$ and 1 respectively and (c) and (d) for $dL^*/\lambda = -0.03$ and $\alpha = 0$ and 1 respectively again. Observe subcritical and supercritical bifurcations, and transitions from equilibria (steady lasing) to periodic and chaotic behaviour. Observe also that the details (and indeed the presence of any instabilities) depend strongly on the values of dL^* and α.

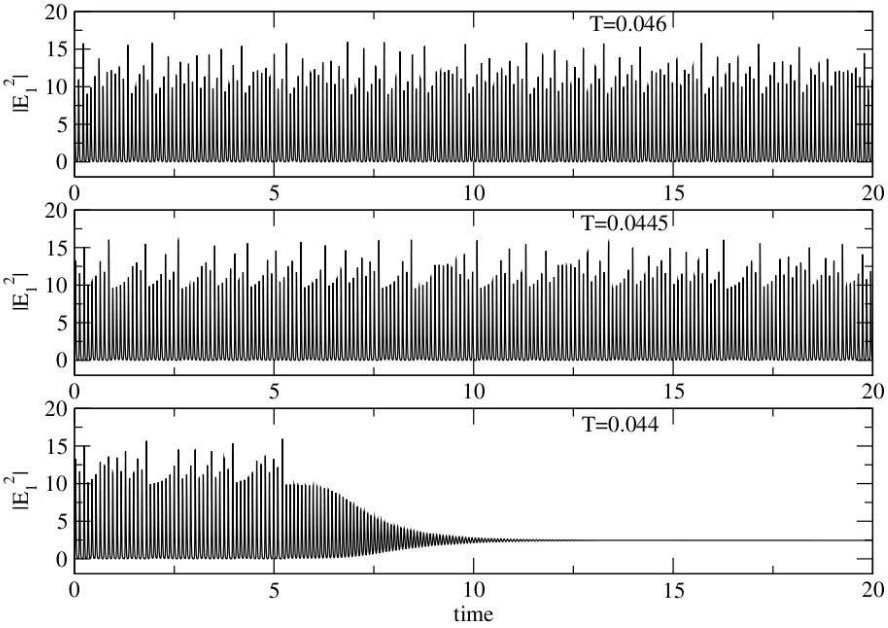

Figure 5.3: The dynamics plotted of $|E_1^2|$ for the parameters as in Figure 5.2(a) and decreasing values of $T = 0.46$, $T = 0.445$ and $T = 0.44$. Observe the chaotic sequence of peaks for the top two panels is replaced with a transient in the last. The middle panel is bistable with the continuation of the equilibrium shown in the lower panel. Note the presence of intermittent bursts away from a saddle periodic orbit. In the lower panel we infer the existence of a boundary crisis where the stable manifold of this saddle periodic orbit acts as a basin boundary. This saddle periodic orbit can be matched to the periodic oscillations before decay.

γ_E	4×10^{11}	s^{-1}	Photon decay rate
γ_N	2×10^{9}	s^{-1}	Population decay rate
γ_M	0	s^{-1}	Mirror losses
n_A	3.4		Refractive index in the laser cavity for $N = N_{th}$
n_B	3.4		Refractive index in the passive resonator
N_{ts}	2×10^{24}	m^{-3}	Population density at transparency
Γ	0.1		Confinement factor
ξ	5×10^{-20}	m^2	Differential gain coefficient
c	3×10^{8}	ms^{-1}	Speed of light
L	280×10^{-6}	m	Length of laser
Λ	6		Normalised pump rate
T	varies		Transmissivity factor
dL^*	varies		Optical-length difference
α	varies		Linewidth enhancement factor

Table 5.1: Parameters and their typical values used in simulations.

Chapter 6

Numerical bifurcation analysis of the laser model

We use the path following package AUTO to investigate the stability of solutions of (5.21) with (5.24) and in particular to better understand the transitions observed in Figure 5.2. Note that even apparently simple bifurcations (on varying T and dL^*) cannot be computed by hand because the parameters in the equations are only determined once one has solved the transendental equation (5.16). For further information on these and other bifurcations we recommend Kuznetzov [23]. In this chapter we discus the path-following results for the codimension one bifurcations after which, in chapter 7, we discuss some of the codimension two bifurcations in this system. The results are summarised in Figures 6.5 and 6.6.

Initially the system of equations in the rotating frame (5.26) are used in AUTO rather than the reduced system of equations (see Appendix B). AUTO is also used

to solve the trancendental equation and calculate the modal integrals at each point in parameter space, though initial starting values for these need to be calculated in Mathematica [26].

Problems arise due to the symmetries in this system; AUTO is unable to successfully continue path-following bifurcations of periodic orbits whenever X is zero. The system of equations for the rotating frame are used to produce diagrams of bifurcations of stationary points only. These indicate the existence of Bogdanov-Takens and Saddle-node Hopf points (which should have associated bifurcations of periodic orbits). These diagrams also prove useful in verifying the validity of these bifurcations of stationary points in the reduced system later.

The existence of Bogdanov-Takens and Saddle-node Hopf points indicates the existence of further bifurcations of periodic orbits and for example homoclinic orbits. The use of the reduced system of equations (5.27) will allow a more complete bifurcation diagram to be produced (see Appendix C). Unfortunately this could mean that any new bifurcations detected are potentially false bifurcations. Careful checking is needed of the eigenvalues in the output files from AUTO to compare with the eigenvalues from the original system at the same point in parameter space whenever a new bifurcation is detected. If the original eigenvalues are combined in such a way as to produce zero eigenvalues in the reduced system then the bifurcation is false. Results can then be verified using DsTool [2] (see Appendix E) which will plot the dynamics of the system for given points in parameter space and can be used to build a clearer picture of the dynamics in each region around bifurcations.

6.1 Steady Bifurcations

A variety of types of bifurcations appear on varying the parameters T, dL^* for fixed α; these include Hopf bifurcations and folds (codimension one), Bodganov Takens, Bautin and Saddle Node Hopf (codimension two).

The value of α reflects the material and design properties of a laser and quantifies how the refractive index changes with the population inversion at a given frequency. α would typically lie between 1 and 10 for semiconductor lasers [42], which is why the high sensitivity on α in this system is of interest. More recently semiconductor lasers with $\alpha = 0$ have been designed, as in [30] and [31].

For $\alpha = 0$ corresponding to Figure 5.2(a), Figure 6.1 shows that there are two Hopf curves shown in in red, a fold in blue and two Bogdanov Takens points where one of the hopf curves terminates on opposite sides of the fold.

For $\alpha = 0.1$, Figure 6.2 shows already a significant change in the diagram for only a small increase in α. The curves Hopf and Saddle-node curves move downwards while the upper BT point slides along the fold towards the upper cusp point. This suggests that the bifurcation details are sensitive to changes in α.

For $\alpha = 1$, Figure 6.3 shows that the upper loop on the subcritical hopf has disappeared as the BT point rounds the cusp. As the fold approaches the larger hopf structure a SNH point develops and divides leaving a section of supercritical fold between the points. This explains why figure(5.2b,d) are so different from Figure 5.2(a,c). At $\alpha = 2$, Figure 6.4 shows that the upper SNH point rounds the neighbouring cusp of the fold.

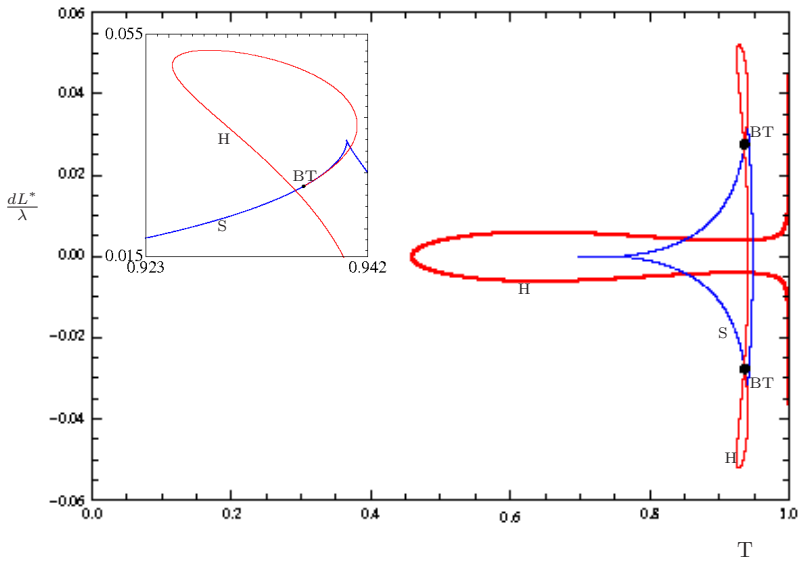

Figure 6.1: Bifurcation diagram for $\alpha = 0$: steady solutions. Axes are T, and dL^*/λ. In passing through one of the bifurcation lines in parameter space the dynamics in phase space will bifurcate. In this diagram we show just the bifurcations of steady solutions. Sub and supercritical Hopf bifurcations, H, are shown in thin and thick red lines respectively. Saddle-node bifurcations, S, are shown in blue. Inset is a zoom showing in more detail how the sub-critical Hopf bifurcation meets the saddle node at a Bogdanov Takens, BT, point. Near a Bogdanov Takens point we expect to see a homoclinic bifurcation.

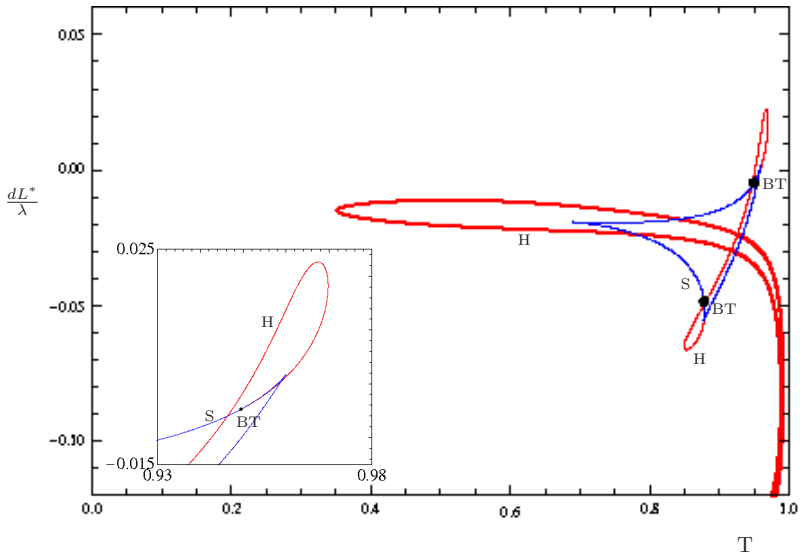

Figure 6.2: Bifurcation diagram for $\alpha = 0.1$: steady solutions. In contrast to Figure 6.1 the structure is dragged down for larger T, but the bifurcation diagram is otherwise very similar. Note that the BT point in this region is approaching the cusp of the fold.

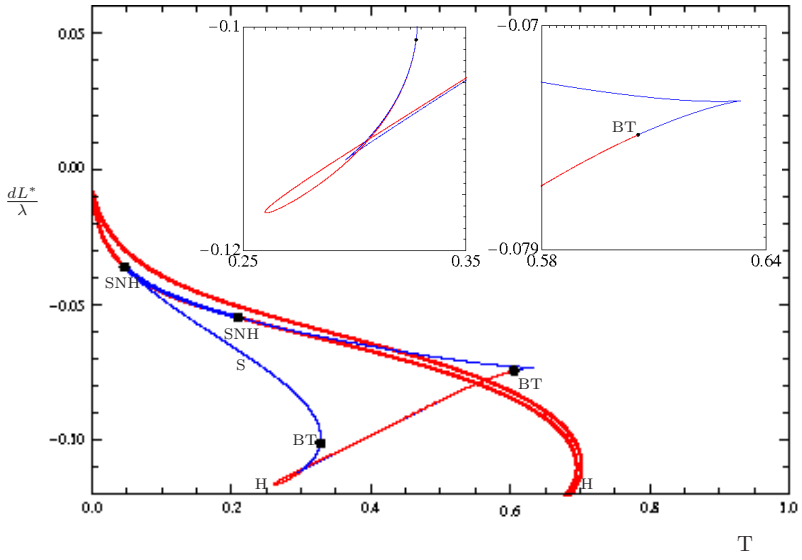

Figure 6.3: Bifurcation diagram for $\alpha = 1$: steady solutions. The upper BT point has passed through the cusp of the fold compared with Figures 6.1 and 6.2, and the upper loop of the Hopf bifurcation has disappeared. We also see that the Saddle-node and super-critical Hopf bifurcations meet at Saddle-node Hopf points, SNH. The S and H curves first meet at approximately $\alpha = 0.45$.

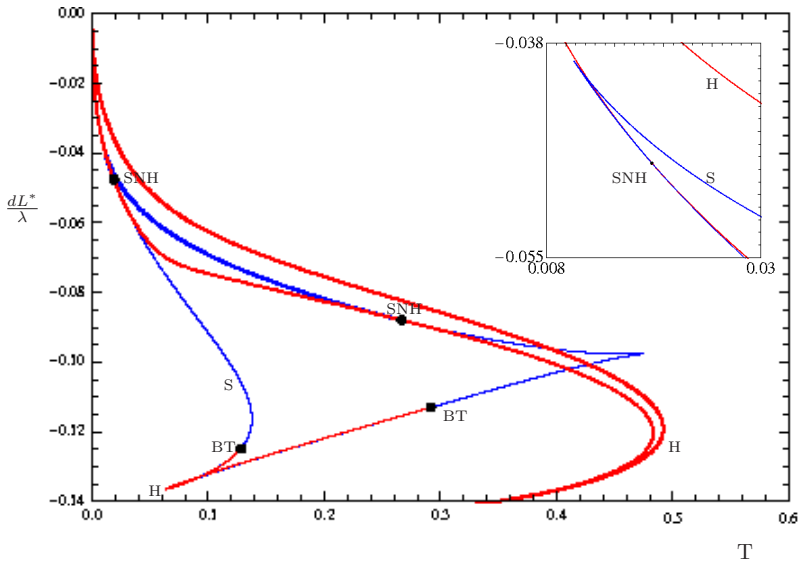

Figure 6.4: Bifurcation diagram for $\alpha = 2$: steady solutions. Compared to Figure 6.3, the features are accentuated and the left most SNH point has passed through the upper cusp of the fold bifurcation.

6.2 Periodic Orbits

In addition to the steady bifurcations discussed, a range of bifurcations of periodic orbits should observed in the system and these are found by removing the symmetries in the system of equations. The existence of Saddle-node Hopf and Bogdanov-Takens points as well as the dynamics displayed earlier in Figure (5.2a) for $\alpha = 0$ and Figure (5.2d) for $\alpha = 1$ indicates that there should also be many bifurcations of periodic orbits. In particular, at codimension one we will see Saddle-nodes of a limit cycle (SL), period doubling (PD), torus (T) and homoclinic bifurcations (h) in addition to Hopf bifurcations (H).

We now revisit the bifurcation diagrams computed already to add in the bifurcations of periodic orbits. Figure 6.5 shows a more complete bifurcation diagram for $\alpha = 0$ on including the periodic solution bifurcations. Figure 6.6 illustrates how this changes for $\alpha = 1$; observe the presence of Saddle-node Homoclinic, Torus and Period doubling bifurcations in what is becoming a very complicated bifurcation structure.

In region 1 on Figure 6.5 there is a simple stable steady solution, at 2 there are two additional steady solutions, at 3 there is in addition a periodic orbit, while at 4 there is one steady solution and one periodic orbit. Remember that steady solutions in the reduced system correspond to a relative equilibrium in the rotating frame and a periodic orbit in the original system. Periodic orbits in the reduced system correspond to a relative periodic orbit in the rotating frame and a torus in the original system. Codimension-2 points will be discussed in Chapter 7.

6.3 Conclusions

In this chapter a composite cavity model was used to analyse the behaviour of a single-mode semiconductor laser coupled to an external cavity with strong optical feedback. Although only two electromagnetic modes are used, they need to be re-calculated at each point in parameter space. Initial diagrams showing bifurcations of stationary solutions show a high sensitivity to changes in the linewidth enhancement factor, and a range of bifurcations and transitions were found by a mixture of two parameter path following and simulation. We discuss in particular a novel non-central Saddle-node Homoclinic bifurcation.

The bifurcation analysis in two parameters throws up several bifurcations that are not generic for one parameter but are for two. In particular we discuss the appearence of Bodganov Takens, Bautin and cusp singularities. A novel feature we have seen in this analysis is a degenerate Saddle-node Hopf interaction at codimension two that has not been previously documented. We focus on this in Chapter 7.

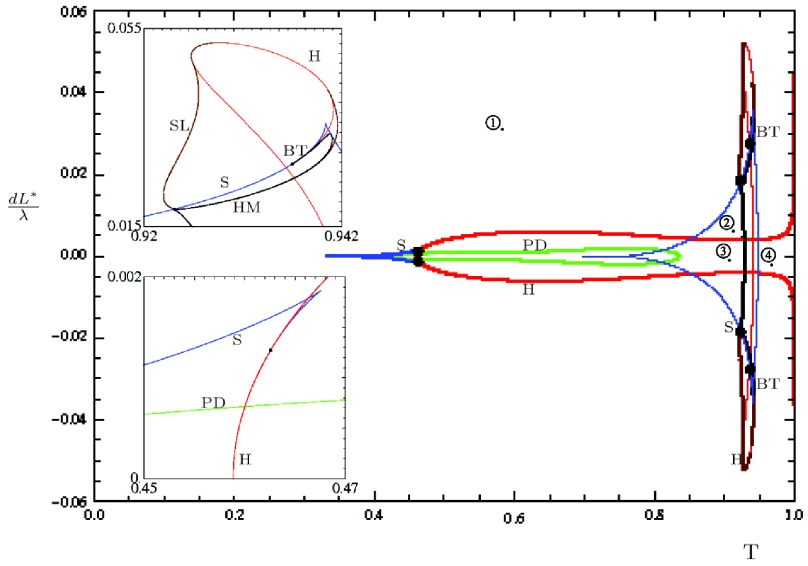

Figure 6.5: Bifurcation diagram for the reduced equations at $\alpha = 0$: steady and periodic solutions. Hopf, H, and Saddle-node, S, lines are as in Figure 6.1. Also shown is period doubling, PD, and homoclinic bifurcation, h, drawn in black which joins the two BT points, and also saddle node of limit cycles drawn in brown. Note that the (mostly) sub-critical Hopf bifurcation becomes super-critical in the regions between the Bautin points, B, where the SL's meet the H curve. Note all meet at a codimension 2 interaction, Z. Typical dynamics at point 1-4 are described in the text.

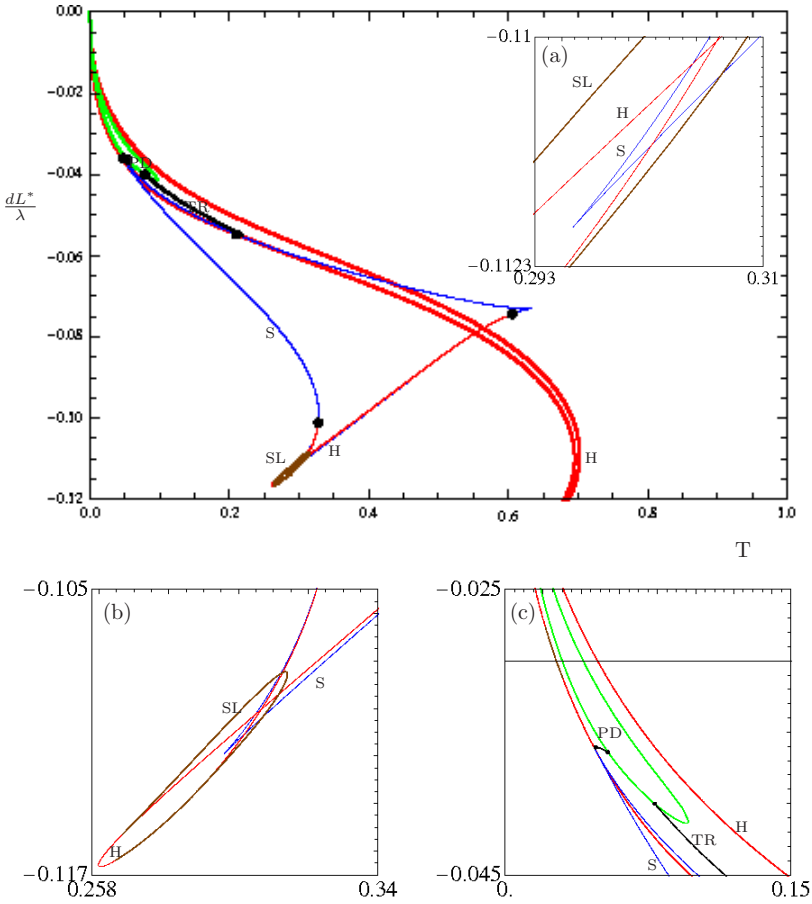

Figure 6.6: Bifurcation diagram for $\alpha = 1$: steady and periodic solutions. Homoclinic bifurcations, h, joining with the two saddle node Hopf points can be seen in black. Note the presence of torus bifurcations (T) from SH to PD at a codimension two interaction. Note the presence of torus bifurcations, T, from SH to PD lines at a codimension two interaction.

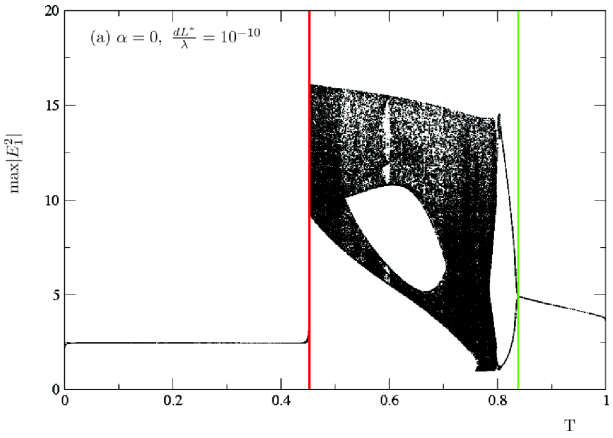

Figure 6.7: Here we have a repeat of Figure 5.2(a) which shows the maximum value of I_1 for varying T for $\alpha = 0$ and fixed dL^*. Note that the vertical lines indicate bifurcation points matching exactly to bifurcations shown in Figure 6.5.

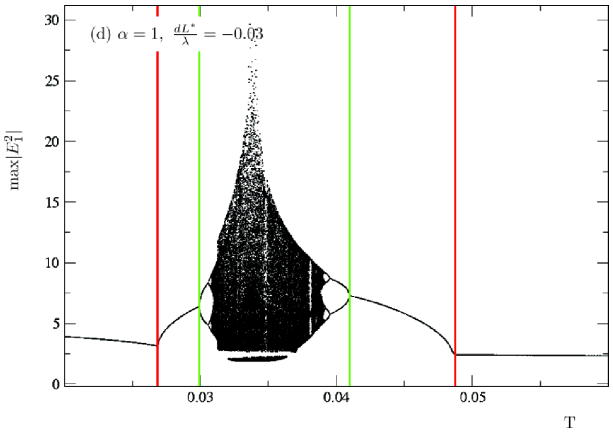

Figure 6.8: Here we have a repeat of Figure 5.2(d) which shows the maximum value of I_1 for varying T for $\alpha = 1$ and fixed dL^*. Note that the vertical lines indicate bifurcation points matching exactly to bifurcations shown in Figure 6.6 and indicated by the horizontal line in panel (c).

Chapter 7

Codimension 2 bifurcations in the laser problem

There are several codimension-2 bifurcations which arise when analysing the laser problem on varying T, dL^* and α, as seen in Figures 6.1 to 6.6. For all values of α there are two Bogdanov-Takens points, and as α increases a pair of saddle node Hopf bifurcation points are born, initially starting out as a single point where a saddle node and Hopf curve become tangent in parameter space. In addition to this there are two Bautin points, seen in the second inset in Figure 6.5, and a point which for now is labelled Z in the first inset in Figure 6.5 which will be explored in more depth during this chapter.

The Bogdanov-Takens and Saddle-node Hopf points are observable in the original system, before it is reduced to the orbit space. However, it is not possible to continue bifurcations of periodic orbits involved in these points due to the symmetry in the

original system. In the reduced system it is possible to fully continue bifurcations of periodic orbits and determine the nature of these codimension-2 points.

7.1 Bogdanov-Takens

These points are also known as a double-zero bifurcation as at this point in parameter space an equilibrium has linearization with with two zero eigenvalues. There are two types of Bogdanov-Takens points (as there are two types of Hopf curves), depending on whether the periodic orbit involved in the interaction is stable or unstable.

In this bifurcation a Hopf curve terminates on a Saddle-node, producing a homoclinic orbit. The derivation of the normal form can be found in [23, p316], and gives the result in [23, p322, Theorem 8.4] summarised by

$$\dot{y}_1 = y_2 \tag{7.1}$$

$$\dot{y}_2 = \beta_1 + \beta_2 y_1 + y_1^2 + s y_1 y_2 \tag{7.2}$$

where $s = \pm 1$ and $O(||y||^3)$ terms are discarded.

The dynamics of the system exactly on the Bogdanov-Takens point are the same, regardless of s as shown in Figure 7.1, but the value of s determines the dynamics surrounding the point. An illustration of these dynamics for $s = -1$ can be found on p324 of [23], however for the laser system we have the case where $s = +1$ which can be seen in Figure 7.2.

The nature of the Bogdanov-Takens point may be determined by observation of the eigenvalues of the system in the AUTO output files to determine the nature

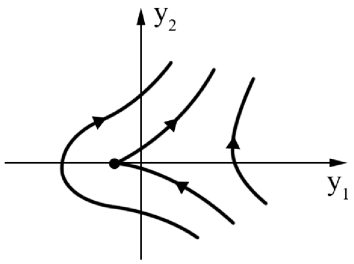

Figure 7.1: The dynamics of a system at a Bogdanov-Takens point. $\beta_1 = \beta_2 = 0$ in (7.2)

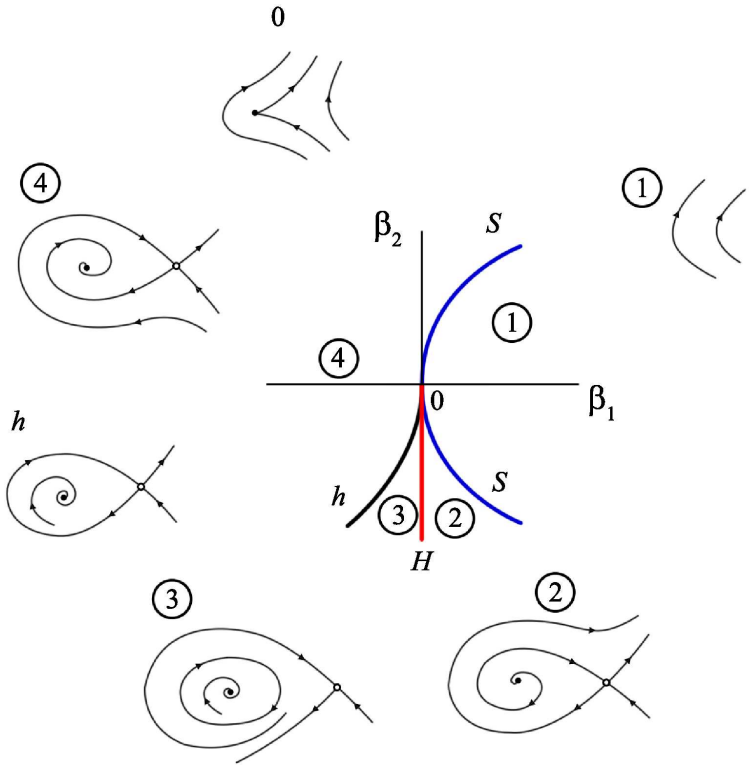

Figure 7.2: Unfolding of the Bogdanov-Takens bifurcation 7.2 with $s = +1$.

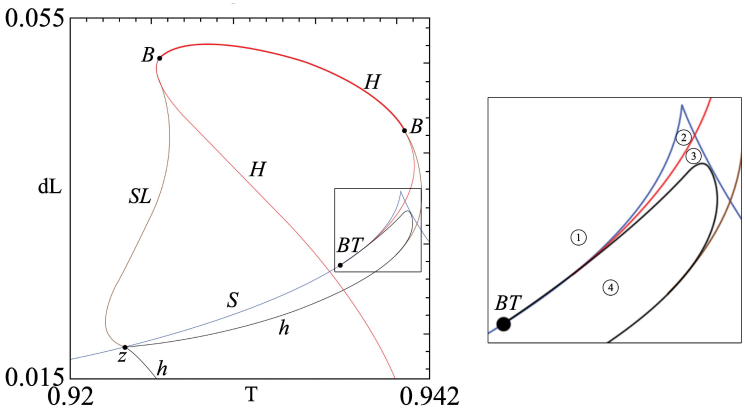

Figure 7.3: Bogdanov-Takens bifurcation with $s = +1$ in the two parameter space T and dL^*/λ for the laser system $\alpha = 0$. This is a detail of Figure (6.5)

of the Hopf bifurcation involved. A supercritical Hopf bifurcation would indicate $s = -1$, and a subcritical Hopf would indicate $s = +1$ for the Bogdanov-Takens point. Alternatively the use of a program such as DsTool to plot the dynamics would allow observation of the dynamics in the four surrounding regions. This method, though slower to determine the type of point in this case, will prove useful later in the chapter. Figure 7.3 shows the regions on the bifurcation diagram which correspond to each of the regions in Figure 7.2.

The interaction between the Hopf curve and the Bogdanov-Takens and Bautin points can be seen in Figure 7.4. More detail is shown to also indicate the nature of the Hopf curve as well as the change from sub to supercritical Hopf at the Bautin points which will now be discussed.

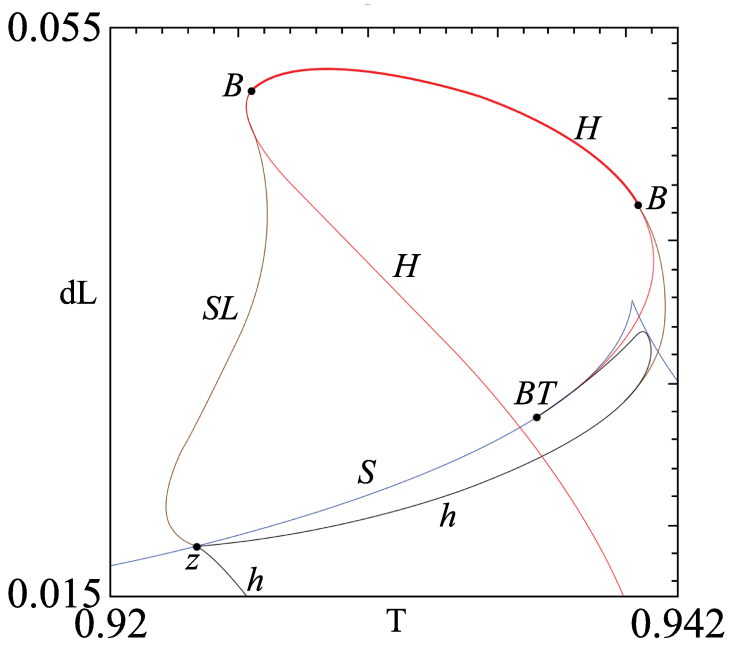

Figure 7.4: A region of the lasers parameter space, for Figure(6.5) with $\alpha = 0$, showing three types of codimension-2 points; Bogdanov-Takens (BT), Bautin (B), and a non-central Saddle-node Homoclinic point with additional non-centrality (Z). Also indicated here is the nature of the Hopf curve; the supercritical region is shown in bold red, while the subcritical part of the curve is in fine red.

7.2 Bautin Bifurcation points

These codimension-2 points are also known as generalised Hopf bifurcations and, as indicated in Figure 7.4, seperate subcritical and supercritical branches of a Hopf bifurcation curve. These points are indicated by a pair of purely imaginary eigenvalues and zero value for the first Lyapunov coefficient [23, p309] and the normal form in polar coordinates is

$$\dot{r} = r(\beta_1 + \beta_2 r^2 + sr^4 \tag{7.3}$$

$$\dot{\psi} = 1 \tag{7.4}$$

At this point in parameter space a Saddle-node of limit cycles terminates on a Hopf curve, seperating sub from supercritical. This would imply that in a surrounding region of the Bautin point there is a pair of limit cycles with differing stability which either anihilate one another in a saddle node of limit cycles bifurcation, or one merges with a stationary point in a Hopf bifurcation.

Similarly to the Bogdanov-Takens point there are two types of Bautin point. The case for $s = -1$ is illustrated in Kuznetsov [23, p314] in which case the two limit cycles lie between the Saddle-node of limit cycles (SL) and the subcritical part of the Hopf curve, with a stable stationary point between the SL curve and the supercritial Hopf curve. The $s = +1$ case is shown in Figure 7.5 in which case the pair of periodic orbits involved in the bifurcation lie between the SL curve and the supercritical part of the Hopf curve, with an unstable stationary point between the SL and the subcritical Hopf curve.

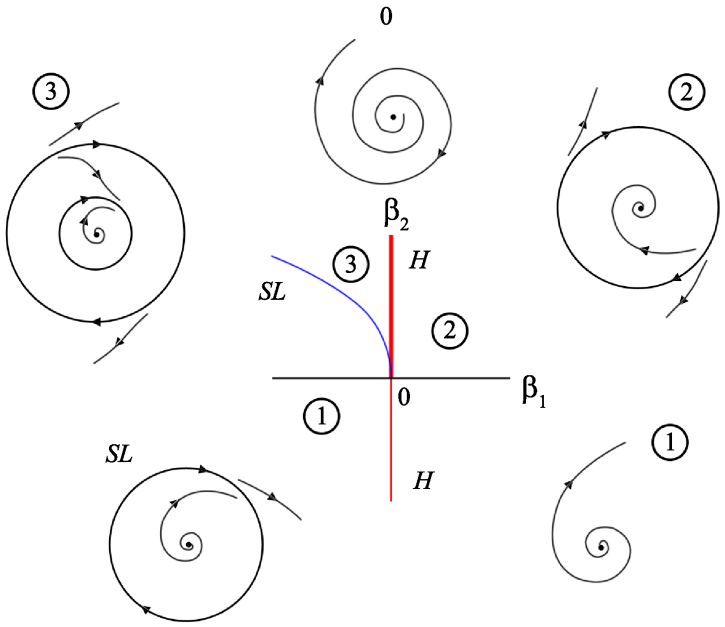

Figure 7.5: Unfolding of the Bautin bifurcation, normal form 7.4, for the case $s = 1$.

In the case of the laser, continuation software, AUTO, can be used to follow the periodic orbits in parameter space. By observing the eigenvalues in the AUTO output files it is possible to continue the unstable periodic orbit born on the subcritical part of the Hopf curve (or the stable periodic orbit born on the supercritical Hopf curve) until it either merges with a saddle to form a homoclinic orbit, or bifurcates at a saddle node of limit cycles by merging with another periodic orbit. Figure 7.6 shows the regions in which the periodic orbits exist.

Taking a closer look at the regions surrounding the Bautin points in Figure 7.6 it is possible to see that in all these cases the Bautin points are type $s = -1$, as shown in [23, p314].

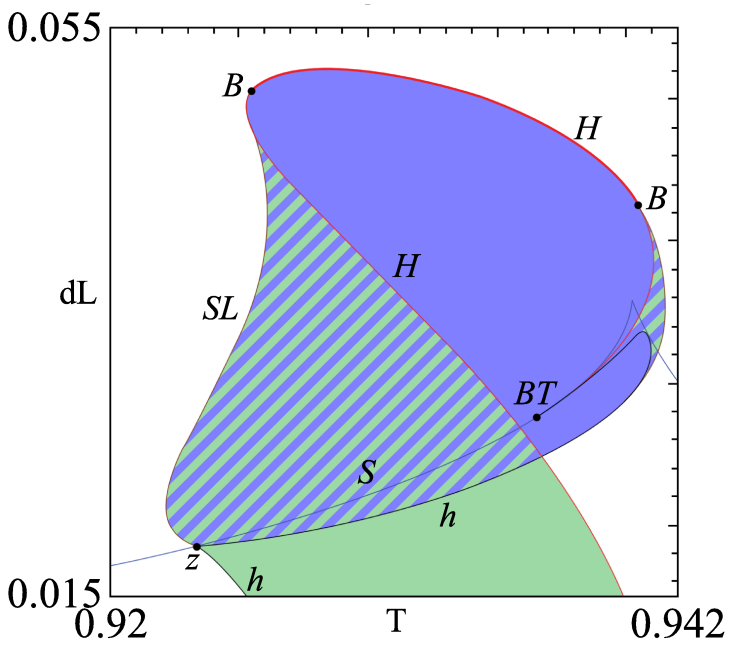

Figure 7.6: The regions in which the unstable periodic orbits exist are shown in green, while the regions in which the stable periodic orbit exists is shown in blue. There is a narrow region between the Bogdanov-Takens, Z, and the right hand Bautin point, in which there are two unstable periodic orbits and a stable periodic orbit simultaneously.

7.3 Saddle-Node Hopf Bifurcation points

This codimension-2 point can be found for larger values of α in the laser system, for example in Figures 6.3 and 6.6 for $\alpha = 1$, and 6.4 for $\alpha = 2$. As well as Saddle-node Hopf, these bifurcation points are also referred to as Fold-Hopf, zero Hopf, or Gavrilov-Guckenheimer points.

This bifurcation occurs when a Saddle-node and Hopf curve meet tangentially in parameter space, when there is a zero eigenvalue and a pair of purely imaginary eigenvalues. As, for certain cases, Torus bifurcations may eminate from these points Saddle-node Hopf points often imply a local cause of chaos. We do not give the normal form and unfolding here, but note that it has been studied in [23, p332]. On analysing the Saddle-node Hopf points shown in Figure 7.7 the dynamics indicate that these are classified with $s = -1, \theta > 0$ as shown in Figure 7.8[23, p343].

7.4 Non-central SN Homoclinic with additional non-centrality

When considering bifucations of stationary and periodic solutions we encounter an unusual point shown in Figure 7.9. A similar point can be found in the paper by S. Wieczorek [41], although this new point appears to have an additional non-central direction.

For $\alpha = 0$ there is a complicated interaction between several bifurcations in the region of $T = 0.92, 0.93$, Homoclinic bifurcations joining with the two saddle node

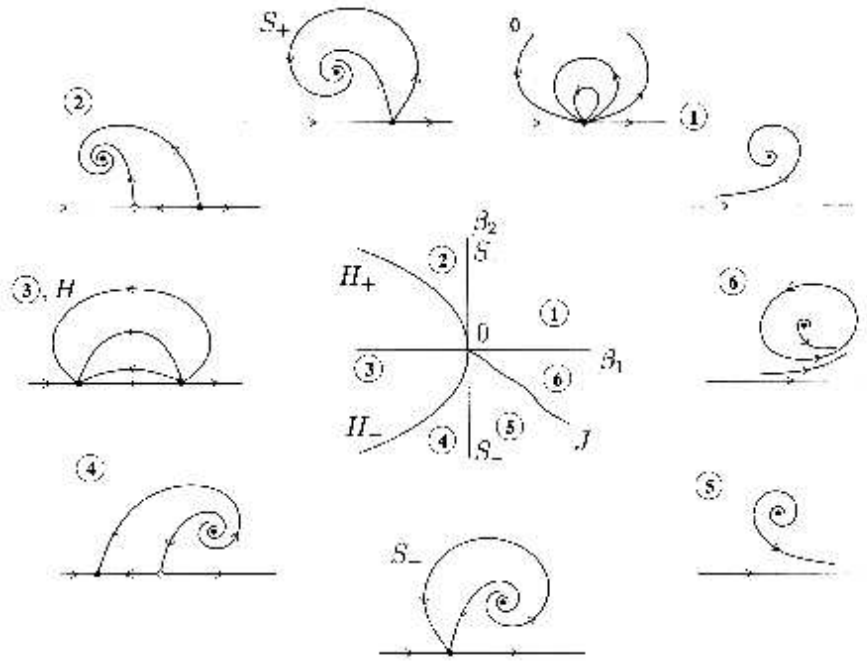

Figure 7.7: Unfolding of the Saddle-node Hopf Bifurcation as shown in [23, p343].

Hopf points can be seen in black. dL^*/λ is in the region of $(\pm 0.015, 0.02)$. Here we see the homoclinic bifurcation pass through the point where a saddle node of limit cycles crosses a Saddle-node bifurcation. Figure 7.9 is a zoom of one of these two points and also shows the stationary points and periodic orbits that exist in each region around the point. If you were to balance on this point in parameter space you would find a saddle with double homoclinic connection shown on the right of Figure 7.9, though neither connection would be in the central direction. A tiny perturbation would move the dynamics into one of the surrounding regions of the bifurcation diagram.

On a side note, when crossing from regions 1 or 6 in Figure 7.11 through the saddle node a very fast change happens to one of the developing point's eigenvalues

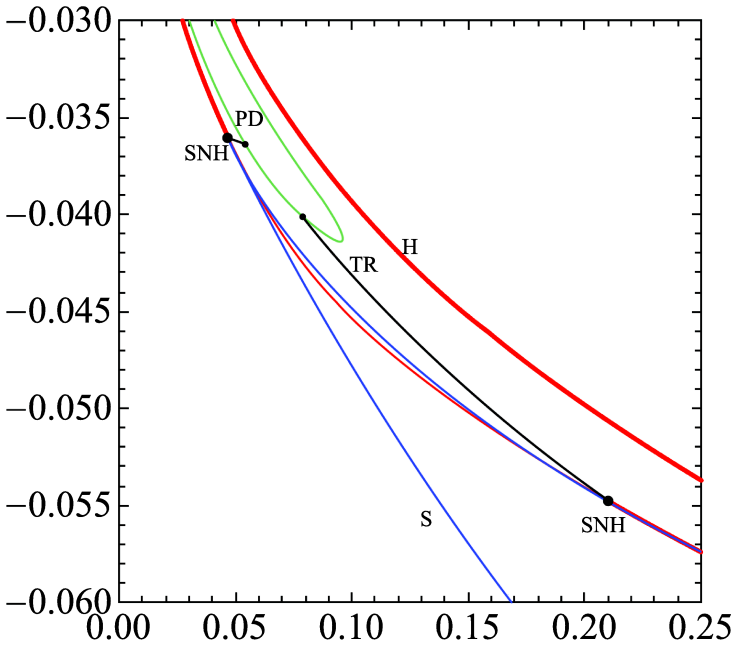

Figure 7.8: Fold Hopf bifurcations in the laser system for $\alpha = 1$ (a region from Figure 6.3).

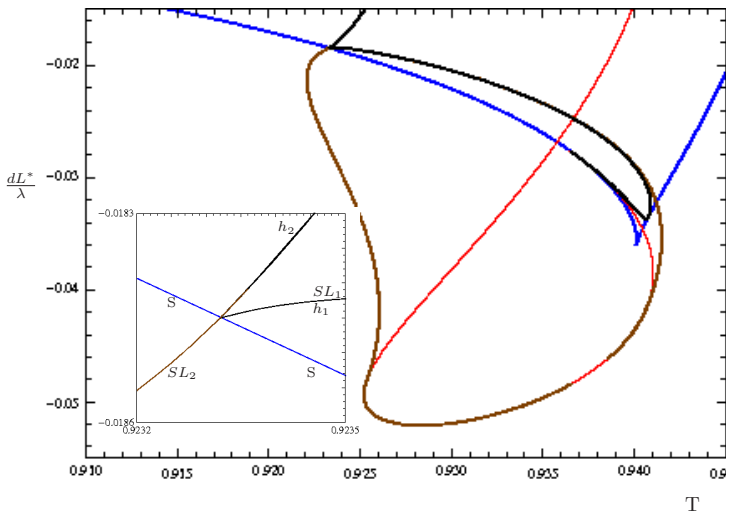

Figure 7.9: Bifurcation diagram for $\alpha = 0$. Central figure shows a zoom of a special point we refer to as a Non-central SNHopf.

turning another direction complex rapidly. This is not a bifurcation, but is also shown in the figure, as you see the saddle gain a spiralling direction. The other point however, retains its real eigenvalue.

In Figure 7.10 we see the phase portraits of the two homoclinic orbits as they approach the Non-central SNH. There is the possibility that this could be two points very close together. This behaviour is also shown in [18] and the question remains why these two points should be so close. If we compare the phase portraits in the regions around the bifurcation in both the 2D case from [18] and the 3D case as

seen in Figure 7.9 which we are particulary interested in we see that the necessity for an additional saddle is removed in this new 3D case.

7.5 Checking the validity of bifurcations

The existance of false bifurcations has been a real possibility during this work. Several methods could be utilised to combat this issue including:

- Plotting the dynamics of the original system using DsTool [2] for specific points in $T - dL^*$ parameter space. Note that the modes for this need to be calculated in Mathematica [26].
- Comparison of eigenvalues in the old and new systems to check how these have been combined at detected bifurcation points.
- Plotting $I_1 I_2 - (I_3^2 + I_4^2)$: this should be zero unless the bifurcation detected is a false one.

For example, Figure 7.12 shows how plots produced in DsTool (in the rotating system; see Appendix E) can illustrate the dynamics at chosen points in parameter space. This figure indicates that there are further Period Doubling bifurcations.

Eigenvalues in the rotating and reduced systems can also be compared for fixed parameter values. The output file d.filename contains the parameter values and eigenvalues for each step in the continuation. Next we will see part of this file for $\alpha = 0$, $dL^*/\lambda = 3.4 \times 10^{-10}$, $T = 0.45$. Firstly the eigenvalues in the rotating system:

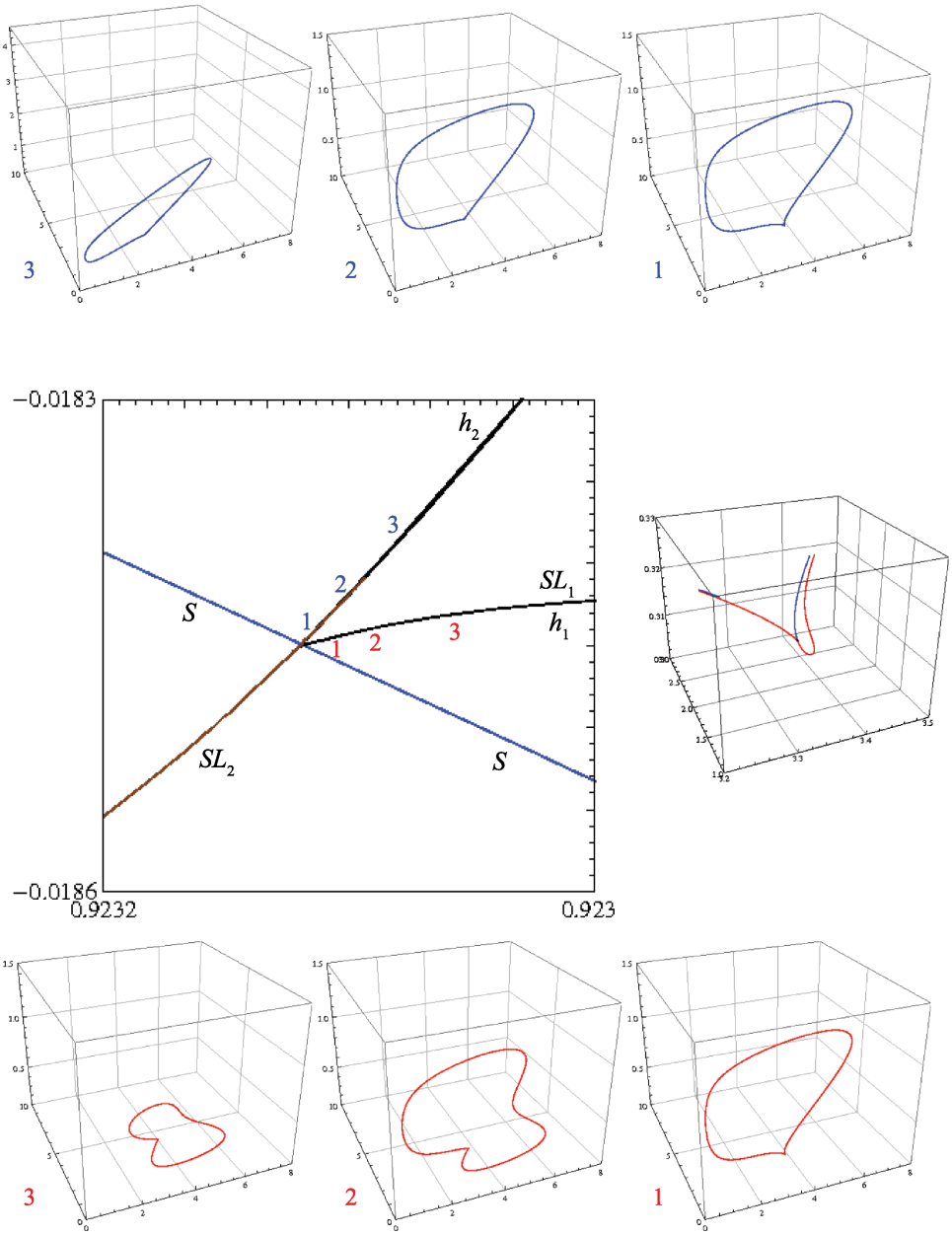

Figure 7.10: Plots of the homoclinic orbit as it approaches Z from h1 (blue) and from h2 (red).

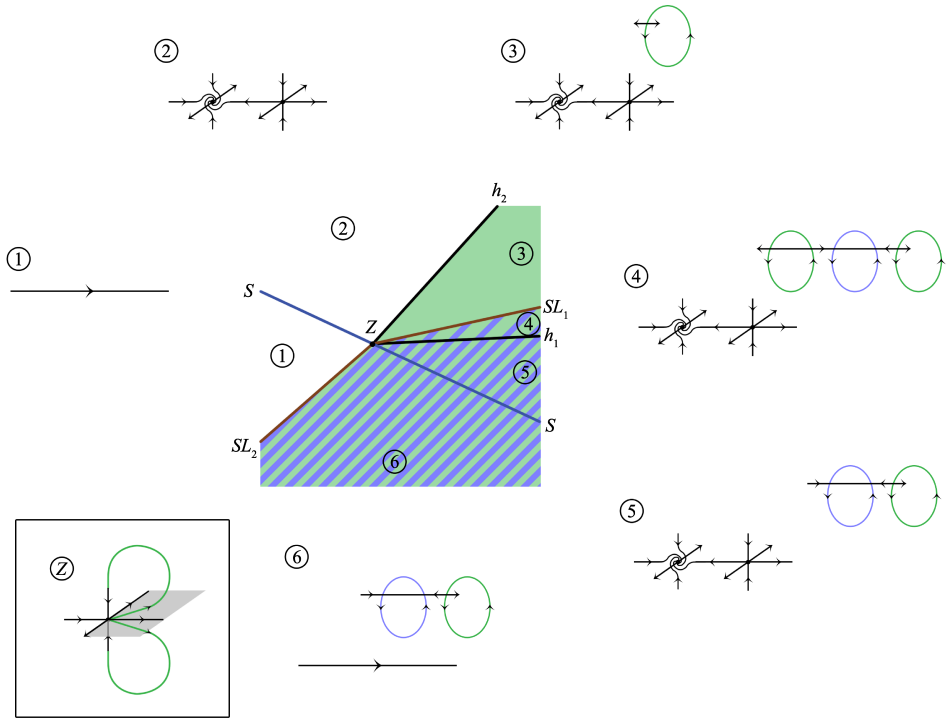

Figure 7.11: This diagram illustrates the dynamics in each region surrounding the Non-central Saddle-Node Homoclinic point, Z.

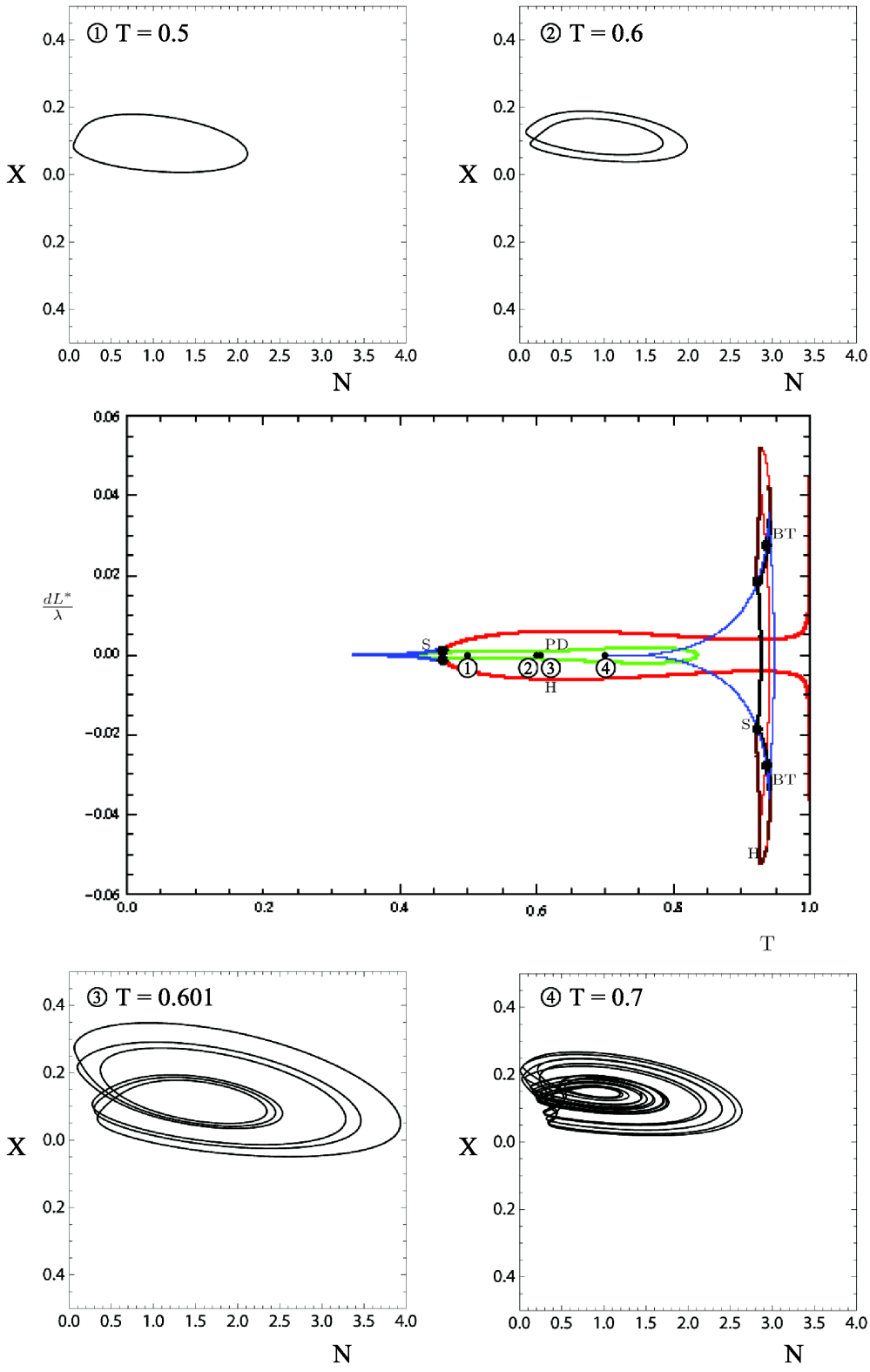

Figure 7.12: The central panel shows the bifurcation diagram as in Figure 6.5 for $\alpha = 0$. Points 1-4 correspond to $T = 0.5$, 0.6, 0.601, 0.7 for $dL^*/\lambda = 0$. This shows there are further Period Doubling bifurcations.

```
  BR    PT  IT

   1  8689   0      4.500335E-01               -1.123322E+00  7.713036E+02
1.564424E+00  7.039063E-01 -1.406917E+00  7.767913E-02
   1  8689   1      4.500335E-01               -1.123322E+00  7.713036E+02
1.564424E+00  7.039063E-01 -1.406917E+00  7.767913E-02


 ==> Location of special point :  Iteration   0   Stepsize = -3.53279E-02

  BR    PT  IT

   1  8689   0      4.500000E-01               -1.123322E+00  7.712683E+02
1.564425E+00  7.039743E-01 -1.406884E+00  7.767118E-02
   1  8689   1      4.500000E-01               -1.123322E+00  7.712683E+02
1.564425E+00  7.039743E-01 -1.406884E+00  7.767118E-02


 ==> Location of special point :  Convergence.    Stepsize = -4.75295E-07

   1  8689        Fold Function    9.47228E-04

   1  8689        BP   Function    1.20347E+12

   1  8689        Hopf Function   -3.82053E-01

   1  8689        Eigenvalues:     Stable:   6

   1  8689        Eigenvalue  1  -3.820529E-01 -7.807684E+01

   1  8689        Eigenvalue  2  -3.820529E-01  7.807684E+01

   1  8689        Eigenvalue  3  -6.473619E+00  0.000000E+00

   1  8689        Eigenvalue  4  -6.473619E+00  0.000000E+00

   1  8689        Eigenvalue  5  -5.798747E+01  0.000000E+00

   1  8689        Eigenvalue  6  -7.694989E+01  0.000000E+00
```

```
  BR    PT  TY LAB    PAR(0)        L2-NORM         U(1)          U(2)

   1 -8689  UZ   2  4.500000E-01  7.712723E+02 -1.123322E+00  7.712683E+02

    U(3)          U(4)          U(5)          U(6)

1.564425E+00  7.039743E-01 -1.406884E+00  7.767118E-02

------------------------------------------------------------------------------
```

and then for the reduced system for the same parameter values:

```
------------------------------------------------------------------------------

  BR    PT  IT

   1  8689   0      4.500320E-01               -1.123322E+00  7.713021E+02

2.447423E+00  2.474899E+00  1.101213E+00  2.201012E+00

   1  8689   1      4.500320E-01               -1.123322E+00  7.713021E+02

2.447423E+00  2.474899E+00  1.101213E+00  2.201012E+00


 ==> Location of special point :  Iteration   0   Stepsize = -3.37788E-02

  BR    PT  IT

   1  8689   0      4.500000E-01               -1.123322E+00  7.712683E+02

2.447427E+00  2.474902E+00  1.101315E+00  2.200965E+00

   1  8689   1      4.500000E-01               -1.123322E+00  7.712683E+02

2.447427E+00  2.474902E+00  1.101315E+00  2.200965E+00


 ==> Location of special point :  Convergence.    Stepsize = -4.75451E-07

   1  8689        Fold Function    9.47225E-04
```

```
   1  8689        BP   Function   -1.39539E+14

   1  8689        Hopf Function   -3.82053E-01

   1  8689        Eigenvalues:     Stable:   7

   1  8689        Eigenvalue  1  -3.820529E-01 -7.807684E+01

   1  8689        Eigenvalue  2  -3.820529E-01  7.807684E+01

   1  8689        Eigenvalue  3  -6.473619E+00  0.000000E+00

   1  8689        Eigenvalue  4  -6.473619E+00  0.000000E+00

   1  8689        Eigenvalue  5  -5.798747E+01  0.000000E+00

   1  8689        Eigenvalue  6  -7.694989E+01  0.000000E+00

   1  8689        Eigenvalue  7  -1.159464E+02  0.000000E+00


  BR    PT  TY LAB    PAR(0)        L2-NORM         U(1)          U(2)

   1 -8689  UZ   2  4.500000E-01  7.712809E+02 -1.123322E+00  7.712683E+02

    U(3)          U(4)          U(5)          U(6)

 2.447427E+00  2.474902E+00  1.101315E+00  2.200965E+00
```

Note that we can define user points (UZ) at particular points in parameter space to compare the eigenvalues in the two systems. Some eigenvalues remain the same (in this case all but one), but others in the reduced system are a complicated combination of the eigenvalues in the rotating system.

During the analysis the false bifurcation shown in Figure 7.13 was detected and verified to be false. This aparent additional fold bifurcation can be shown to be false using the third of the methods available to us. Figure 7.14 shows how $I_1 I_2 - (I_3^2 + I_4^2)$

varies as the false bifurcation is continued. In comparison Figure 7.15 shows that $I_1 I_2 - (I_3^2 + I_4^2)$ remains zero as part of the Hopf bifurcation is continued.

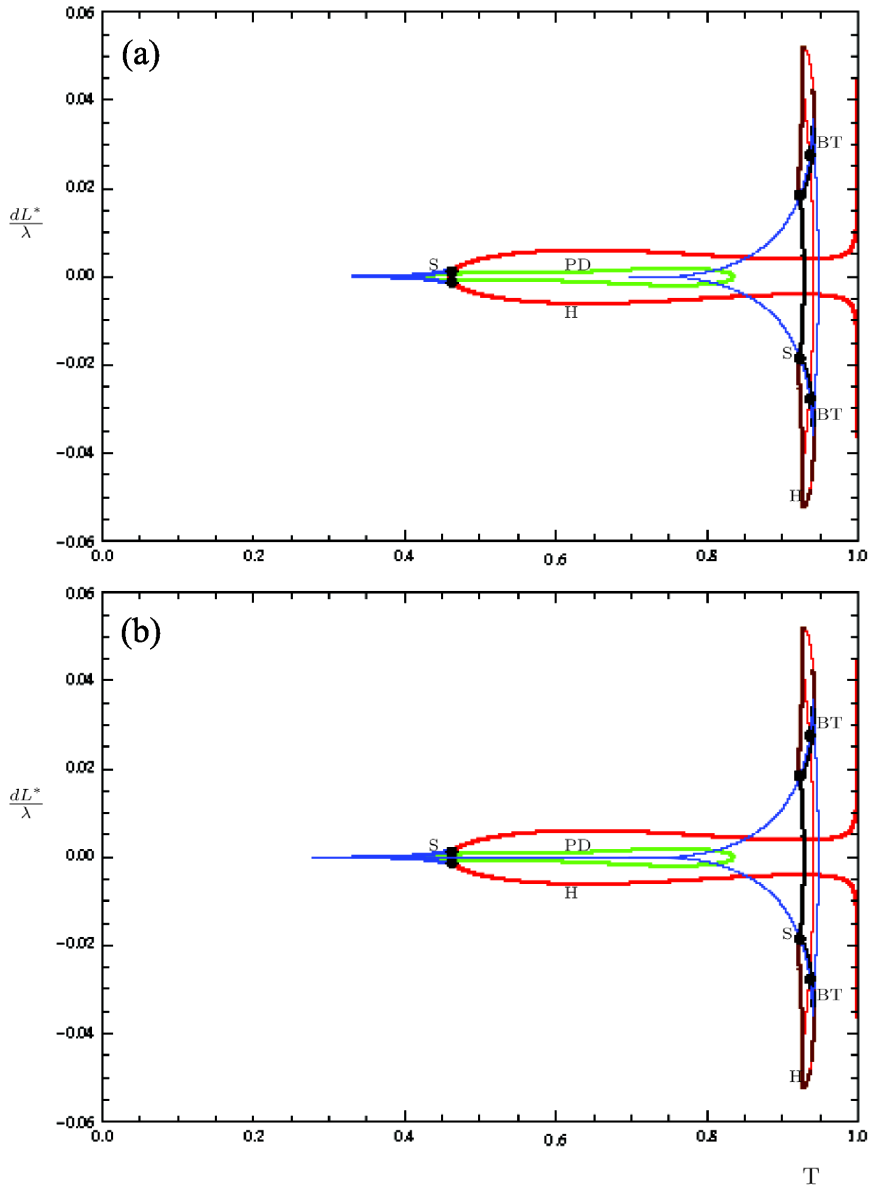

Figure 7.13: Here the additional Saddle-node bifurcation produced by the reduced system in the second panel does not correspond to a bifurcation in the original system.

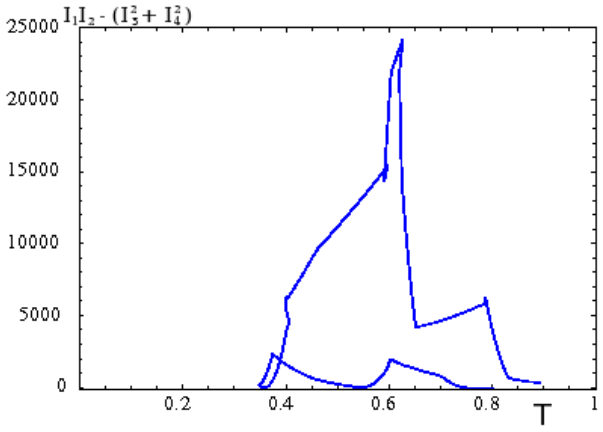

Figure 7.14: In continuing the additional Saddle-Node bifurcation shown in the second panel in Figure 7.13 we see that $I_1I_2 - (I_3^2 + I_4^2)$ is non-zero and so this is indeed a false bifurcation.

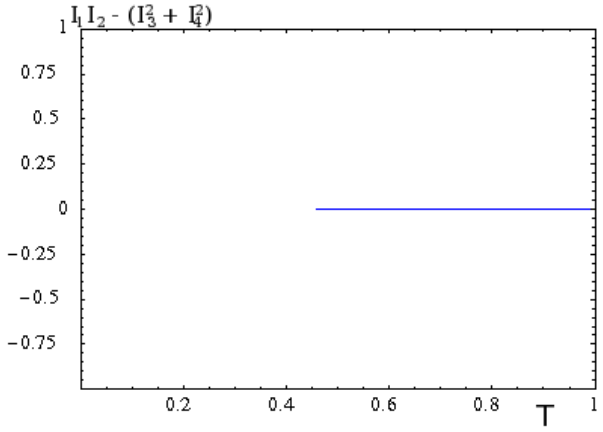

Figure 7.15: In contrast to Figure 7.14 this figure shows how $I_1I_2 - (I_3^2 + I_4^2)$ remains zero as the Hopf bifurcation is continued. This is indeed a correct bifurcation and is verified by DsTool and Matlab.

Chapter 8

Bifurcation to Lasing

In this chapter, I consider a particular type of Pitchfork bifurcation, that occurs in systems with symmetries as found in the example of a laser with strong optical feedback (as discussed in Chapters 5-7). The particular solution we consider is the bifurcation to lasing in the system. Note that (5.21) and (5.24) has a solution where $E_1 = E_2 = 0$ and $N = \Lambda - 1$ with symmetry $\mathbf{SO}(2)$. The eigenvalue corresponding to perturbations in the N direction is -1 from (5.24). We compute here the eigenvalues in the remaining directions to locate any bifurcations. Note that this cannot be easily done analytically as the couplings C_{ij} depend in a highly non-trivial way on the parameters T and dL^*/λ. I will describe the region in parameter space for this laser in which a pitchfork bifurcation might occur. I show that although part of the bifurcation diagram in the previous chapter may look like a pitchfork bifurcation, it is merely close by. I discuss how the pitchfork bifurcation is calculated in a special case where $\alpha = dL^* = 0$ and at what pump current this would occur in the laser.

Note that for $\alpha = 0$, $dL = 0$ we have $C_{11} = C_{22} = 1$ and $C^A_{11} = C^A_{22} = \frac{1}{2}$ (see Figures 8.1, 8.4). This then implies $\gamma = \gamma_1 = \gamma_2 = \frac{\gamma_E}{\gamma_N}$. Note $\Omega_{21} = \Omega$ and $C^A_{12} = C^A_{21}$. The equations then become

$$0 = -2\gamma I_1 + 2\gamma \left(\frac{1}{2} F I_1 + C F I_3 \right) \tag{8.1}$$

$$0 = -2\gamma I_2 + 2\gamma \left(\frac{1}{2} F I_2 + C F I_3 \right) \tag{8.2}$$

$$0 = -2\gamma I_3 - \Omega I_4 + \gamma F I_3 + C\gamma F (I_1 + I_2) \tag{8.3}$$

$$0 = -2\gamma I_4 + \Omega I_3 + \gamma F I_4 \tag{8.4}$$

$$0 = \Lambda - (I_5 + 1) - \frac{F}{2}(I_1 + I_2 + 4C I_3) \tag{8.5}$$

and as before $F = 1 + \beta I_5$. The aim is to solve these to find an equation in I_5. From the first two equations (8.1) and (8.2) we have

$$I_1 = \frac{2CF}{2 - F} I_3$$

and

$$I_2 = \frac{2CF}{2 - F} I_3 = I_1 = I$$

where we now let $I_1 = I_2 = I$.

From the fourth equation (8.4) we obtain

$$I_4 = \frac{\Omega}{2\gamma CF} I \tag{8.6}$$

Then from the third (8.3) we obtain

$$0 = (-\gamma^2(F-2)^2 - \Omega^2 + 4\gamma^2 C^2 F^2)I \tag{8.7}$$

When equation (8.6) and equation (8.7) are equated and I is substituted it is clear that either

$$I = 0 \tag{8.8}$$

is a solution or

$$-\gamma^2(F-2)^2 - \Omega^2 + 4\gamma^2 C^2 F^2 = 0 \tag{8.9}$$

The final equation (8.5) with relevant substitutions made will give the value for I once I_5 has been found using the previous equation. This then gives the values of I_n at the pitchfork bifurcation.

Note that (8.9) is quadratic in I_5 giving a transcritical bifurcation to lasing. However, as only the case $I \geq 0$ is relevant this corresponds to a pitchfork bifurcation in the original variables.

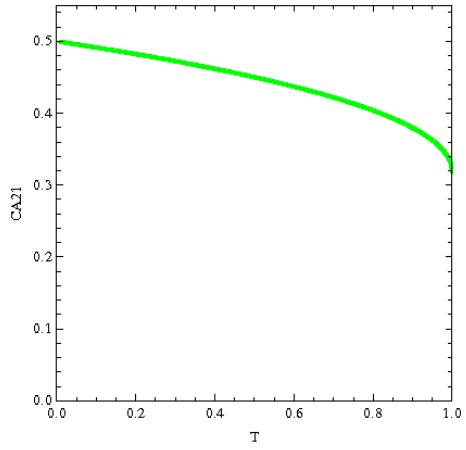

Figure 8.1: With $\alpha = dL = 0$, AUTO is used to output the value of C_{21}^A as T is increased from 0 to 1. At these values of α and $dL^*/lambda$, C_{21}^A is not constant.

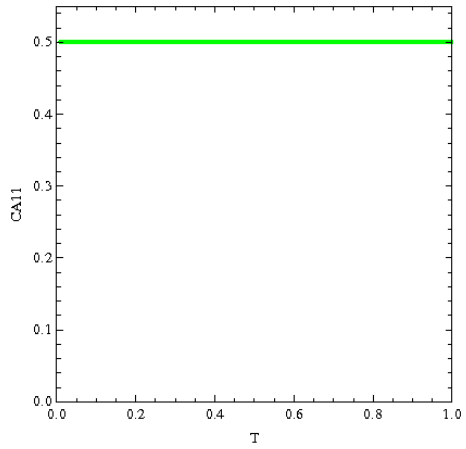

Figure 8.2: With $\alpha = dL = 0$, AUTO is used to output the value of C_{11}^A as T is increased from 0 to 1. At these values of α and dL^*/λ, C_{11}^A is fixed at 0.5 allowing us to simplify the equations further.

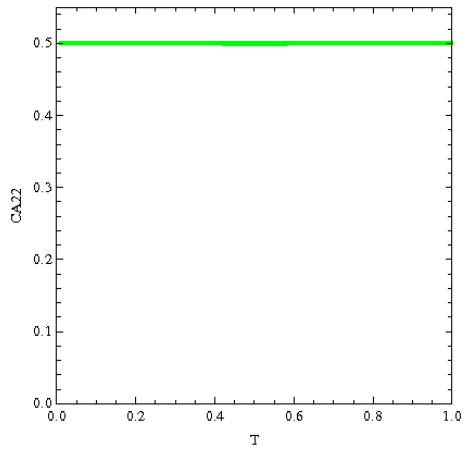

Figure 8.3: With $\alpha = dL = 0$, AUTO is used to output the value of C_{22}^A as T is increased from 0 to 1. At these values of α and dL^*/λ C_{22}^A is fixed at 0.5 allowing us to simplify the equations further.

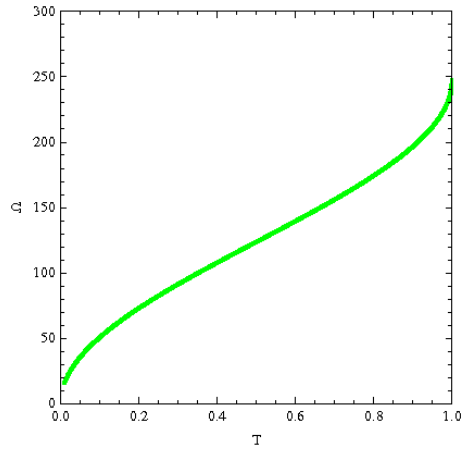

Figure 8.4: With $\alpha = dL = 0$, AUTO is used to output the value of Ω as T is increased from 0 to 1. At these values of α and dL^*/λ Ω is not constant and so it must remain in the calculation.

Chapter 9

Conclusions

In Chapter 1 we considered the importance of lasers in modern technology and the need to understand their dynamics. A brief history of how lasers, in particular semiconductor lasers, came about. With the invention of the semiconductor laser exploration of the complicated non-linear behaviour they often exhibited started. The noteable work by Lang and Kobayashi and others [24] [28] [34] in the early 1980's were some of these first explorations. More recently challenges have arisen to model lasers with feedback (from an external mirror) or coupled with many other lasers which are common in optical communication techniques [20]. We also discussed the necessity to understand the stable and unstable behaviour of these laser systems. It has been a focus of this research project to model a laser with strong optical feedback; that is, one with an external mirror set part way down an optical fibre originally thought by the manufacturers to stablise the lasers operations. We have seen in later chapters that this is not the case and in fact makes the laser highly

sensitive to small parameter changes.

We went on to discuss the symmetric nature of many laser systems [21] and the difficulties that arise from using path-following software such as AUTO [6] to analyse the stability. In section 1.2 we discussed how bifurcations were often related to changes in symmetry and we considered types of linear symmetry which might apply to local bifurcations. In order to discuss the dynamics in more detail we used group theory to describe the symmetry in systems of ODEs. This required a short introduction to the topic which can be found in section 1.3.

In Chapter 2 differential equations with symmetries were considered further and we also considered in section 2.1 symmetries for bifurcation problems, in particular an example of a Hopf bifurcation. We discussed the problems with studying bifurcation problems with symmetry due to potentially having eigenvalues with high multiplicity. In order to solve this problem we considered the work of Chossat [3] and the idea that new variables (which are functions of the original variables) could be used to re-write the system of equations as a representation of the orbit space. We continued with this line of thought and considered how we might do this in the most efficient way in order to remove the symmetries in the system.

In section 2.3 we introduced the idea of invariants and equivariants and defined a Hilbert basis. A Hilbert basis can be used in order to remove the symmetries in the system, still reducing it to the orbit space. We saw that a Hilbert basis was not necessarily unique and relations between elements could exist. They can also be of any size and so in order to reduce the dimension of the new system a minimal

Hilbert basis should be found.

In section 2.4 we considered several examples of the use of invariants to reduce systems to the orbit space. This included an example which used a Hilbert basis with relation which was later relevant to the laser system discussed in later chapters.

The next challenge was to consider how eigenvalues of the Jacobians of the original and reduced systems of equations might be related. Chapter 3 included a review of the work of Koenig and Chossat [3], [19] in order to relate bifurcations found in the reduced system to those in the original system. The choice of basis used to create the reduced system will affect the eigenvalues and how they are related to the original eigenvalues. In section 3.2 we discussed previous work by Chossat and Koenig on the topic and then considered how the eigenvalues of the reduced system can be related back to the original system in order to interpret results. A previously derived theorem from Chossat [3] was used to explain how the eigenvalues in the systems related to one another. This meant the possibility of detecting bifurcations in the reduced system which were false (i.e. not in the original system).

In Chapter 4 we gave examples of how eigenvalues in the reduced system were combinations of those in the original system. The way in which they are combined is vitally important as it may lead to false zero eigenvalues in the reduced system which would cause path-following software to detect a bifurcation, though this would be false. In section 4.1 we considered an example similar to the laser system introduced in Chapter 5. We saw that the problem was highly complex and although it was not possible to complete the computation it indicated some of the issues for the later

chapter.

The main contribution of the thesis came in Chapters 5-8. We first introduced the problem of the laser with strong optical feedback. The composite cavity mode approach [39],[40] was used to create a model for the system. Equations (5.21) and (5.24) formed the original system of equations. An initial basis was chosen so that the system was considered in the rotating frame allowing the use of continuation software. This formed equations (5.26) which were initially used with path-following software to detect bifurcations in the system, though this system still contained symmetries. Figure 5.2 indicated the dynamics to be expected once path-following was performed fully. In section 5.2 we considered how the symmetries could be removed by choosing a set of invariants to transform the system into the equations (5.27). Section 5.3 then discussed how the stationary points and periodic orbits in each of the three systems were related to one another, allowing results to be interpreted for the original model of the system.

The transcendental equation (dependent on T and dL^*) was solved for two modes and this was set up as an additional pair of equations in the continuation software so that it was solved at each point in parameter space. In future it would be usuful to explore the effect of more than two modes.

Bifurcation analysis was first done on equations (5.26) in Section 6.1. This created a series of Bifurcation diagrams for different values of α which showed Hopf and Saddle-node bifurcations. These also indicated Bogdanov Takens and Saddle-node Hopf points. It was not possible to maintain continuation of bifurcations of

periodic orbits in the rotating system of equations as X became zero. Therefore the reduced system, equations (5.27), were used to produce the bifurcation diagrams which included bifurcations of periodic orbits. This produced bifurcation diagrams consistent with the approximations made using Matlab and also indicated additional codimension 2 points; Bautin points and an unusual point which we describe as a Non-central Saddle-node Homoclinic point.

The high sensitivity on α was very noticeable. It is possible that the linewidth enhancement factor is affected by the number of inverted atoms. In future it would be interesting to build a dependence of α on N to see if this has an effect on the stability regions of the model. Another topic for further investigation would be when the other parameters (e.g. Λ) are varied.

In Chapter 7 we considered Bogdanov-Takens, Bautin, and Saddle-node Hopf points. We considered the normal forms of these and classified the points found in the laser system. We also considered the Non-central Saddle-node Hopf points. The dynamics in each region was determined by careful analysis of the eigenvalues and how these altered in crossing into each new region in parameter space around the point. AUTO was used to continue the two homoclinic connections towards the point and DsTool was used to verify the remaining changes in the dynamics. A false bifurcation was found in Figures 7.13 and 7.14 and described.

Finally, in Chapter 8 we discuss a particular case (the bifurcation to lasing) where we can progress further with an analytical bifurcation analysis. However, in this case we need to use AUTO to calculate the dependence of various parameters

on T. It remains to be seen wheter these results can be extended to realistic laser problems, but we have discussed some important steps along the way.

Bibliography

[1] F.T. Arecchi, R. Meucci, G. Puccioni, and J. Tredicce. Experimental evidence of subharmonic bifurcations, multistability, and turbulence in a Q-switched gas laser. *Phys. Rev. Lett.*, 49(17):1217–1220, 1982.

[2] A. Back, J. Guckenheimer, M.R. Myers, F.J. Wicklin, and P.A. Worfolk. DsTool: Computer assisted exploration of dynamical systems. *Notices Am. Math. Soc.*, 39:303–309, 1992.

[3] P. Chossat. The reduction of equivariant dynamics to the orbit space for compact group actions. *Acta Applicandae Mathematicae*, 70(1):71–94, 2002.

[4] P. Chossat and R. Lauterbach. *Methods in equivariant bifurcations and dynamical systems*. World Scientific Pub Co Inc, 2000.

[5] W.W. Chow. *IEEE J. Quantum Electron.*, QE-22(1174), 1986.

[6] E. Doedel, A. Champneys, T. Fairgrieve, B. Sandstede, Yu. Kuznetsov, and X. Wang. *AUTO 2000: continuation and bifurcation software for ordinary differential equations*. http://indy.cs.concordia.ca/auto/main.html, 2000.

[7] A. Einstein, A. Engel, and E.L. Schücking. *The Collected Papers of Albert Einstein: English Translation*. 1917.

[8] H. Erzgraber, D. Lenstra, B. Krauskopf, APA Fischer, and G. Vemuri. Feedback phase sensitivity of a semiconductor laser subject to filtered optical feedback: experiment and theory. *Physical Review E*, 76(2):26212, 2007.

[9] M. Field and M. Golubitsky. *Symmetry in Chaos*. Oxford University Press, North Carolina, USA, 1992.

[10] A. Gavrielides, V. Kovanis, and T. Erneux. Analytical stability boundaries for a semiconductor laser subject to optical injection. *Optics Communications*, 136(3-4):253–256, 1997.

[11] M. Golubitsky, D.G. Schaeffer, and I. Stewart. *Singularities and groups in bifurcation theory*. Springer Verlag, 1988.

[12] K. Green, B. Krauskopf, and D. Lenstra. External cavity mode structure of a two-mode VCSEL subject to optical feedback. *Optics Communications*, 277(2):359–371, 2007.

[13] J. Hecht. *Laser Pioneers*. Academic Press Inc., San Diego, 1992.

[14] J. Hecht. *The Laser Guidebook*. McGraw-Hill Professional, 1999.

[15] T. Heil, I. Fischer, W. Elsasser, B. Krauskopf, K. Green, and A. Gavrielides. Delay dynamics of semiconductor lasers with short external cavities: Bifurcation scenarios and mechanisms. *Physical Review E*, 67(6):66214, 2003.

[16] I.N. Herstein. *Topics in Algebra 2nd ed.* Wiley: New York, 1975.

[17] J.E. Humphreys. *Introduction to Lie Algebras and Representation Theory.* Springer, 1972.

[18] A.I. Khibnik, B. Krauskopf, and C. Rousseau. Global study of a family of cubic Lienard equations. *Nonlinearity*, 11:1505, 1998.

[19] M. Koenig. Linearization of vector fields on the orbit space of the action of a compact Lie group. In *Mathematical Proceedings of the Cambridge Philosophical Society*, volume 121, 03, pages 401–424. Cambridge Univ Press, 1997.

[20] B. Krauskopf and D. Lenstra. Fundamental issues of nonlinear laser dynamics, vol. 548 of. In *AIP Conf. Proc*, 2000.

[21] B. Krauskopf, G.H.M. van Tartwijk, and G.R. Gray. Aspects of symmetry in lasers with optical feedback. *Proceedings of SPIE*, 3625:646–655, 1999.

[22] M. Krupa. Bifurcations of Relative Equilibria. *SIAM J. Math. Anal.*, 21(6):1453–1486, 1990.

[23] Y.A. Kuznetsov, I.A. Kuznetsov, and Y. Kuznetsov. Elements of applied bifurcation theory. 1995.

[24] R. Lang and K. Kobayashi. External optical feedback effects on semiconductor injection laser properties. *IEEE Journal of Quantum Electronics*, 16(3):347, 1980.

[25] T.H. Maiman. Stimulated optical radiation in ruby. *Nature*, 187:493–494, 1960.

[26] Wolfram Research. *Mathematica Version 7*. Wolfram Research, Inc., Champaign, Illinois., 2008.

[27] M.H. Rose, M. Lindberg, W.W. Chow, S.W. Koch, and M. Sargent III. Composite-cavity-mode approach to single-mode semiconductor-laser feedback instabilities. *Physical Review A*, 46(1):603–611, 1992.

[28] J. Sacher, D. Baums, P. Panknin, W. Elsasser, and E.O. Gobel. Intensity instabilities of semiconductor lasers under current modulation external light injection and delayed feedback. *Phys. Rev. A*, 45(3):1893–1905, 1992.

[29] M. Sargent III, MO Scully, and WE Lamb Jr. Laser Physics Addison-Wesley. *Reading, Mass*, 1974.

[30] H.C. Schneider, W.W. Chow, and S.W. Koch. Anomalous carrier-induced dispersion in quantum-dot active media. *Phys. Rev. B*, 66:041310(R), 2002.

[31] P.M. Smowton, E.J. Pearce, H.C. Schneider, W.W. Chow, and M. Hopkinson. Filamentation and linewidth enhancement factor in InGaAs quantum dot lasers. *Appl. Phys. Lett.*, 81:3251–3253, 2002.

[32] M.B. Spencer and W.B. Lamb. *Phys. Rev. A*, 5(893), 1972.

[33] W.M. Steen and W.M. Steen. *Laser material processing*. Springer Verlag, 2003.

[34] G.H.M. van Tartwijk and G.P. Agrawal. Laser instabilities: a modern perspective. *Prog. Quant. Electron*, 22:43–122, 1998.

[35] G.D. Van Wiggeren and R. Roy. Communication with chaotic lasers. *Science*, 279:1198–1200, 1998.

[36] D.A.R. Wallace. *Groups, rings, and fields*. Springer Verlag, 1998.

[37] C.O. Weiss, A. Godone, and A. Olafsson. Routes to chaotic emission in a CW He-Ne Laser. *Phys. Rev. A*, 28:892–895, 1983.

[38] C.O. Weiss and R. Vilaseca. *Dynamics of Lasers*. VCH Verlagsgesellschaft, Weinheim, Germany, 1991.

[39] S. Wieczorek and W.W. Chow. Bifurcations and interacting modes in coupled lasers: A strong-coupling theory. *Physical Review A*, 69(3):33811, 2004.

[40] S. Wieczorek and W.W. Chow. Global view of nonlinear dynamics in coupled-cavity lasers-a bifurcation study. *Optics communications*, 246(4-6):471–493, 2005.

[41] S. Wieczorek and B. Krauskopf. Bifurcations of n-homoclinic orbits in optically injected lasers. *Nonlinearity*, 18:1095, 2005.

[42] S. Wieczorek, B. Krauskopf, TB Simpson, and D. Lenstra. The dynamical complexity of optically injected semiconductor lasers. *Physics Reports*, 416(1-2):1–128, 2005.

Appendix A

Germs of smooth functions

It is usual to express the decomposition theorems in terms of germs of smooth functions; see for example [11]. Germs are a "local" concept of functions useful for bifurcation problems. To define a germ we first define

$$C^\infty(\mathbb{R}^p, \mathbb{R}^q) = \{f : \mathbb{R}^p \to \mathbb{R}^q \ : \ f^{(k)} \text{ is continuous for all } x \in \mathbb{R} \text{ and } k = 0, 1, 2, ...\}$$

and consider an equivalence relation on C^∞ by $f \sim g$ at 0 if there is an $\varepsilon > 0$ such that

$$f(x) = g(x)$$

for all $|x| < \varepsilon$. Clearly, if $f \sim g$ and $g \sim h$ then $f \sim h$ and $f \sim g \Rightarrow g \sim f$ meaning that $\sim$ is an equivalence relation.

The equivalence classes of C^∞ for $\sim$ are called *germs of functions* at 0. Note that germs of functions have well-define derivative even though they are not necessarily define at any point other than 0; this is because all functions which equivalent in a neighbourhood of 0 must have the same Taylor series there.

Appendix B

AUTO code for simulating equations (5.26)

```
#include "auto_f2c.h"

/* ---------------------------------------------------------------------- */

/* ---------------------------------------------------------------------- */

/*   excav: The External Cavity Laser

/* ---------------------------------------------------------------------- */

/* ---------------------------------------------------------------------- */

/* ---------------------------------------------------------------------- */

/* ---------------------------------------------------------------------- */

int func (integer ndim, const doublereal *u, const integer *icp,

          const doublereal *par, integer ijac,

          doublereal *f, doublereal *dfdu, doublereal *dfdp) {
```

```
    /* Evaluates the algebraic equations or ODE right hand side */
    /* Input arguments : */
  /*      ndim   :   Dimension of the ODE system */
  /*      u      :   State variables */
  /*      icp    :   Array indicating the free parameter(s) */
  /*      par    :   Equation parameters */
    /* Values to be returned : */
  /*      f      :   ODE right hand side values */
    /* Normally unused Jacobian arguments : IJAC, DFDU, DFDP (see manual) */
    // Variables
  doublereal dk1 = u[0], dk2 = u[1], E1 = u[2], ReE2 = u[3], ImE2 = u[4],
 N = u[5];
  // Continuation parameters
  doublereal T = par[0], doL = par[1], Lambda = par[2], alpha = par[3];
  // Fixed parameters
  doublereal gammaE = 4*pow(10,11), gammaN = 2*pow(10,9), Gamma = 0.1,
gammaM = 0.0, nA = 3.4, nB = 3.4, Nts = 2*pow(10,24), xi = 5*pow(10,-20),
c = 3*pow(10,8), beta = 1+((2*c*Gamma*xi*Nts)/(nB*gammaE));
  // Coupling and composite mode parameters
  doublereal LA = 0.000280;
  doublereal LoA = nA*LA, ko = 6283185.307179587;
  doublereal k1 = dk1+ko, k2 = dk2+ko;
```

```
  // Re-scale doL
  doublereal scale = 1.0*pow(10,-10);
  // A1, A2, B1, B2
  double A1 = sqrt((nB*LoA)/((nB*LoA*(0.5-sin(2*dk1*LoA)/(4*k1*LoA)))+(nB*
(LoA+doL*scale)*((sin(dk1*LoA)*sin(dk1*LoA))/(sin(dk1*LoA+ko*doL*scale+dk1*
doL*scale)*sin(dk1*LoA+ko*doL*scale+dk1*doL*scale)))*(0.5-(sin(2*(dk1*LoA+
ko*doL*scale+dk1*doL*scale))/(4*k1*(LoA+doL*scale)))))+((nB+nB)*sqrt((1-T)
/T)*sin(dk1*LoA)*sin(dk1*LoA)/k1)));
  double A2 = sqrt((nB*LoA)/((nB*LoA*(0.5-sin(2*dk2*LoA)/(4*k2*LoA)))+(nB*
(LoA+doL*scale)*((sin(dk2*LoA)*sin(dk2*LoA))/(sin(dk2*LoA+ko*doL*scale+dk2
*doL*scale)*sin(dk2*LoA+ko*doL*scale+dk2*doL*scale)))*(0.5-(sin(2*(dk2*LoA
+ko*doL*scale+dk2*doL*scale))/(4*k2*(LoA+doL*scale)))))+((nB+nB)*sqrt((1-T
)/T)*sin(dk2*LoA)*sin(dk2*LoA)/k2)));
  double B1 = -A1*sin(dk1*LoA)/sin(dk1*LoA+ko*doL*scale+dk1*doL*scale);
  double B2 = -A2*sin(dk2*LoA)/sin(dk2*LoA+ko*doL*scale+dk2*doL*scale);
  // C's
  doublereal CA11 = (A1*A1/2)*(1-(sin(2*dk1*LoA)/(2*k1*LoA)));
  doublereal CA12 = (A1*A2/(2*LoA))*(sin((dk2-dk1)*LoA)/(k2-k1)-sin((dk2+
dk1)*LoA)/(k2+k1));
  doublereal CA22 = (A2*A2/2)*(1-sin(2*dk2*LoA)/(2*k2*LoA));
  doublereal CB11 = ((B1*B1*(LoA+doL*scale))/(2*LoA))*(1-sin(2*(dk1*LoA+ko
*doL*scale+dk1*doL*scale))/(2*k1*(LoA+doL*scale)));
```

```
  doublereal CB12 = (B1*B2/(2*LA))*((sin((LoA+doL*scale)*(dk1-dk2))/(nB*(
k1-k2)))-(sin((LoA+doL*scale)*(dk1+dk2)+2*ko*doL*scale)/((k1+k2)*nB)));
  doublereal CB22 = (B2*B2*(LoA+doL*scale)/(2*LoA))*(1-sin(2*(dk2*LoA+ko*
doL*scale+dk2*doL*scale))/(2*k2*(LoA+doL*scale)));
  doublereal C11 = CA11+CB11;
  doublereal C12 = CA12+CB12;
  doublereal C22 = CA22+CB22;
  doublereal U1Sq0 = A1*A1*sin(dk1*LoA)*sin(dk1*LoA);
  doublereal U2Sq0 = A2*A2*sin(dk2*LoA)*sin(dk2*LoA);
  // Rescaled parameters
  // gamma1, gamma2, Gamma1, Gamma2
  doublereal gamma1 = gammaE*C11/(2*gammaN);
  doublereal gamma2 = gammaE*C22/(2*gammaN);
  doublereal Gamma1 = gamma1+(U1Sq0*gammaM/gammaN);
  doublereal Gamma2 = gamma2+(U2Sq0*gammaM/gammaN);
  doublereal Omega1 = (k1*c/gammaN), Omega2 = (k2*c/gammaN);
  // f[0] and f[1] find k1 and k2, then f[2]->f[5] are E1dot, ReE2dot,
ImE2dot, Ndot. Note that the equations for f[0] and f[1] are multiplied
by 1000. This does not affect AUTO as it will path follow where f[0]=f[1]=0,
 but means that the eigenvalues never approach zero - must avoid this extra
way of detecting false bifurcations!
  f[0] = -1000*(nB*sin(dk1*LoA)*cos(ko*doL*scale+dk1*(LoA+doL*scale))+nA*
```

```
sin(ko*doL*scale+dk1*(LoA+doL*scale))*cos(dk1*LoA)-(nA+nB)*sqrt((1-T)/T)*
sin(dk1*LoA)*sin(ko*doL*scale+dk1*(LoA+doL*scale)));
  f[1] = 1000*(nB*sin(dk2*LoA)*cos(ko*doL*scale+dk2*(LoA+doL*scale))+nA*
sin(ko*doL*scale+dk2*(LoA+doL*scale))*cos(dk2*LoA)-(nA+nB)*sqrt((1-T)/T)*
sin(dk2*LoA)*sin(ko*doL*scale+dk2*(LoA+doL*scale)));
  f[2] = -Gamma1*E1+gamma1*(CA11*(1+beta*N)*E1+CA12*((1+beta*N)*ReE2+alpha*
beta*(1+N)*ImE2));
  f[3] = -Gamma2*ReE2-(Omega1-Omega2)*ImE2+gamma2*CA22*((1+beta*N)*ReE2+
alpha*beta*N*ImE2)+gamma2*CA12*(1+beta*N)*E1-gamma1*(CA11*alpha*beta*N+
CA12*(alpha*beta*(1+N)*ReE2-(1+beta*N)*ImE2)/E1)*ImE2;
  f[4] = -Gamma2*ImE2-(Omega2-Omega1)*ReE2+gamma2*CA22*((1+beta*N)*ImE2-
alpha*beta*N*ReE2)-gamma2*CA12*alpha*beta*(1+N)*E1+gamma1*(CA11*alpha*
beta*N+CA12*(alpha*beta*(1+N)*ReE2-(1+beta*N)*ImE2)/E1)*ReE2;
  f[5] = Lambda-(1+N)-(1+beta*N)*(CA11*(E1*E1)+2*CA12*E1*ReE2+CA22*(ReE2*
ReE2+ImE2*ImE2));
  return 0;
  }
/* ---------------------------------------------------------------------- */
/* ---------------------------------------------------------------------- */
int stpnt (integer ndim, doublereal t,
           doublereal *u, doublereal *par) {
  /* Input arguments : */
```

```
  /*      ndim   :   Dimension of the ODE system */

  /* Values to be returned : */

  /*      u      :   A starting solution vector */

  /*      par    :   The corresponding equation-parameter values */

  /* Initialize the equation parameters */

  par[0] = (doublereal)0.1; /* T */

  par[1] = (doublereal)3.4;  /* doL/scale */

  par[2] = (doublereal)6.0; /* Lambda */

  par[3] = (doublereal)0.0;  /* alpha */

  /* Initialize the solution (dk1, dk2, E1, ReE2, ImE2, N) These starting
values are found using DsTool.*/

  u[0] = (doublereal) -1.1255924910482362;

  u[1] = (doublereal) 336.85480959977735;

  u[2] = (doublereal) 1.573137426127045;

  u[3] = (doublereal) 1.3900452821889273;

  u[4] = (doublereal) -0.76112748279911779;

  u[5] = (doublereal) 0.013697706910560149;

  return 0;

}
```

Appendix C

AUTO code for the simulating equations (5.27)

```
#include "auto_f2c.h"

/* ---------------------------------------------------------------------- */

/* ---------------------------------------------------------------------- */

/*   excav: The External Cavity Laser

/* ---------------------------------------------------------------------- */

/* ---------------------------------------------------------------------- */

/* ---------------------------------------------------------------------- */

/* ---------------------------------------------------------------------- */

int func (integer ndim, const doublereal *u, const integer *icp,

          const doublereal *par, integer ijac,

          doublereal *f, doublereal *dfdu, doublereal *dfdp) {
```

```
  /* Evaluates the algebraic equations or ODE right hand side */

  /* Input arguments : */

  /*      ndim   :   Dimension of the ODE system */

  /*      u      :   State variables */

  /*      icp    :   Array indicating the free parameter(s) */

  /*      par    :   Equation parameters */

  /* Values to be returned : */

  /*      f      :   ODE right hand side values */

  /* Normally unused Jacobian arguments : IJAC, DFDU, DFDP (see manual) */

  // Variables

  doublereal dk1 = u[0], dk2 = u[1], X = u[2], Y = u[3], ReZ = u[4],
ImZ = u[5], N = u[6];

  // Continuation parameters

  doublereal T = par[0], doL = par[1], Lambda = par[2], alpha = par[3];

  // Fixed parameters

  doublereal gammaE = 4*pow(10,11), gammaN = 2*pow(10,9), Gamma = 0.1,
gammaM = 0.0, nA = 3.4, nB = 3.4, Nts = 2*pow(10,24), xi = 5*pow(10,-20),
c = 3*pow(10,8), beta = 1+((2*c*Gamma*xi*Nts)/(nB*gammaE));

  // Coupling and composite mode parameters

  doublereal LA = 0.000280;

  doublereal LoA = nA*LA, ko = 6283185.307179587;

  doublereal k1 = dk1+ko, k2 = dk2+ko;
```

```
  // Re-scale doL
  doublereal scale = 1.0*pow(10,-10);
  // A1, A2, B1, B2
  double A1 = sqrt((nB*LoA)/((nB*LoA*(0.5-sin(2*dk1*LoA)/(4*k1*LoA)))+(nB
*(LoA+doL*scale)*((sin(dk1*LoA)*sin(dk1*LoA))/(sin(dk1*LoA+ko*doL*scale+
dk1*doL*scale)*sin(dk1*LoA+ko*doL*scale+dk1*doL*scale)))*(0.5-(sin(2*(dk1
*LoA+ko*doL*scale+dk1*doL*scale))/(4*k1*(LoA+doL*scale)))))+((nB+nB)*
sqrt((1-T)/T)*sin(dk1*LoA)*sin(dk1*LoA)/k1)));
  double A2 = sqrt((nB*LoA)/((nB*LoA*(0.5-sin(2*dk2*LoA)/(4*k2*LoA)))+(nB*
(LoA+doL*scale)*((sin(dk2*LoA)*sin(dk2*LoA))/(sin(dk2*LoA+ko*doL*scale+dk2*
doL*scale)*sin(dk2*LoA+ko*doL*scale+dk2*doL*scale)))*(0.5-(sin(2*(dk2*LoA
+ko*doL*scale+dk2*doL*scale))/(4*k2*(LoA+doL*scale)))))+((nB+nB)*sqrt((1-
T)/T)*sin(dk2*LoA)*sin(dk2*LoA)/k2)));
  double B1 = -A1*sin(dk1*LoA)/sin(dk1*LoA+ko*doL*scale+dk1*doL*scale);
  double B2 = -A2*sin(dk2*LoA)/sin(dk2*LoA+ko*doL*scale+dk2*doL*scale);
  doublereal CA11 = (A1*A1/2)*(1-(sin(2*dk1*LoA)/(2*k1*LoA)));
  doublereal CA12 = (A1*A2/(2*LoA))*(sin((dk2-dk1)*LoA)/(k2-k1)-sin((dk2+
dk1)*LoA)/(k2+k1));
  doublereal CA22 = (A2*A2/2)*(1-sin(2*dk2*LoA)/(2*k2*LoA));
  doublereal CA21 = CA12;
  doublereal CB11 = ((B1*B1*(LoA+doL*scale))/(2*LoA))*(1-sin(2*(dk1*LoA+
ko*doL*scale+dk1*doL*scale))/(2*k1*(LoA+doL*scale)));
```

```
  doublereal CB12 = (B1*B2/(2*LA))*((sin((LoA+doL*scale)*(dk1-dk2))/(nB*
(k1-k2)))-(sin((LoA+doL*scale)*(dk1+dk2)+2*ko*doL*scale)/((k1+k2)*nB)));
  doublereal CB22 = (B2*B2*(LoA+doL*scale)/(2*LoA))*(1-sin(2*(dk2*LoA+ko*
doL*scale+dk2*doL*scale))/(2*k2*(LoA+doL*scale)));
  doublereal C11 = CA11+CB11;
  doublereal C12 = CA12+CB12;
  doublereal C22 = CA22+CB22;
  doublereal U1Sq0 = A1*A1*sin(dk1*LoA)*sin(dk1*LoA);
  doublereal U2Sq0 = A2*A2*sin(dk2*LoA)*sin(dk2*LoA);
  // Rescaled parameters
  // gamma1, gamma2, Gamma1, Gamma2
  doublereal gamma1 = gammaE*C11/(2*gammaN);
  doublereal gamma2 = gammaE*C22/(2*gammaN);
  doublereal Gamma1 = gamma1+(U1Sq0*gammaM/gammaN);
  doublereal Gamma2 = gamma2+(U2Sq0*gammaM/gammaN);
  doublereal Omega1 = (k1*c/gammaN), Omega2 = (k2*c/gammaN);
  doublereal Omega = Omega2 - Omega1;
  doublereal Fs = 1+beta*5;
  doublereal Cs = sqrt((Omega*Omega -4*(gamma1*gamma1)*(Fs-1)*(Fs-1))*(2-
Fs)/(2*(Fs*Fs)*gamma1*(Fs-1)));
  // f[0] and f[1] are from the previous thing to find k1 and k2, then
f[2]->f[5] are E1dot, ReE2dot, ImE2dot, Ndot. Note that the equations
```

```
for f[0] and f[1] are multiplied by 1000. This does not affect AUTO as
it will path follow where f[0]=f[1]=0, but means that the eigenvalues
never approach zero - must avoid this extra way of detecting false
bifurcations! Note that in the write up X, Y, ReZ, ImZ, N appear as I1,
I2, I3, I4, I5.

  f[0] = -1000*(nB*sin(dk1*LoA)*cos(ko*doL*scale+dk1*(LoA+doL*scale))+nA
*sin(ko*doL*scale+dk1*(LoA+doL*scale))*cos(dk1*LoA)-(nA+nB)*sqrt((1-T)/
T)*sin(dk1*LoA)*sin(ko*doL*scale+dk1*(LoA+doL*scale)));

  f[1] = 1000*(nB*sin(dk2*LoA)*cos(ko*doL*scale+dk2*(LoA+doL*scale))+nA
*sin(ko*doL*scale+dk2*(LoA+doL*scale))*cos(dk2*LoA)-(nA+nB)*sqrt((1-T)/
T)*sin(dk2*LoA)*sin(ko*doL*scale+dk2*(LoA+doL*scale)));

  f[2] = -2*Gamma1*X+2*gamma1*(CA11*(1+beta*N)*X+CA12*((1+beta*N)*ReZ-
alpha*beta*(1+N)*ImZ));

  f[3] = -2*Gamma2*Y+2*gamma2*(CA22*(1+beta*N)*Y+CA12*((1+beta*N)*ReZ+
alpha*beta*(1+N)*ImZ));

  f[4] = -ImZ*(Omega2-Omega1)-ReZ*(Gamma1+Gamma2)+gamma1*CA11*(alpha*
beta*(N)*ImZ+(1+beta*N)*ReZ)+gamma2*CA22*(-alpha*beta*(N)*ImZ+(1+beta*
N)*ReZ)+CA21*(1+beta*N)*(gamma1*Y+gamma2*X);

  f[5] = ReZ*(Omega2-Omega1)-ImZ*(Gamma1+Gamma2)+gamma1*CA11*((1+beta*N)
*ImZ-alpha*beta*(N)*ReZ)+gamma2*CA22*((1+beta*N)*ImZ+alpha*beta*(N)*ReZ)
+CA21*alpha*beta*(1+N)*(gamma2*X-gamma1*Y);

  f[6] = Lambda-(1+N)-(1+beta*N)*(CA11*X+2*CA12*ReZ+CA22*Y);
```

```
  return 0;
  }
/* ---------------------------------------------------------------------- */
/* ---------------------------------------------------------------------- */
int stpnt (integer ndim, doublereal t,
           doublereal *u, doublereal *par) {
  /* Input arguments : */
  /*      ndim   :   Dimension of the ODE system */
  /* Values to be returned : */
  /*      u      :   A starting solution vector */
  /*      par    :   The corresponding equation-parameter values */
  /* Initialize the equation parameters */
  par[0] = (doublereal)0.1; /* T */
  par[1] = (doublereal)3.4;  /* doL/scale */
  par[2] = (doublereal)6.0; /* Lambda */
  par[3] = (doublereal)0.0;  /* alpha */
  /* Initialize the solution (dk1, dk2, X, Y, ReZ, ImZ, N)*/
  u[0] = (doublereal) -1.1255924910482362;
  u[1] = (doublereal) 336.85480959977735;
  u[2] = (doublereal) 2.4747613614816237;
  u[3] = (doublereal) 2.511540931607816;
  u[4] = (doublereal) 2.1867322574227313;
```

```
  u[5] = (doublereal) 1.197358129245161;

  u[6] = (doublereal) 0.013697706910560149;

  return 0;

}
```

Appendix D

Matlab code for simulating bifurcations diagrams

This produces Figure [d]5.2 for example. In order to use this we need input from a file, data4.dat, that is produced by an AUTO run. For example, to create data4.dat a run in AUTO with $\alpha = 1$, $dL^*/\lambda = -0.03$, is made from $T = 0$ to $T = 1$. The step length between each value of T can be chosen to increase or decrease the resolution of the final image to be made using Matlab. The values of T and the values of the variables at that point are output in outputs.txt (which is later saved as data4.dat) so that Matlab has the values of the variables for each value of T in order to simulate the dynamics at each point. data4.dat is available in the supplementary information.

Firstly lasrat4.m:

```
function ydot=lasrat4(t, y)
```

```
global G1 G2 a b CA11 CA12 CA22 CA21 Lambda O1 O2


ydot=[-2*G1*y(1)+2*G1*(CA11*(1+b*y(5))*y(1)+CA12*((1+b*y(5))*y(3)
-a*b*(1+y(5))*y(4)));...
    -2*G2*y(2)+2*G2*(CA22*(1+b*y(5))*y(2)+CA12*((1+b*y(5))*y(3)
+a*b*(1+y(5))*y(4)));...
    -y(4)*(O2-O1)-y(3)*(G1+G2)+G1*CA11*(a*b*(y(5))*y(4)+(1+b*y(5))
*y(3))+G2*CA22*(-a*b*(y(5))*y(4)+(1+b*y(5))*y(3))+CA21*(1+b*y(5))*
(G1*y(2)+G2*y(1));...
    y(3)*(O2-O1)-y(4)*(G1+G2)+G1*CA11*((1+b*y(5))*y(4)-a*b*(y(5))*y(3))
+G2*CA22*((1+b*y(5))*y(4)+a*b*(y(5))*y(3))+CA21*a*b*(1+y(5))*(G2*y(1)
-G1*y(2));...
    Lambda-(1+y(5))-(1+b*y(5))*(CA11*y(1)+2*CA12*y(3)+CA22*y(2))];
```

Secondly lasratrun4.m:

```
clear;
global G1 G2 a b CA11 CA12 CA22 CA21 CB11 CB12 CB22 Lambda O1 O2
load data4.dat;
S=data4;
tempout=[0 0];
figure(1);
clf;
save outputs.txt -ascii tempout
```

```
y0=S(1,4:8);

for j=1:size(S,1);

    T=S(j,1);

    yy=S(j,2:3);

    a=1;

    doL=-1020;

    Lambda=6;

    gE=400000000000;

    gN=2000000000;

    G=0.1;

    nA=3.4;

    nB=3.4;

    Nts=2000000000000000000000000;

    xi=0.00000000000000000005;

    c=300000000;

    b=1+((2*c*G*xi*Nts)/(nB*gE));

    LA=0.000280;

    LoA=nA*0.000280;

    ko=6283185.307179587;

    scale=0.0000000001;

#Check:

    -(nB*sin(yy(1)*LoA)*cos(ko*doL*scale+yy(1)*(LoA+doL*scale))+nA*sin
```

```
(ko*doL*scale+yy(1)*(LoA+doL*scale))*cos(yy(1)*LoA)-(nA+nB)*sqrt((1-T)
/T)*sin(yy(1)*LoA)*sin(ko*doL*scale+yy(1)*(LoA+doL*scale)))
    (nB*sin(yy(2)*LoA)*cos(ko*doL*scale+yy(2)*(LoA+doL*scale))+nA*sin(
ko*doL*scale+yy(2)*(LoA+doL*scale))*cos(yy(2)*LoA)-(nA+nB)*sqrt((1-T)/
T)*sin(yy(2)*LoA)*sin(ko*doL*scale+yy(2)*(LoA+doL*scale)))
    k1=yy(1)+ko;
    k2=yy(2)+ko;
    A1 = sqrt((nB*LoA)/((nB*LoA*(0.5-sin(2*yy(1)*LoA)/(4*k1*LoA)))
+(nB*(LoA+doL*scale)*((sin(yy(1)*LoA)*sin(yy(1)*LoA))/(sin(yy(1)*LoA+ko
*doL*scale+yy(1)*doL*scale)*sin(yy(1)*LoA+ko*doL*scale+yy(1)*doL*scale
)))*(0.5-(sin(2*(yy(1)*LoA+ko*doL*scale+yy(1)*doL*scale))/(4*k1*(LoA+
doL*scale)))))+((nB+nB)*sqrt((1-T)/T)*sin(yy(1)*LoA)*sin(yy(1)*LoA)/
k1)));
    A2 = sqrt((nB*LoA)/((nB*LoA*(0.5-sin(2*yy(2)*LoA)/(4*k2*LoA)))+
(nB*(LoA+doL*scale)*((sin(yy(2)*LoA)*sin(yy(2)*LoA))/(sin(yy(2)*LoA
+ko*doL*scale+yy(2)*doL*scale)*sin(yy(2)*LoA+ko*doL*scale+yy(2)*doL
*scale)))*(0.5-(sin(2*(yy(2)*LoA+ko*doL*scale+yy(2)*doL*scale))/(4*
k2*(LoA+doL*scale)))))+((nB+nB)*sqrt((1-T)/T)*sin(yy(2)*LoA)*sin(yy
(2)*LoA)/k2)));
    B1 = -A1*sin(yy(1)*LoA)/sin(yy(1)*LoA+ko*doL*scale+yy(1)*doL*scale);
    B2 = -A2*sin(yy(2)*LoA)/sin(yy(2)*LoA+ko*doL*scale+yy(2)*doL*scale);
    CA11 = (A1*A1/2)*(1-(sin(2*yy(1)*LoA)/(2*k1*LoA)));
```

```
    CA12 = (A1*A2/(2*LoA))*(sin((yy(2)-yy(1))*LoA)/(k2-k1)-sin((yy(2)+yy(1))
*LoA)/(k2+k1));

    CA22 = (A2*A2/2)*(1-sin(2*yy(2)*LoA)/(2*k2*LoA));

    CA21 = CA12;

    CB11 = ((B1*B1*(LoA+doL*scale))/(2*LoA))*(1-sin(2*(yy(1)*LoA+ko*doL*scale
+yy(1)*doL*scale))/(2*k1*(LoA+doL*scale)));

    CB12 = (B1*B2/(2*LA))*((sin((LoA+doL*scale)*(yy(1)-yy(2)))/(nB*(k1-k2)))
-(sin((LoA+doL*scale)*(yy(1)+yy(2))+2*ko*doL*scale)/((k1+k2)*nB)));

    CB22 = (B2*B2*(LoA+doL*scale)/(2*LoA))*(1-sin(2*(yy(2)*LoA+ko*doL*scale
+yy(2)*doL*scale))/(2*k2*(LoA+doL*scale)));

    C11=CA11+CB11;

    C22=CA22+CB22;

    G1=gE*C11/(2*gN);

    G2=gE*C22/(2*gN);

    O1=k1*c/gN;

    O2=k2*c/gN;

    %% transient

    tspan=[0 6];

    options = odeset('Stats','on','AbsTol',1e-12,'RelTol',1e-12);

    [t,y]=ode45(@lasrat4,tspan,y0,options);
%% generate the final plot

    tspan=[6 8];
```

```
    y1=y(size(y,1),:);
    options = odeset('Stats','on','AbsTol',1e-12,'RelTol',1e-12);
    [t,y]=ode45(@lasrat4,tspan,y1,options);
    M=length(t);
    for k=1
        x=1:M; w=y(:,k);
        for i=2:M-1;
            ai=i+1; bi=i-1;
            if w(i)>w(bi) & w(i)>w(ai)
     %           disp(['x= ',num2str(x(i)),' w = ',num2str(w(i)),'
','num2str(w(bi)),' ',num2str(w(ai))]);
                p(i)=i;
                m(i)=w(i);
                tempout=[T,w(i)'];
                save outputs.txt -ascii -append tempout
            end
        end
        %figure(1);
       % hold on
       % plot(T,m,'.');
    end
end
```

Appendix E

DsTool: Code to Simulate Equations (5.26)

```
/* ------------------------------------------------------------------------

   proc used to define the vector field

   ------------------------------------------------------------------------ */

int excav(f,x,p)

double f[],x[],p[];

{

  //  variables

  double E1, ReE2, ImE2,  N;

  E1 = x[0]; ReE2 = x[1]; ImE2 = x[2];  N = x[3];

  // specified parameters

  double gammaE, gammaN, Gamma, Lambda, gammaM, alpha;
```

```
  //dk1, dk2;
  gammaE = p[0]; gammaN = p[1]; Gamma = p[2]; Lambda = p[3]; gammaM = p[4];
alpha = p[5];
  //dk1 = p[6]; dk2 = p[7];
  double ko = 6283185.307179587;
  // k1 = ko+dk1, k2 = ko+dk2;
  // laser medium parameters
  double nb = 3.4, Nts = 2*pow(10,24), xi = 5*pow(10,-20) , c = 3*pow(10,8);
  // coupling and composite mode parameters
  double  L = 280*pow(10,-6), T = 0.1, doL = 3.4*pow(10,-10);
  double Normconst = nb*nb*L, LoA = nb*L, LoB = nb*L+doL;
  //Find roots (Newton method)
  //NB g=df/dx
  const double accuracy = 1.0e-14;
  double dknew1 = -200.0; // starting value
  double dkold1 = 0.0;
  double f1,g1;
  do
    {
      dkold1 = dknew1;
      f1 = nb*sin(dkold1*LoA)*cos(ko*(doL)+dkold1*(LoA+doL))+nb*sin(ko*
(doL)+dkold1*(LoA+doL))*cos(dkold1*LoA)-(nb+nb)*sqrt((1-T)/T)*sin(dkold1
```

```
*LoA)*sin(ko*(doL)+dkold1*(LoA+doL));
      g1 = (doL+LoA)*nb*cos(dkold1*LoA)*cos(-doL*ko-dkold1*(doL+LoA))+
LoA*nb*cos(dkold1*LoA)*cos(-doL*ko-dkold1*(doL+LoA))+
(-doL-LoA)*(nb+nb)*sqrt((1-T)/T)*cos(-doL*ko-dkold1*(doL+LoA))*sin(dkold1
*LoA)+LoA*(nb+nb)*sqrt((1-T)/T)*cos(dkold1*LoA)*sin(-doL*ko-dkold1*(doL+
LoA))+LoA*nb*sin(dkold1*LoA)*sin(-doL*ko-dkold1*(doL+LoA))+
(doL+LoA)*nb*sin(dkold1*LoA)*sin(-doL*ko-dkold1*(doL+LoA));
      dknew1 = dkold1-(f1/g1);
    }
  while ( fabs(dknew1-dkold1) > accuracy);

  double dknew2 = 400.0; // starting value
  double dkold2 = 0.0;
  double f2,g2;
  do
    {
      dkold2 = dknew2;
      f2 = nb*sin(dkold2*LoA)*cos(ko*(doL)+dkold2*(LoA+doL))+nb*sin(ko*
(doL)+dkold2*(LoA+doL))*cos(dkold2*LoA)-(nb+nb)*sqrt((1-T)/T)*sin(dkold2
*LoA)*sin(ko*(doL)+dkold2*(LoA+doL));
      g2 = (doL+LoA)*nb*cos(dkold2*LoA)*cos(-doL*ko-dkold2*(doL+LoA))+
LoA*nb*cos(dkold2*LoA)*cos(-doL*ko-dkold2*(doL+LoA))+
```

```
(-doL-LoA)*(nb+nb)*sqrt((1-T)/T)*cos(-doL*ko-dkold2*(doL+LoA))*sin(dkold2
*LoA)+LoA*(nb+nb)*sqrt((1-T)/T)*cos(dkold2*LoA)*sin(-doL*ko-dkold2*(doL+
LoA))+LoA*nb*sin(dkold2*LoA)*sin(-doL*ko-dkold2*(doL+LoA))+
(doL+LoA)*nb*sin(dkold2*LoA)*sin(-doL*ko-dkold2*(doL+LoA));
      dknew2 = dkold2-(f2/g2);
    }
  while ( fabs(dknew2-dkold2) > accuracy);

  double dk1 = dknew1;
  double dk2 = dknew2;
  double k1 = dk1 + ko, k2 = dk2 + ko;

  //printf("%f %f \n", dk1, dk2);

  double A1 = sqrt((nb*LoA)/((nb*LoA*(0.5-sin(2*dk1*LoA)/(4*k1*LoA)))+
(nb*(LoA+doL)*((sin(dk1*LoA)*sin(dk1*LoA))/(sin(dk1*LoA+ko*doL+
dk1*doL)*sin(dk1*LoA+ko*doL+dk1*doL)))*(0.5-(sin(2*(dk1*LoA+ko*doL+
dk1*doL))/(4*k1*(LoA+doL)))))+((nb+nb)*sqrt((1-T)/T)*sin(dk1*LoA)*sin(dk1
*LoA)/k1)));

  double A2 = sqrt((nb*LoA)/((nb*LoA*(0.5-sin(2*dk2*LoA)/(4*k2*LoA)))+(nb
*(LoA+doL)*((sin(dk2*LoA)*sin(dk2*LoA))/(sin(dk2*LoA+ko*doL+dk2*doL)*sin(
```

```
dk2*LoA+ko*doL+dk2*doL)))*(0.5-(sin(2*(dk2*LoA+ko*doL+dk2*doL))/(4*k2*(
LoA+doL)))))+((nb+nb)*sqrt((1-T)/T)*sin(dk2*LoA)*sin(dk2*LoA)/k2)));

  double B1 = -A1*sin(dk1*LoA)/sin(dk1*LoA+ko*doL+dk1*doL);

  double B2 = -A2*sin(dk2*LoA)/sin(dk2*LoA+ko*doL+dk2*doL);

  //printf("%f %f %f %f \n", A1, A2, B1, B2 );


  double CA11 = (A1*A1/2)*(1-(sin(2*dk1*LoA)/(2*k1*LoA)));
  double CA12 = (A1*A2/(2*LoA))*(sin((dk2-dk1)*LoA)/(k2-k1)-
sin((dk2+dk1)*LoA)/(k2+k1));
  double CA22 = (A2*A2/2)*(1-sin(2*dk2*LoA)/(2*k2*LoA));

  double CB11 = ((B1*B1*(LoA+doL))/(2*LoA))*(1-sin(2*(dk1*LoA+ko*doL+
dk1*doL))/(2*k1*(LoA+doL)));
  double CB12 = (B1*B2/(2*L))*((sin((LoA+doL)*(dk1-dk2))/(nb*(k1-k2)))-
(sin((LoA+doL)*(dk1+dk2)+2*ko*doL)/((k1+k2)*nb)));
  double CB22 = (B2*B2*(LoA+doL)/(2*LoA))*(1-sin(2*(dk2*LoA+ko*doL+
dk2*doL))/(2*k2*(LoA+doL)));
```

```
  double CA21 = CA12;
  double CB21 = CB12;

  double C11 = CA11+CB11;
  double C12 = CA12+CB12;
  double C21 = C12;
  double C22 = CA22+CB22;

  double U1Sq0 = A1*A1*sin(dk1*LoA)*sin(dk1*LoA);
  double U2Sq0 = A2*A2*sin(dk2*LoA)*sin(dk2*LoA);

  //printf("%f %f %f \n", CA12, CB12, C12);

  // rescalled parameters
  double  beta = 1+((2*c*Gamma*xi*Nts)/(nb*gammaE)), gamma1 =
gammaE*C11/(2*gammaN), gamma2 = gammaE*C22/(2*gammaN);
  double Gamma1 = gamma1+(U1Sq0*gammaM/gammaN), Gamma2 =
gamma2+(U2Sq0*gammaM/gammaN), F = 1+beta*N, G = beta*(1+N);

  double
    Omega1 = (k1*c/gammaN),
```

```
    Omega2 = (k2*c/gammaN);

  f[0] = -Gamma1*E1+gamma1*CA11*F*E1+gamma1*CA21*F*ReE2+
gamma1*CA21*alpha*G*ImE2;

  f[1] = -Gamma2*ReE2-ImE2*(Omega1-Omega2)+gamma2*CA22*(ReE2*F+
ImE2*alpha*beta*N)-ImE2*gamma1*CA11*alpha*beta*N+
((gamma1*CA21*ImE2*(F*ImE2-alpha*G*ReE2))/E1)+gamma2*CA12*F*E1;

  f[2] = -Gamma2*ImE2+ReE2*(Omega1-Omega2)-gamma2*CA12*alpha*G*E1+
gamma1*CA11*alpha*beta*N*ReE2+gamma2*CA22*(F*ImE2-alpha*beta*N*ReE2)+
((gamma1*CA21*ReE2*(alpha*G*ReE2-F*ImE2))/E1);

  f[3] = Lambda-(1+N)-F*(CA11*(E1*E1)+2*CA12*E1*ReE2+
CA22*(ReE2*ReE2+ImE2*ImE2));

  //printf("%f %f %f %f \n", f[0],f[1],f[2],f[3]);

  //printf("%f %f %f %f \n", E1, ReE2, ImE2, N);
 return(0);
}
```

```
/* ------------------------------------------------------------------------

   proc to define the default data for the dynamical system

   Note: You may change the entries for each variable but

         DO NOT change the list of items.  If a variable is

         unused, NULL or zero the entry, as appropriate.

   ------------------------------------------------------------------------ */

int excav_init()

{

  /* define the dynamical system in this segment

     ------------------------------------------------------------------------

  int    n_varb=4;

/* dim of the phase spase */

  static char   *variable_names[]={"E1","ReE2","ImE2","N"};

/* list of phase varb names */

  static double variables[]={1.0,0.0,1.0,0.0};

/* initial conditions for the variables */

  static double variable_min[]={0.0,-3.0,-3.0,-0.3};

/* default varb min for display */

  static double variable_max[]={3.0,3.0,3.0,0.3};

/* default varb max for display */

  static char   *indep_varb_name="time";

/* name of indep variable  */
```

```
  double indep_varb_min=0.;
/* default indep varb min r display */
  double indep_varb_max=100.;
/* default indep varb max r display */


  int    n_param=6;
/* dim of the parameter space */
  static char   *parameter_names[]={"gammaE","gammaN","Gamma","Lambda",
"gammaM","alpha"};  /* list of param names */
  static double parameters[]={400000000000.0,2000000000.0,0.1,2.0,0.0,0.0};
 /* initial parameter values */
  static double parameter_min[]={0.0,0.0,0.0,0.0,0.0,0.0,0.0,0.0};
 /* default param min for display */
  static double parameter_max[]={1.0,1.0,1.0,1.0,1.0,1.0,1.0,1.0};
 /* default param max for display */


  int    n_funct=1;
/* number of user-defined functions */
  static char   *funct_names[]={"E2"};
/* list of param names */
  static double funct_min[]={-1};
/* default varb max for display */
```

```
  static double funct_max[]={1};
/* default varb max for display */


  int    manifold_type = EUCLIDEAN;
 /* EUCLIDEAN or PERIODIC (periodic variables) */
  static int    periodic_varb[] = {FALSE,FALSE,FALSE,FALSE};
/* if PERIODIC, which variables are periodic */
  static double period_start[] = {0.,0.,0.,-PI};
 /* if PERIODIC, beginning of fundamental domain */
  static double period_end[] = {0., 0.,0., PI};
/* if PERIODIC, end of fundamental domain */


  int    mapping_toggle=FALSE;
 /* is this a map? */
  int    inverse_toggle=FALSE;
/* if so, is inverse FALSE, APPROX_INV, or EXPLICIT_INV?*/


  /*  In this section, input NULL or the name of the function which contains... *
  int           (*def_name)()=excav;
/* the eqns of motion */
  int           (*jac_name)()=NULL;
/* the jacobian (deriv w.r.t. space) */
```

```
  int           (*aux_func_name)()=excav_func;
/* the auxiliary functions */
  int           (*inv_name)()=NULL;
/* the inverse or approx inverse */
  int           (*dfdt_name)()=NULL;
/* the deriv w.r.t time */
  int           (*dfdparam_name)()=NULL;
/* the derivs w.r.t. parameters */


c_filename = __FILE__;  /* display this file for help with this system */


/* ------------------ end of dynamical system definition ------------------ */
#include <ds_define.c>
}
```